Charles University
Faculty of Science

Study programme: Biology

Branch of study: Cellular and Developmental Biology

Bc. Kristýna Čunátová

The role of tissue specific isoforms of subunit 4 in assembly and function of cytochrome *c* oxidase

Úloha tkáňově specifických izoforem podjednotky 4 v sestavování a funkci cytochrom *c* oxidázy

Diploma thesis

Supervisor: Mgr. Petr Pecina, Ph.D.

Prague, 2018

Prohlášení:

Prohlašuji, že jsem závěrečnou práci zpracovala samostatně a že jsem uvedla všechny použité informační zdroje a literaturu. Tato práce ani její podstatná část nebyla předložena k získání jiného nebo stejného akademického titulu.

V Praze, 30.4.2018

Podpis

Acknowledgements

I would like to thank my supervisor, Mgr. Petr Pecina, Ph.D., for guiding and supporting me. You have set an example of excellence as a researcher, mentor, and someone who instilled in me a passion for science.

I would also like to thank RNDr. Tomáš Mráček, Ph.D., and to all members of the Department of Bioenergetics at the Czech Academy of Sciences. I am very grateful to all of You for Your encouragement and making the workplace a fun place to be.

Finally, I would like to thank Jiří Veltruský who always stood by my side, and my family for the love and constant support throughout my entire life.

This study was supported by the grant project from Grant Agency of the Czech Republic (16-13671S).

Abstrakt

Systém oxidační fosforylace (OXPHOS) je zodpovědný za produkci naprosté většiny ATP v savčích organismech. Tento proces, lokalizovaný ve vnitřní mitochondriální membráně, je mimo jiné regulován jaderně kódovanými podjednotkami cytochrom *c* oxidázy (COX), která je terminálním enzymem elektron transportního řetězce. Podjednotka Cox4 se účastní regulace OXPHOS systému a spolu s podjednotkou Cox1 utváří první intermediát v sestavování COX. Není-li tento intermediát správně sestaven, nedojde následně ke vložení Cox2 katalytické podjednotky a tím k maturaci katalyticky funkčního COX enzymu. Mimo to je Cox4 podjednotka přítomna ve dvou izoformách (Cox4i1, Cox4i2), které hypoteticky slouží k optimalizaci funkce respiračního řetězce během změn v zásobování tkání kyslíkem. Funkční dopad výměny izoforem nebyl nicméně doposud v savčích tkáních a buňkách podrobně prozkoumán.

V rámci této práce byly pomocí CRISPR CAS9-10A párující nikázy připraveny jedinečné modely HEK293 buněk s úplnou absencí (knock-out, KO) podjednotky Cox4, a byly dále charakterizovány. Vyřazení funkce obou izoforem Cox4i1 a Cox4i2 (COX4i1/4i2 KO klony) vedlo ke generalizovanému snížení COX podjednotek spojenému s úplnou absencí sestavené COX. Množství detekovaných podjednotek komplexu I, stejně jako obsah sestaveného komplexu I, byly sníženy u COX4i1/4i2 KO klonů. Naopak, množství komplexu II, komplexu III a komplexu V nebylo výrazně narušeno. V souladu s tímto pozorováním i metabolické značení 13 mitochondriálně kódovaných proteinů odhalilo narušení proteosyntézy podjednotek COX i komplexu I, zatímco komplex III a komplex V nebyly ovlivněny. Změny mitochondriální proteosyntézy rovněž korelovaly se sníženým množstvím mitochondriálních ribozomálních proteinů. Dle očekávání nebyla u COX4i1/4i2 KO klonů detekována mitochondriální respirace, jejíž nefunkčnost byla kompenzována zvýšenou glykolytickou kapacitou.

COX4i1/4i2 KO modely připravené v HEK293 buněčné linii vykazovaly fenotyp úplné ztráty COX, vedoucí k plné závislosti buněk na nemitochondriální ATP produkci. Navrhujeme, že narušení mitochondriální proteosyntézy představuje sekundární efekt dysfunkce elektron transportního řetězce. COX4i1/4i2 dvojité KO klony připravené v rámci předkládané diplomové práce budou použity jako nástroj pro vytvoření knock-in modelů Cox4i1 i Cox4i2 izoformy, které poslouží k objasnění jejich biologické úlohy.

Klíčová slova: cytochrom *c* oxidáza, COX, Cox4 izoformy, Cox4i1, Cox4i2, CRISPR

Abstract

Oxidative phosphorylation apparatus (OXPHOS) is responsible for production of majority of ATP in mammalian organisms. This process, occurring in the inner mitochondrial membrane, is partly regulated by nuclear-encoded subunits of cytochrome *c* oxidase (COX), the terminal enzyme of electron transport chain. Cox4 subunit, participating in OXPHOS regulation, is an early-assembly state subunit, which is necessary for incorporation of Cox2 catalytic subunit, thus for assembly of catalytically functional COX enzyme. Moreover, regulated expression of two isoforms (Cox4i1, Cox4i2) of Cox4 subunit is hypothesized to optimize respiratory chain function according to tissue oxygen supply. However, the functional impact of the isoform switch for mammalian tissues and cells is still only partly understood.

In the present thesis, unique HEK293 cell line-based model with complete absence of subunit Cox4 (knock-out, KO) was prepared employing novel CRISPR CAS9-10A paired nickase technology and further characterized. Knock-out of both isoforms Cox4i1 and Cox4i2 (COX4i1/4i2 KO clones) showed general decrease of majority of Cox subunits resulting in total absence of fully assembled COX. Moreover, detected Complex I subunits as well as the content of assembled Complex I were decreased in COX4i1/4i2 KO clones. On the contrary, levels of Complex II, Complex III, and Complex V were not significantly affected. Pulse-chase metabolic labelling of 13 mtDNA-encoded proteins synthesized in mitochondria uncovered impairment of COX and Complex I subunits proteosynthesis, while Complex III and Complex V subunits were not significantly affected. Correspondingly, partial impairment of mitochondrial proteosynthesis correlated with decreased level of mitochondrial ribosomal proteins. As expected, mitochondrial respiration was undetected in COX4i1/4i2 KO cells, and was compensated by increased glycolytic capacity.

In summary, the HEK293 cell line-based cellular model of COX4i1/4i2 KO displayed phenotype of total COX absence, making cells fully reliant on OXPHOS-independent ATP production. In addition, we hypothesise that the impairment of mitochondrial proteosynthesis represents a secondary effect of electron transport chain dysfunction. COX4i1/4i2 double KO prepared in this project will serve as a tool for knock-in of either Cox4i1 or Cox4i2 isoform to clarify biological role of these isoforms.

Key words: cytochrome *c* oxidase, COX, Cox4 isoforms, Cox4i1, Cox4i2, CRISPR

List of content

List of abbreviations

ADP	adenosine diphosphate
AOX	alternative terminal oxidase
ATP	adenosine triphosphate
BN-PAGE	blue native polyacrylamide gel electrophoresis
BNC	binuclear center
bp	base pair
C	complex
COX	cytochrome *c* oxidase
ECAR	extracellular acidification rate
ETC	electron transport chain
FADH	flavin adenine dinucleotide
gRNA	guide RNA
HEK293	human embryonic kidney cell line
HeLa	cell line derived from cervical carcinoma of Henrietta Lacks
HIF-1	hypoxia inducible factor-1
HREs	hypoxia-response elements
IMM	inner mitochondrial membrane
IMS	intermembrane space
kDa	kilodaltons
KI	knock-in
KO	knock-out
LSI	late state intermediate complex
MEFs	mice embryonal fibroblasts
MITRAC	mitochondrial translation regulation assembly intermediate of COX
MS LFQ	mass spectrometry label free quantification
mtDNA	mitochondrial deoxynucleic acid
NADH	nicotinamide adenine dinucleotide
nDNA	nuclear deoxynucleic acid
OCR	oxygen consumption rate
ORE	oxygen responsive element
OREFs	ORE binding factors
OXPHOS	oxidative phosphorylation
PAMSCs	pulmonary arterial muscle cells
PIC	protease inhibitor cocktail
PLS	proton loading site
pmf, Δp	proton motive force
ROS	reactive oxygen species
wt	wild-type

1. Introduction

1.1. Oxidative phosphorylation apparatus

Energy demands of mammalian cells are mainly covered by ATP synthesis carried out by oxidative phosphorylation apparatus (OXPHOS) located in the central bioenergetic organelle, mitochondria. OXPHOS is composed of five multi-subunit complexes embedded in the inner mitochondrial membrane (IMM), as shown in Figure 1.1. Electrons from reduced substrates of complexes I and II are transported through electron carriers to the terminal OXPHOS enzyme, cytochrome *c* oxidase (COX, Complex IV), which reduces the terminal electron acceptor, oxygen, to water. Electron transport is achieved by increasing redox potential of individual active centers of complexes and carriers. Complex I, Complex III and Complex IV couple electron transport with translocation of protons across the membrane into intermembrane space (IMS). Proton gradient is then utilized by Complex V (ATP synthase) for ATP production (Nicholls and Ferguson, 2013).

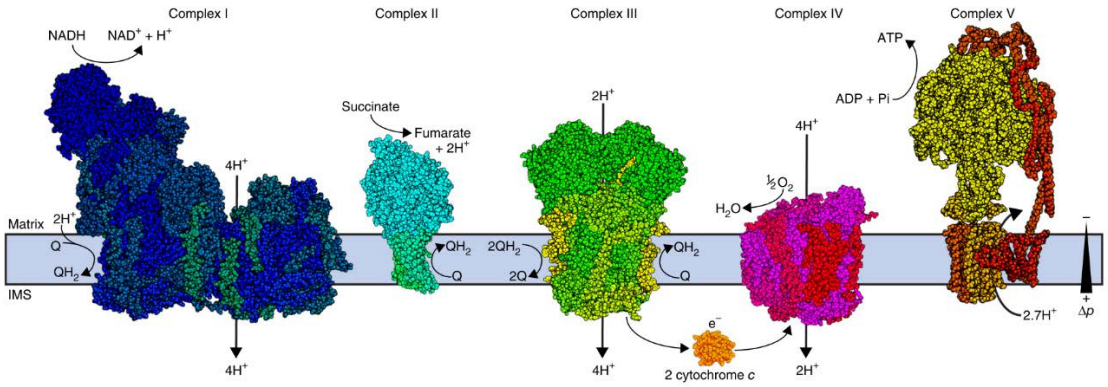

Figure 1.1: Scheme of OXPHOS apparatus localized in the inner mitochondrial membrane (Letts and Sazanov, 2017). OXPHOS is composed of five multi-subunit complexes: Complex I (NADH dehydrogenase, CI), Complex II (Succinate dehydrogenase, CII), Complex III (cytochrome bc1, CIII), Complex IV (Cytochrome c oxidase, COX) and Complex V (ATP synthase, CV).

1.2. Biogenesis of OXPHOS complexes

In evolution, most of mitochondrial genes were transferred into nucleus. However, human mitochondrial DNA still encodes thirteen subunits of OXPHOS complexes. Thus, OXPHOS complexes are composed of subunits encoded by both mitochondrial (mtDNA) and nuclear (nDNA) DNA. This means that expression and posttranslational modifications of individual subunits in mitochondria and cytosol need to be coordinated

by crosstalk between nucleus and mitochondria to prevent accumulation of assembly intermediates with no catalytic function (Dennerlein, Wang and Rehling, 2017). Multiple levels of OXPHOS proteins expression, such as mRNA maturation and stability, translational coordination, ribosomal biogenesis, and translation (Hällberg and Larsson, 2014), may regulate OXPHOS capacity. Also, many cofactors secure proper homeostasis and assembly of subunits into apoenzyme (Fontanesi et al., 2006).

Moreover, there is an evidence of interdependency between individual complexes, as aberration of one OXPHOS complex may affect assembly or stability of the other. The best understood is interdependence between CI and CIII (Ugalde *et al.*, 2004; Diaz, Enríquez and Moraes, 2012). But, relation was also described between CI and COX, whereas complete absence of COX affects amount of CI holoenzyme monomer and also CI within supercomplexes at the level of CI assembly (Diaz *et al.*, 2006; Li *et al.*, 2007). On the other hand, it was shown that nonsense mutations in Cox1 subunit (catalytic core subunit of COX) affect amount of CI at the level of stability, rather than assembly (Hornig-Do *et al.*, 2012).

Thus, coordination of many processes is crucial for assembly of each complex and their alterations may lead to certain diseases.

1.3. Supercomplexes

Individual electron transport chain (ETC) complexes were shown to form higher organization structures, which may modulate efficiency of electron transport. Existence of supercomplexes is consistent with the plasticity model (Acín-Pérez *et al.*, 2008; Enríquez, 2016), which suggests coexistence of both solid-state (Chance and Williams, 1955) and random collision models (Chazotte and Hackenbrock, 1989) of IMM (see Figure 1.2). In addition to COX dimers (IV_2) and supercomplexes III_2IV_1, I_1III_2, yet another one termed respirasome ($I_1III_2IV_1$) was described, which may increase efficiency of ETC by electrons channeling (Letts and Sazanov, 2017). However, content and ratio of various supercomplexes differ among species and tissues (Schägger and Pfeiffer, 2000).

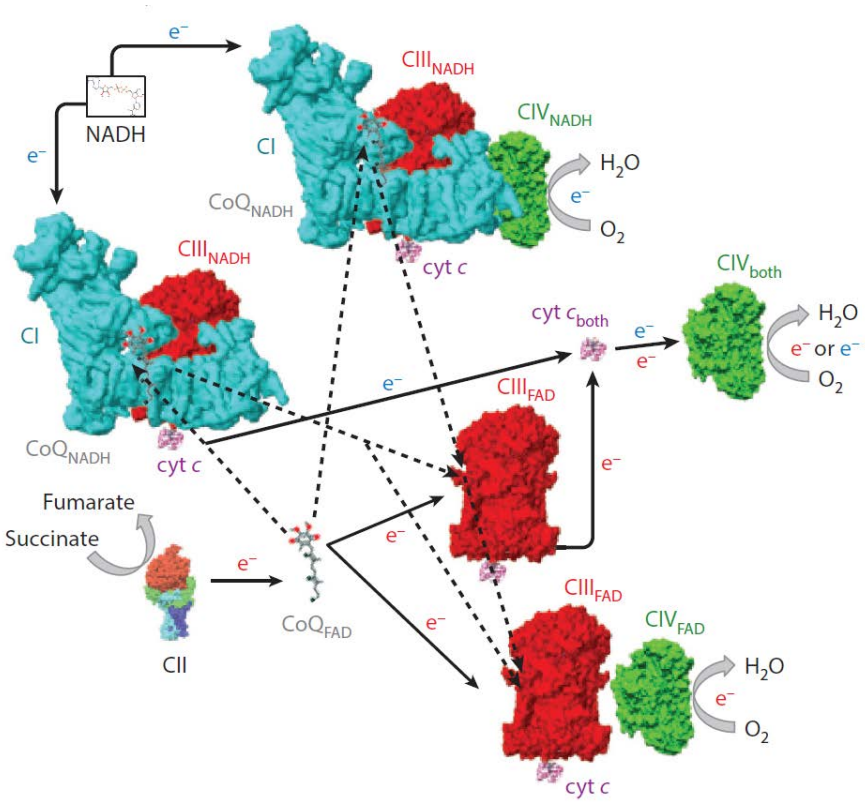

Figure 1.2: Plasticity model of the inner mitochondrial membrane (Enríquez, 2016). Plasticity of respiratory chain organization serves to modulate electron transfer pathways from substrates to terminal acceptor oxygen.

In mammals, arrangements of supercomplexes composed of Complex I, Complex III and Complex IV (Figure 1.3) were studied mostly by 1-D/2-D BN-PAGE and 1-D CN-PAGE (Wittig and Schägger, 2005). The most abundant supercomplex found in bovine heart is $I_1III_2IV_n$ (n = 1-4) supercomplex (Schägger and Pfeiffer, 2000). Its 3-D structure was originally studied by MALDI-MS and by cryo-electron microscopy (Schäfer *et al.*, 2006). Then, the most detailed architecture at 5.8 Å of ovine supercomplex (Letts et al. , 2016) and at 4.0 Å of porcine heart supercomplex (Wu *et al.*, 2016) were solved. Recently, structure of human $I_1III_2IV_1$ supercomplex was published, suggesting existence of circular $I_2III_2IV_2$ megacomplex (Guo *et al.*, 2017). Moreover, authors propose $I_2II_2III_2IV_2$ megacomplex, which contains also CII inserted between CI and CIV in $I_2III_2IV_2$ (Guo *et al.*, 2017). Supercomplexes relevance *in vivo* was approved by mass spectrometry revealing intact mitochondria interactome (Liu *et al.*, 2018).

Despite current studies focusing on supercomplex architecture, their precise physiological role is not resolved yet. Suggested functions include electron channeling,

ROS production prevention, as well as their involvement in assembly and stabilization of individual complexes (Letts and Sazanov, 2017; Milenkovic *et al.*, 2017).

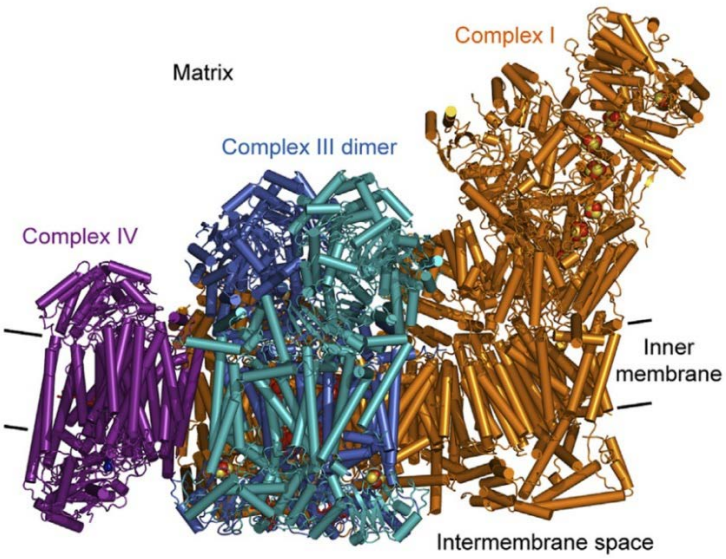

Figure 1.3: Structure of respirasome (Milenkovic *et al.*, 2017). Model of respirasome structure based on cryo-electron microscopy data.

1.4. Cytochrome *c* oxidase

Cytochrome *c* oxidase (COX), the member of heme-Cu oxidases, is the terminal enzyme of mitochondrial ETC indispensable for transfer of electrons to the terminal electron acceptor, the oxygen, and for contribution in formation of proton gradient necessary for ATP production by ATP synthase in mammalian cells. Moreover, COX is proposed to have important function in regulation within whole OXPHOS system (Nicholls and Ferguson, 2013).

1.4.1. COX structure

COX monomer of mammalian enzyme is composed of thirteen subunits encoded by both, mitochondrial and nuclear genome (see Figure 1.4). Initially, COX subunit composition was characterized by high-resolution SDS-PAGE (Kadenbach *et al.*, 1983) and later approved by X-ray crystallography of bovine heart COX dimer (Tsukihara *et al.*, 1996). Catalytic core of COX enzyme is assembled of mitochondria-encoded subunits (Cox1, Cox2, Cox3) which are tightly surrounded by ten nuclear-encoded subunits (Cox4, Cox5a, Cox5b, Cox6a, Cox6b, Cox6c, Cox7a, Cox7b, Cox7c, Cox8). Nomenclature of

subunits by Kadenbach is widely accepted and corresponds to decreasing molecular weight of subunits observed by SDS-PAGE. Subunits with similar molecular weight are distinguished by a letter (Kadenbach and Merle, 1981). Among several other proteins associating with COX as putative subunits that are not retained in isolated enzyme (see Section 1.4.5.), NDUFA4 (or COXFA4) has become widely accepted as bona-fide stoichiometric COX subunit (Pitceathly and Taanman, 2018).

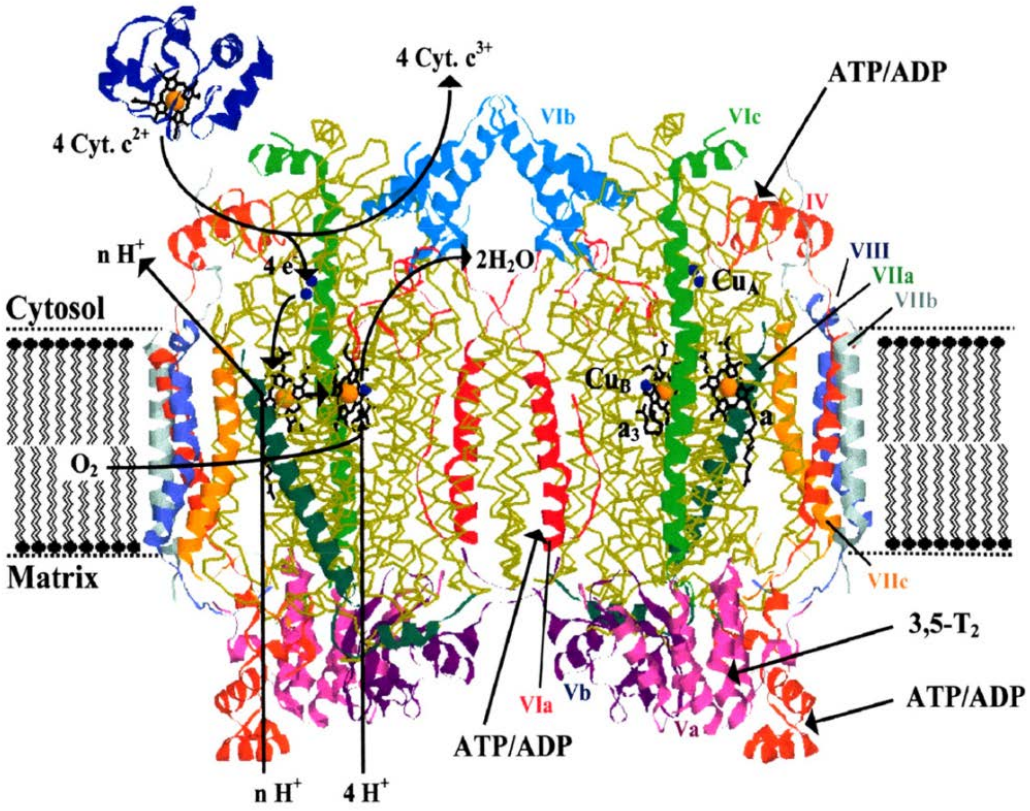

Figure 1.4: Structure of bovine COX dimer (Kadenbach and Hüttemann, 2015).

1.4.2. Mitochondria-encoded catalytic core subunits

Mammalian COX catalytic core is composed of three mitochondria-encoded subunits (Cox1 Cox2, Cox3) responsible for catalytic function of the enzyme. Some aerobic bacteria contain cytochrome aa3 type of the terminal oxidase, which shows structural and functional homology to eukaryotic mitochondrial enzyme core. In contrast with multi-subunit composition of mitochondrial COX, the enzyme of *Paracoccus denitrificans* contains only four subunits. Functionally crucial subunits Cox1 and Cox2 are highly conserved across the organisms at the amino acid level and also at the level of structure (Iwata *et al.*, 1995; Tsukihara *et al.*, 1996).

Cox1 subunit consists of twelve transmembrane α-helices and three catalytic centers of COX enzyme - heme *a* and binuclear center (BNC) composed of heme a_3 and Cu_B atom. Cox2 subunit is composed of two transmembrane α-helices and bimetallic Cu_A catalytic center (Cu^I/Cu^{II}). Moreover, Cox2 hydrophilic domain in IMS forms binding site for cytochrome *c*. Cox3 subunit consists of seven transmembrane α-helices and stabilizes catalytic center of COX (Kaila, Verkhovsky and Wikström, 2010; Nicholls and Ferguson, 2013). Without Cox3 subunits, stoichiometry of pumped protons decreases in both bacterial and mitochondrial enzyme. So it seems, that Cox3 subunits connection with Cox1 could maintain efficient proton pumping and also oxygen diffusion (Hosler, 2004; Sharma *et al.*, 2015). Moreover, loss of Cox3 increases possibility of suicide inactivation of COX by inactivation of electron transfer between heme *a* and heme a_3 (Bratton, Pressler and Hosler, 1999).

1.4.3. Catalytic function of COX

COX enables electron transfer from cytochrome c to the terminal electron acceptor, oxygen, which is reduced to water (as shown in Figure 1.5). Electrons are received from cytochrome *c* on intermembrane side of COX enzyme by docking of cytochrome *c* thanks to electrostatic interactions of conserved lysine residues of cytochrome *c* with carboxyl groups of hydrophilic part of Cox2 subunit (Millett *et al.*, 1983). Further, electrons are sequentially transferred through Cu_A center to heme *a*. Heme *a* is called electron-queuing site thanks to dependency of following transfer of electrons to BNC (heme a_3 and $Cu_{B)}$ on proton translocation (Babcock and Wikström, 1992). Distance between heme centers - 7 Å - is conserved in heme-Cu oxidases (Kaila, Verkhovsky and Wikström, 2010). Although, direct transfer of electrons from Cu_A center to heme *a*3 was observed in mutated oxidases, efficiency of enzyme was significantly decreased (Kannt *et al.*, 1999).

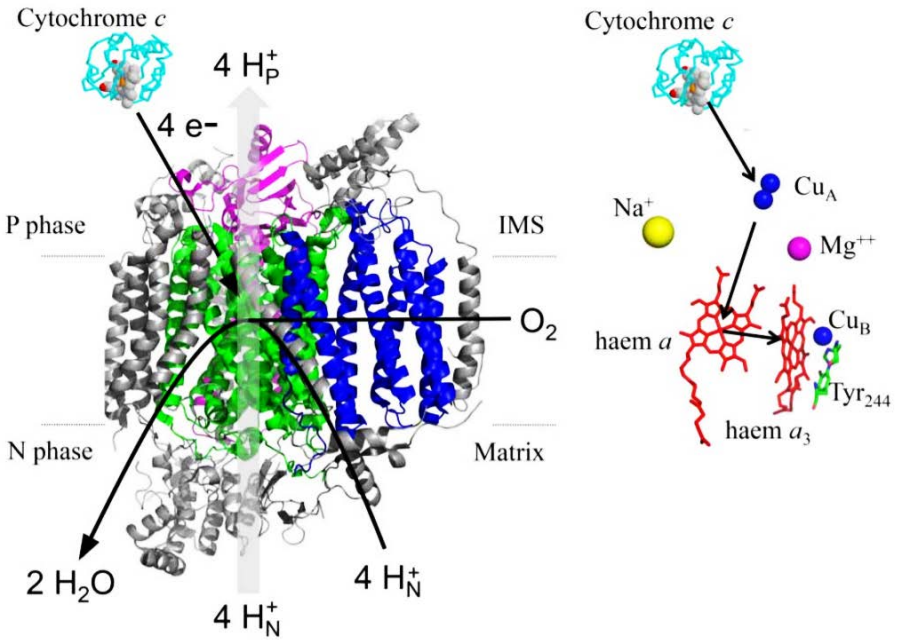

Figure 1.5: Schematic depiction of COX catalytic function (Rich, 2017).

Nonpolar channel enables diffusion of the oxygen into catalytic center of COX enzyme (Tsukihara *et al.*, 1996; Sharma *et al.*, 2015). Heme-oxygen adduct is formed by binding of oxygen into BNC (Chance, Saronio and John S. Leigh, 1975). Oxygen bond is disrupted immediately after binding of oxygen into BNC. One electron for oxygen reduction is provided by tyrosine residue (Tyr208), second electron by Cu_B and two remaining electrons come from iron cations of heme *a*3. Simultaneous transfer of four electrons is crucial as a precaution of reactive oxygen species (ROS) production (Ludwig *et al.*, 2001). Then, BNC is regenerated by four reduction steps of catalytic cycle. In each step, one electron from heme *a* and one proton from matrix (chemical proton) are translocated into BNC, while one proton is pumped into IMS (Kaila, Verkhovsky and Wikström, 2010).

Electron transfer is coupled to translocation of protons across the IMM, which builds up transmembrane electrochemical proton gradient, called protonmotive force (pmf), which is used by ATP synthase for ATP production. Each transferred electron corresponds to translocation of two positive charges across IMM. Chemical proton is translocated from matrix into catalytic center, where it contributes to reduction of the oxygen and compensates electron charge of electron transferred from IMS. Physical proton, which is pumped from matrix into IMS, does not contribute to chemical reaction itself, but it's motion is indirectly coupled to the reaction (Kaila, Verkhovsky and

Wikström, 2010). Electron transfer tunneling through metallic centers creates strong electric field in protein, which enables proton translocation due to water molecules polarized into a chain. Therefore, barrier for initial transfer of proton from acceptor to first water molecule is decreased. When proton reaches acceptor, polarity of water molecules is reversed (Kaila, Verkhovsky and Wikström, 2010).

Mechanism of proton pumping is not clarified despite biophysical studies on models as mitochondrial COX isolated from bovine heart or prokaryotic variant of COX from *P. denitrificans*. Nowadays, two different hypotheses of mechanism of proton pumping through COX are proposed. First hypothesis operates with proton loading site (PLS) in propionate domain of heme *a*3, which accepts physical protons translocated from matrix by D-pathway, while hem *a* is occupied by electron. Proton in PLS increases redox potential of BNC and therefore performs electron transfer into BNC. Then, chemical proton is attracted from matrix into BNC, which repulses physical proton from PLS into IMS. This mechanism is supported by molecular dynamics simulations and also by observed water molecules formation between Glu242 and heme *a*3 before electron is transferred into BNC (Fadda, Yu and Pomès, 2008). Second hypothesis presumes as a first step chemical proton translocation into BNC, which corresponds to conformational change allowing translocation of physical proton into PLS (Brzezinski and Larsson, 2003).

Translocation of protons is achieved by proton pathways (located in Cox1 subunit) predicted in bacteria and eukaryote by site-specific mutagenesis and COX crystal structure (Hosler *et al.*, 1993; Tsukihara *et al.*, 1996). These pathways are depicted in Figure 1.6. K-pathway (named by Lys319 residue in bovine COX enzyme) is supposed to translocate first or even second chemical proton into BNC center (Tyr280 in bovine COX enzyme) (Konstantinov *et al.*, 1997; Vygodina *et al.*, 1997; Ruitenberg *et al.*, 2000). In bacteria, it was shown that K-pathway contains water molecules and proton translocation occurs there (Kaila, Verkhovsky and Wikström, 2010). Remaining chemical and physical protons are translocated by D-pathway (Asp91 residue in bovine COX enzyme), which also contains water molecules, polar amino acid residues and leads into BNC center (Glu242 in bovine COX enzyme) (Konstantinov *et al.*, 1997; Vygodina *et al.*, 1997). Nonpolar cavity located near Glu242 residue may be filled by water molecules formed during reaction in BNC (Wikström, Verkhovsky and Hummer, 2003). Third, H-pathway, was predicted by crystal structure of bovine heart COX enzyme (Tsukihara *et*

al., 1996; Yoshikawa *et al.*, 1998) and further approved by mutational analyses of bovine COX (Kamiya *et al.*, 2007; Shimokata *et al.*, 2007; Yano *et al.*, 2016; Luo *et al.*, 2018). Hypothesis of increased stoichiometry of pumped protons by H-pathway under low membrane potential was proposed (Kadenbach, Ramzan and Vogt, 2013). However, studies on bacterial COX mutants targeted on its proposed structure did not approve H-pathway existence in bacterial COX (Pfitzner *et al.*, 1998; Lee *et al.*, 2000; Salje, Ludwig and Richter, 2005; Wikström *et al.*, 2015). Thus, H-pathway may be an unique structure for proton translocation in mammalian COX (reviewed by Rich 2017; Yoshikawa and Shimada 2015).

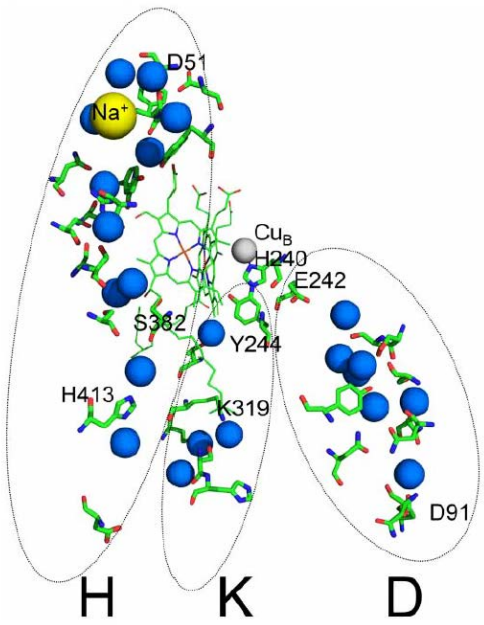

Figure 1.6: Proton pathways localized in Cox1 subunit (Rich, 2017).

1.4.4. Nuclear-encoded subunits as evolutionary superstructure

Conserved catalytic core of eukaryotic COX is complemented by as much as ten nuclear-encoded subunits, which are not crucial for catalytic function of COX. Nevertheless, nuclear-encoded subunits may modulate COX activity upon various conditions due to its regulatory function within the enzyme. Moreover, some nuclear-encoded subunits show tissue-specific and development-specific isoforms (encoded by different genes), possibly enabling fine-tuning of COX function in individual tissues.

Nuclear-encoded subunits, which are specific for eukaryotic organisms, represent innovation in COX structure and function (see Figure 1.7). Although, some mitochondrial

genes were relocated from mitochondrial genome into nucleus after endosymbiosis, nuclear-encoded subunits do not appear to have origin in mitochondrial genome (Szklarczyk and Huynen, 2010). No homologous genes were found in either *Rickettsia prowazekii* (the closest taxon to the hypothetic endosymbiont), or in *Reclinomonas americana* genome, which retained largest number of genes in mtDNA (Lang, Burger and O'Kelly, 1997; Andersson *et al.*, 1998; Das, Miller and Stern, 2004). Many nuclear-encoded subunits may be found in genome of *Drosophila melanogaster*, *Saccharomyces cerevisiae* and *Arabidopsis thaliana*, which suggests appearance of these subunits before the split of eukaryotic linages (Das, Miller and Stern, 2004; Pierron *et al.*, 2012). Moreover, some nuclear-encoded subunits show two or three isoforms, which were created by duplication of incriminated gene, therefore being paralogues. It is unknown, if isoforms rise from duplication of individual genes or whole genome duplication (Blomme *et al.*, 2006; Little *et al.*, 2010). After duplication of genes, selective pressures could have shaped specialized function of isoform pair and for tissue-specific expression of the subunit, in a process called subfunctionalization (Lynch *et al.*, 2001; Pierron *et al.*, 2012).

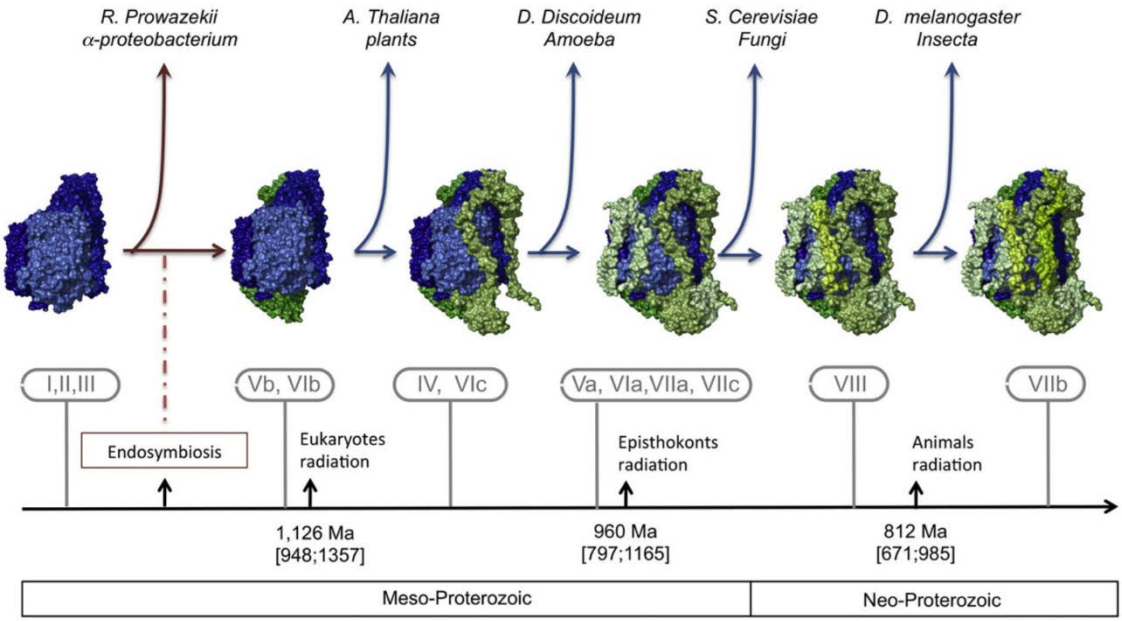

Figure 1.7: Evolution of COX subunits composition (Pierron *et al.*, 2012).

Subunits Cox5a, Cox5b, Cox6c and Cox7c do not show isoform pairs in mammals, but some of them have regulatory function. Subunit Cox5a, which is located on matrix side of the enzyme, specifically binds 3,5-diiodothyronine (T2) in bovine heart COX, which abolishes allosteric ATP-inhibition of COX and stimulates energetic metabolism

of the cell (Cimmino *et al.*, 1996; Lanni *et al.*, 1996). Matrix side Cox5b subunit is important for COX assembly (Galati *et al.*, 2009) and interacts with regulatory subunit of cAMP-dependent protein kinase A, which inhibits COX activity (Yang *et al.*, 1998). Subunits Cox6c and Cox7c were not proven to have any regulatory function yet, despite of their interaction with catalytic core subunits Cox1 and Cox2 (Tsukihara *et al.*, 1996).

Subunits Cox4, Cox6b and Cox7b are each present in mammals as two different isoforms. Cox4 isoforms are described in detail in Chapter 1.5. IMS side oriented Cox6b subunit mediates tight interaction between two monomers of COX in dimer (Tsukihara *et al.*, 1996). Cox6b-1 isoform absence results in doubled enzyme activity of COX without changes in stoichiometry of translocated protons due to monomerization of COX dimer. It occurs due to the loss of cooperative behavior of COX dimer's monomers in cytochrome *c* binding kinetics (Weishaupt and Kadenbach, 1992; Kadenbach and Hüttemann, 2015). Second Cox6b isoform (Cox6b-2) in mammals is specifically expressed only in testis, and thus extends a group of testes-specific proteins, such as ANT4 isoform of adenine nucleotide translocator (Dahout-Gonzalez, 2006) or cytochrome *c* (Hüttemann, Jaradat and Grossman, 2003). However, testis isoform of cytochrome *c* is not conserved in primates (Krzyzosiak *et al.*, 2000). Cox7b-1 isoform of Cox7b subunit is important for COX assembly and activity (Indrieri *et al.*, 2012). To the contrary, function of Cox7b-2 isoform was not determined yet. Nevertheless, mice Cox7b-2 isoform expands the group of testes-specific proteins (Kadenbach and Hüttemann, 2015).

Subunits Cox6a, Cox7a and Cox8 display similar tissue-specific and development-specific manner of isoforms expression. Isoform H (heart) is expressed in heart and skeletal muscle, while isoform L (liver) is ubiquitously expressed in all other tissues (Bonne *et al.*, 1993). Cox6a subunit is in contact with Cox1 subunit of another COX monomer, therefore is supposed to stabilize dimer (Radford *et al.*, 2002). Expression of heart isoform, Cox6a-H, is development-specific, as exchange of Cox6a-L to Cox6a-H occurs during the third month after the birth (Ewart, Zhang and Capaldi, 1991; Boczonadi *et al.*, 2015). Cox7a-H isoform gene deletion in mice leads to decreased COX activity and compensation of the loss by Cox7a-L substitution of Cox7a-H in heart COX, which is not observed with Cox6a-H isoform knock-out (Hüttemann, Klewer, *et al.*, 2012). Another point of interest is possible regulation of Cox7a-L expression by HIF-1α (hypoxia inducible factor 1α), which may alter supercomplexes composition under hypoxia, thus

modulating COX activity (Hwang *et al.*, 2015). Moreover, Cox7a subunit possesses a third possible isoform, SCAF1 (supercomplex assembly factor 1) (Cox7a2L, Cox7aR, SIG81), which has similar expression pattern as Cox7aL (Segade *et al.*, 1996; Schmidt, Goodman and Grossman, 1999). However, some publications still present SCAF1 as a protein homologous to Cox7a subunit (Letts and Sazanov, 2017). For further description of the role of SCAF1 in supercomplexes formation, see Chapter 1.4.5. Cox 8 subunit, which is crucial for enzyme stability (Hallmann *et al.*, 2016), is present in three different isoforms in mammals. However, humans retained only Cox8-L isoform, while Cox8-H lost its function and became a pseudogene (Goldberg *et al.*, 2003). Third, Cox8-3, isoform was identified as a homologous gene in humans, but its tissue specificity is not clarified (Hüttemann, Schmidt and Grossman, 2003).

Mutations in assembly factors genes are frequent cause of mitochondrial diseases coupled with malfunction of COX enzyme. In these cases, residual portion of COX remains functional despite impaired COX assembly (Stibůrek and Zeman, 2010). The putative existence of mutations in nuclear genes encoding COX subunits had long been considered doubtful, as they would lead to total COX absence and thus more severe phenotype. Nevertheless, since 2004, rare mutations leading to hereditary human diseases, as encephalomyopathy and cardiomyopathy, were found in six genes for COX nuclear-encoded subunits. With the development of next generation sequencing techniques, more pathogenic mutations in COX nuclear-encoded subunits genes may be discovered in the future. Mutations characterized to date are listed in Table 1.1.

Gene	Mutation		Disease	Publication
COX4i1	substitution	Lys101Asn	Fanconi anemia	(Abu-Libdeh *et al.*, 2017)
COX6A1	5 bp deletion	247-10_247-6 del CATCT	Axonal form of Charcot-Marie-Tooth syndrome	(Tamiya *et al.*, 2014)
COX6B1	substitution 221G/A in exon 2	Arg19His	Encephalomyopathy	(Massa *et al.*, 2008)
COX6B1	substitution	Arg20Cys	Encephalomyopathy, hydrocephalus, hypertrophic cardiomyopathy	(Abdulhag *et al.*, 2015)
COX7B1	substitution	nonsense mutation	Microphthalmia with linear skin lesions	(Indrieri *et al.*, 2012)
COX7B2	5 SNPs (single nucleotide polymorphisms)	His26Gln substitution	Nasopharyngeal cancer	(Liang, 2004)
COX8A	substitution	115G/C leads to aberrant splicing	Leigh-like syndrome with leukodystrophy and epilepsy	(Hallmann *et al.*, 2016)

Table 1.1: Nuclear-encoded subunits genes mutations leading to mitochondrial diseases.

1.4.5. Proteins associating with COX

Except nuclear-encoded subunits, associating proteins were discovered to comigrate with COX in native electrophoreses, although they were not identified in crystal structure of COX, which contains thirteen subunits (Tsukihara *et al.*, 1996). They are loosely attached to COX and may not be present under all conditions as canonical COX subunits. They are lost from the complex by solubilization preceding structural studies, and thus they were not found by crystallographic techniques. Eventually, associating proteins are present in sub-stoichiometric ratio to subunits of COX monomer. Their role within the complex may be modulation of enzymatic function or assembly of COX into supercomplexes. Several proteins interacting with mammalian COX are described below.

One of associating proteins, MNRR1 (CHCHD2), was co-immunoprecipitated with COX in sub-stoichiometric ratio to Cox1 and Cox2 catalytic subunits. Its predicted function is regulation of dimeric COX or incorporation of COX into supercomplexes (Aras *et al.*, 2015; Grossman *et al.*, 2017). Interaction with COX depends on MNRR1 phosphorylation status. Tyr99 of MNRR1 is phosphorylated by Abl2 kinase, which enhances COX binding and regulates respiratory activity during stress (Aras *et al.*, 2017). NDUFA4, protein originally considered as Complex I subunit (Carroll *et al.*, 2003), was

found to associate with COX where it may activate COX function after biogenesis (Balsa *et al.*, 2012; Pitceathly *et al.*, 2013). Higd1a, which has hypoxia-induced expression (Hayashi *et al.*, 2015), is homolog of yeast protein Rcf1, which has function in supercomplexes assembly (Strogolova *et al.*, 2012). However, in mammals its function seems to be quite different. Higd1a is supposed to directly bind COX and cause structural change around heme *a*, which may enable protons pumping through H-pathway. Thus, Higd1a could sustain ATP production by OXPHOS under hypoxia (Hayashi *et al.*, 2015). Higd2a has function in assembly and stabilization of supercomplexes containing COX, as its yeast homolog Rcf1 (Chen *et al.*, 2012).

SCAF1 (supercomplex assembly factor 1) (Cox7a2L, Cox7aR, SIG81), is another protein associating with COX, which may be located on peripheral part of COX. SCAF1 is supposed to enable COX to incorporate into supercomplexes (Ikeda *et al.*, 2013; Lapuente-Brun *et al.*, 2013; Cogliati *et al.*, 2016). Although, contradicting findings showed that SCAF1 has no role in supercomplexes assembly and that important component for supercomplexes formation is COX itself (Mourier *et al.*, 2014). Recently, model of SCAF1 function was published, which presumes its role in binding COX without Cox7a subunit and forming (stabilizing) the III_2IV supercomplex. This supercomplex would then interact with CI forming the $I_1III_2IV_1$ supercomplex (respirasome). Otherwise, COX containing Cox7a-2 is recruited by supercomplex I_1III_2 forming another population of supercomplexes (respirasomes) while Cox7a-1 containing COX was found only in COX dimers (see Figure 1.8) (Cogliati *et al.*, 2016; Letts and Sazanov, 2017; Milenkovic *et al.*, 2017).

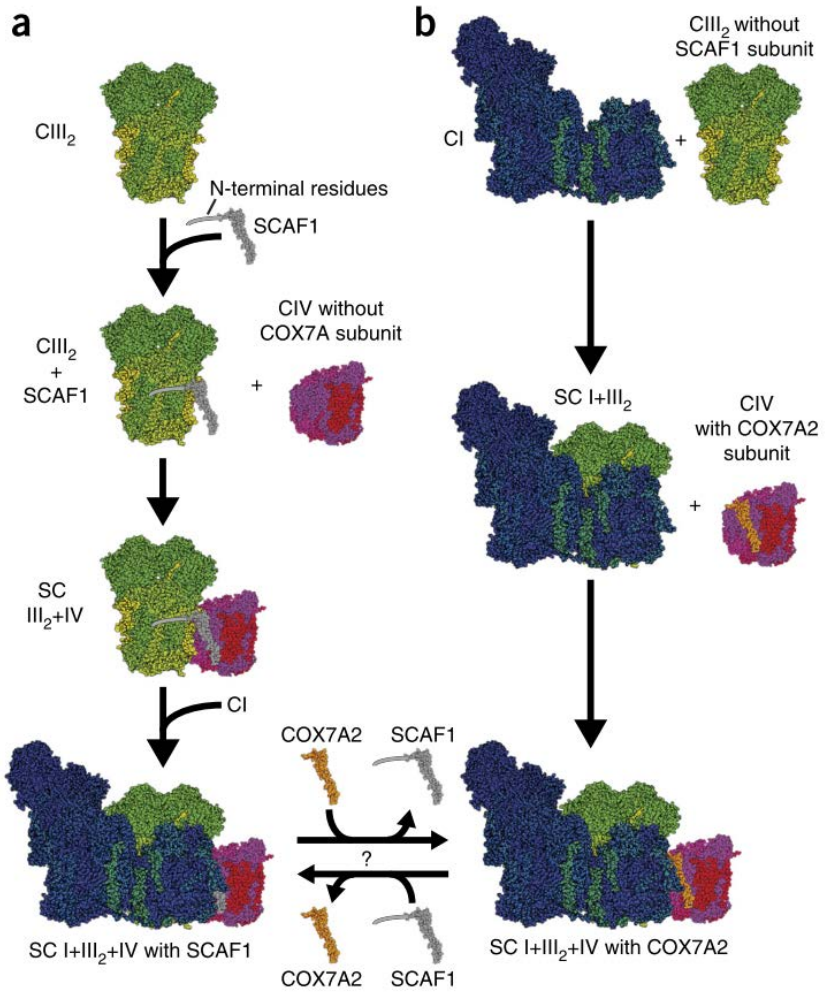

Figure 1.8: Role of SCAF1 in formation of supercomplexes (Letts and Sazanov, 2017).

1.4.6. Assembly of COX enzyme

COX is a multi-subunit enzyme and its proper assembly and stability is necessary for its function. Importance of assembly process is signified by mutations in assembly factor's genes, which lead to congenital defects of COX enzyme in human (Pecina *et al.*, 2004). Moreover, COX is encoded by both mitochondrial and nuclear genome, which requires crosstalk of many processes of subunits biogenesis (as described in Chapter 1.2.). Many cofactors are involved in this process and must be also strictly regulated (Fontanesi *et al.*, 2006). *Saccharomyces cerevisiae* studies uncovered dozens of nuclear-encoded assembly factors required for assembly of each intermediate during building of the enzyme (McEwen *et al.*, 1986; Tzagoloff and Dieckmann, 1990; Khalimonchuk and Rödel, 2005; Fontanesi *et al.*, 2006). Most of these factors were also found in higher eukaryotes, as assembly process seems to be conserved between yeast and human.

De novo COX assembly is a sequential process documented by many studies based on native polyacrylamide gel electrophoresis (as shown in Figure 1.9). Native electrophoresis enables observation of individual COX assembly intermediates, suggests that assembly process is regulated by rate-limiting steps (Nijtmans *et al.*, 1998; Durand *et al.*, 2017). Firstly, Cox1 subunit is synthesized and represents the first S1 intermediate. Cox1 is joined by Cox4 and Cox5a subunits, which are necessary for assembly, forming second intermediate S2 (Fornůsková *et al.*, 2010a). S3 intermediate already contains subunits Cox2, Cox3, Cox 5b, Cox6c, Cox7b, Cox7c, Cox8 (Williams *et al.*, 2004; Fornůsková *et al.*, 2010a). Then, Cox7a and Cox6b are added forming last S4* intermediate, and Cox6a addition results in COX holoenzyme (Fornůsková *et al.*, 2010a).

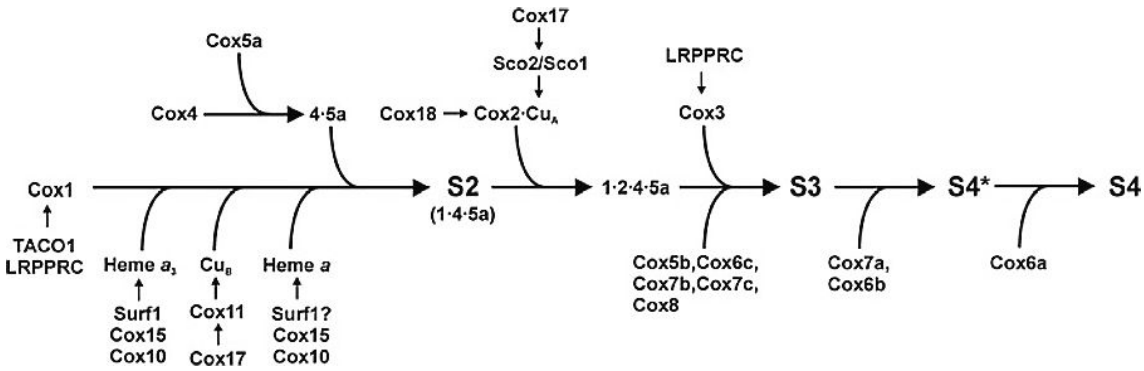

Figure 1.9: Scheme of COX assembly (Fornůsková *et al.*, 2010a).

Alternatively, COX assembly may be viewed as a linear process in which different modules, not subunits, are assembled together into functional enzyme (Timón-Gómez *et al.*, 2017; Vidoni *et al.*, 2017). In modular model, each module containing COX subunits with their assembly factors and chaperons represents assembly checkpoint (Timón-Gómez *et al.*, 2017). For example, in early assembly stage, formation and stability of Cox1 subunit associated with MITRAC complex (mitochondrial translation regulation assembly intermediate of COX) (Dennerlein and Rehling, 2015), is necessary for addition of Cox4-Cox5a sub-module (Mick *et al.*, 2012; Vidoni *et al.*, 2017). Further, COX biogenesis is regulated by assembly-controlled translational plasticity. It means that without nuclear-encoded subunits involved in early stages of COX biogenesis (Cox4), translation of Cox1 subunit is abolished. Then, Cox1 occurs to be present as a ribosome-nascent chain complex containing MITRAC component C12ORF62. Thus, new COX is not assembled and ribosomes may preferentially bind COX1 transcript (Richter-Dennerlein et al., 2016).

Beyond *de novo* assembly, direct incorporation of some nuclear-encoded subunits into holoenzyme, found in other OXPHOS complexes, is also possible in COX. Candidate proteins for this process are subunits involved in later intermediates of the *de novo* assembly, namely Cox6a, Cox6b and Cox7a, which may be incorporated into COX monomer or even COX assembled into supercomplexes (Lazarou *et al.*, 2009). Existence of conserved late state intermediate (LSI) complex, which contains Cox6a and Cox7a subunits with factors for incorporation, supports hypothesis of incorporation. Although, Cox4i1 and Cox6c were not incorporated into holoenzyme, they also form complexes with factors needed for their maturation. Surprisingly, in patients with defects of COX assembly, all these subunits (Cox6a, Cox6b, Cox7a, Cox4i1 and Cox6c) may incorporate into COX established in supercomplex $I_1III_2IV_1$ due to decreased level of these subunits (Lazarou *et al.*, 2009). Described mechanism of nuclear-encoded subunits incorporation into COX holoenzyme may be further applied for the exchange of isoform pairs of nuclear-encoded subunits during changing conditions.

1.5. Cox4 subunit

Cox4 is the largest of nuclear-encoded subunits of COX enzyme and its location nearby catalytic center of the enzyme predisposes it for regulatory function. In mammals, Cox4 subunit exists in two distinct isoforms, which are expressed in tissue-dependent and oxygen-dependent manner, and thus can play a significant role in modulation of COX activity in response to changing conditions. Moreover, Cox4 together with Cox6b are crucial for docking of cytochrome *c* on its binding site on subunit Cox2 (Sampson and Alleyne, 2001). Thus, Cox4 subunit represents possible tool for fine-tuning of COX enzyme and consequently the whole OXPHOS system.

1.5.1. Cox4 isoforms – genetic background and structure

Isoforms of Cox4 subunit were firstly described in yeast (Cox5a and Cox5b homologs of Cox4i1 and Cox4i2) and in tuna (Poyton *et al.*, 1996; Hüttemann, 2000). Later, they were also proved in mammals (human, rat and mouse) by molecular techniques (Hüttemann, Kadenbach and Grossman, 2001). Human isoforms of Cox4 subunit are encoded by different genes situated on different chromosomes (COX4i1 on chromosome 16, COX4i2 on chromosome 20). COX4i1, as well as COX4i2, sequence is approximately

8 kb long. Both genes are composed of five exons, and translational start codon lies in exon II. These similarities point to the likely origin through gene duplication (Hüttemann, Kadenbach and Grossman, 2001).

Cox4 subunit is composed of a transmembrane helix, cytosolic and matrix domain (each contain two helices). Transmembrane helix contacts helices of subunits Cox1, Cox7b and Cox8 (Tsukihara *et al.*, 1996). Comparison of precursor proteins of isoforms Cox4i2 (171 amino acids) and Cox4i1 (169 amino acids) revealed structural differences. N-terminal matrix domain of Cox4i2 contains conserved motive ALKEKEK, which is freely accessible from matrix. Compared to Cox4i1, Cox4i2 C-terminus has extra three positive charges. Moreover, Cox4i2 isoform has three cysteine residues (Cys40, Cys54, Cys108), which are not present in Cox4i1 isoform. Cys84 is not close enough to another cysteine residue and therefore formation of intramolecular disulphide bond is unlikely, but it is conserved across the species. To the contrary, in Cox4i1 isoform, this amino acid position is highly variable. Molecular modelling of human Cox4i2 revealed possible formation of disulphide bond between Cys40 and Cys54 by a small structural change in the loop region formed between these cysteines (Hüttemann, Kadenbach and Grossman, 2001). The most conserved region between isoforms is the transmembrane region contacting helices of Cox1 subunit.

1.5.2. Allosteric regulation

Cox 4 subunit contains ATP/ADP binding sites, which can sense energy status of the cell and therefore regulate activity of the enzyme according to current metabolic needs.

One of ATP/ADP binding sites was found in transmembrane domain. At high ATP/ADP ratio (ATP is bound), affinity of cytochrome c to COX is decreased and it leads to inhibition of enzyme activity (Napiwotzki and Kadenbach, 1998). Under high intra-mitochondrial ATP/ADP ratio, matrix domain also binds ATP, which leads to allosteric inhibition of enzyme activity (Arnold and Kadenbach, 1997). Allosteric ATP-inhibition depends on Cox1 phosphorylation of its cytosolic side by cAMP-dependent protein kinase A (PKA) (Bender and Kadenbach, 2000). One of presumable phosphorylation sites is Ser441 of Cox1 subunit, which is *in vitro* phosphorylated in the presence of cAMP and PKA (Lee, Bender and Kadenbach, 2002). *In vivo*, phosphorylation occurs on another epitope of Cox1 subunit while in presence of allosteric activator ADP leads to inhibition (Lee *et al.*, 2005). This mechanism of regulation, named as “the second mechanism of

respiratory control", is independent on mitochondrial membrane potential (Kadenbach and Arnold, 1999). It was proposed, that allosteric ATP-inhibition controls membrane potential, which is maintained at a low level and thus prevents ROS formation. Dephosphorylation by phosphatases abolishes this control, membrane potential increases, and so does the ROS production under the stress (Kadenbach *et al.*, 2004; Ramzan *et al.*, 2010; Kadenbach, Ramzan and Vogt, 2013). It was proved by site directed mutagenesis, that allosteric inhibition is abolished by Ser58 phosphorylation of Cox4i1 isoform on matrix side by mitochondrial PKA. Mitochondrial PKA is positively regulated by carbonate at the level of mitochondrial adenylate cyclase, while concentration of carbonate increases with elevated activity of Krebs cycle. Therefore, phosphorylation-induced increase of COX activity may regulate mitochondrial metabolic pathways according to energy requirements of mammalian cells (Acín-Pérez *et al.*, 2011).

1.5.3. Cox4 isoforms – expression and function

Cox4i1 isoform is expressed ubiquitously in all mammalian tissues while Cox4i2 isoform is expressed in tissue-dependent manner. Northern blot analysis of human RNA from different tissues confirmed significant expression of Cox4i2 isoform in adult and fetal lung and in fetal muscle. Consistent results were obtained by quantitative PCR of rat tissues, which pointed at the higher content of Cox4i2 in lung, heart and brain. Other tissues showed undetectable amounts of Cox4i2 isoform (Hüttemann, Kadenbach and Grossman, 2001). However, recent publication demonstrated constitutive expression of Cox4i2 isoform at the protein level also in human skeletal muscle (Schiffer *et al.*, 2016).

Minor Cox4i2 expression was also detected in mice cerebral neurons (Horvat, Beyer and Arnold, 2006). This study compared functionally different cerebral neurons with cortical astrocytes, which express only Cox4i1 isoform under normoxia. After cultivation in hypoxic chamber, both cell types showed increased expression of Cox4i2 isoform. Measurement of respiration revealed that if Cox4i2 transcript is present, allosteric ATP-inhibition under the high ATP/ADP ratio is abolished. Presumably, ATP is not bound on matrix domain of Cox4i2 isoform or the conformational changes are not relayed to the catalytic core of the enzyme. This is possibly caused by different structure of Cox4i2 isoform, which can form the above-mentioned disulphide bond. Moreover, differences in C-terminus in intermembrane space may alter binding of cytochrome c and therefore activity of the enzyme (Hüttemann, Kadenbach and Grossman, 2001; Horvat, Beyer and

Arnold, 2006). Authors propose role of COX as an oxygen sensor which enables astrocytes to use anaerobic metabolism (glycolysis) under the hypoxia while neurons, requiring a lot of energy, try to compensate limited availability of energetic substrates at the expense of vulnerability (Horvat, Beyer and Arnold, 2006). Consistently, another study showed increased Cox4i2 expression and decrease of Cox4i1 in striatal astrocytes after cultivation with 3-nitropropionic acid (mitochondrial toxin, *in vitro* model of Huntington's disease). Therefore, induction of Cox4i2 transcription under hypoxia, but also after toxin treatments was proposed. The same pattern was observed in abolished allosteric ATP-inhibition with higher transcription level of Cox4i2 isoform in striatal astrocytes (Singh *et al.*, 2009).

Another research group reported contradictory results which do not indicate abolishment of allosteric ATP-inhibition in Cox4i2 isozyme in bovine lung. Authors compared COX isolated from bovine lung containing approximately the same amount of Cox4i1 and Cox4i2 isoform and liver containing only Cox4i1 isoform. Activity of COX enzyme was two-fold decreased in liver compared to lung enzyme (Hüttemann, Lee, *et al.*, 2012). The same results were obtained by studying Cox4i2-KO mouse models, where the activity of COX enzyme from lung and the level of cellular ATP, was significantly decreased against WT mouse. Allosteric ATP-inhibition was observed in both KO and WT mouse. COX4i2 KO mouse had pathological symptoms of lung deteriorating with age including accumulation of Charcot-Leyden crystals. Thus, Cox4i2 isoform is necessary for physiological lung function. Authors proposed OXPHOS as a therapeutic target for lung pathologies such as asthma (Hüttemann, Lee, *et al.*, 2012).

Although, in some studies higher enzymatic turnover of Cox4i2 containing COX was found (Fukuda *et al.*, 2007; Hüttemann, Lee, *et al.*, 2012), another study obtained opposite results and the question, which isozyme is more active, became controversial (Oliva *et al.*, 2015). Authors of that study have found, that expression of Cox4i1 isoform is increased in human gliomas as an effect of epigenetic gene silencer BMI1 (which is overexpressed in various human tumors). Their cooperative regulation has more deleterious effect on prognosis of patients compared to patients with Cox4i2 isoform. Cox4i1 containing enzyme had significantly higher activity than enzyme containing Cox4i2 isoform. Authors are explaining controversial data by the differences in used models, using mitochondrial fraction for measurement against solubilized enzyme and by variable content of supercomplexes (Oliva *et al.*, 2015).

Physiological significance of Cox4i2 isoform was also shown in human PASMCs (pulmonary artery smooth muscle cells), where Cox4i2 is necessary for acute oxygen sensing. Under hypoxia, Cox4i2 isoform is responsible for hyperpolarization of PASMCs mitochondria by increasing of superoxide content which leads to increase of intracellular calcium and hypoxic pulmonary vasoconstriction (HPV) (Sommer *et al.*, 2017). However, hyperpolarization is not caused by increased COX activity due to Cox4i2 isoform, as was suggested in other studies. PASMCs WT compared with Cox4i2 KO did not show increased respiration (Sommer *et al.*, 2017).

As different models are used in studies mentioned above, it is hard to hypothesize, which Cox4 isoform associates with higher COX activity. Moreover, different ratio of isoforms content in various tissues may distort direct evidence for COX isozymes kinetics. Therefore, study based on cellular model may represent the only objective solution of this controversy.

Moreover, recent publication presents novel human mutation in COX4i1 gene (K101N) affecting conserved Lys residue localized in transmembrane helix domain in a patient with Fanconi anemia. K101N mutation caused decrease in COX activity, ATP production and increase in ROS production. Cox4i1 protein was undetectable in patient's fibroblasts, while CI and CII were not affected (Abu-Libdeh *et al.*, 2017).

1.5.4. Cox4 isoforms – regulation of expression under hypoxia

Increased expression of Cox4i2 isoform under hypoxia was detected in many mammalian cells. Specifically in rat pulmonary smooth muscle cells, HEK 293 cells (Aras *et al.*, 2013), in mice astrocytes (Horvat, Beyer and Arnold, 2006), in human lung cells H460 (Hüttemann *et al.*, 2007), in human HeLa, Hep3B, Hct116 and A594 cells (Fukuda *et al.*, 2007). There is a hypothesis, that the switch in isoform expression is putatively managed by signaling pathway dependent on partial pressure of oxygen in the cell. Two possible mechanisms proposed in literature are illustrated in Figure 1.10, but it is not fully clarified yet, which factors are responsible for regulation of this mechanism.

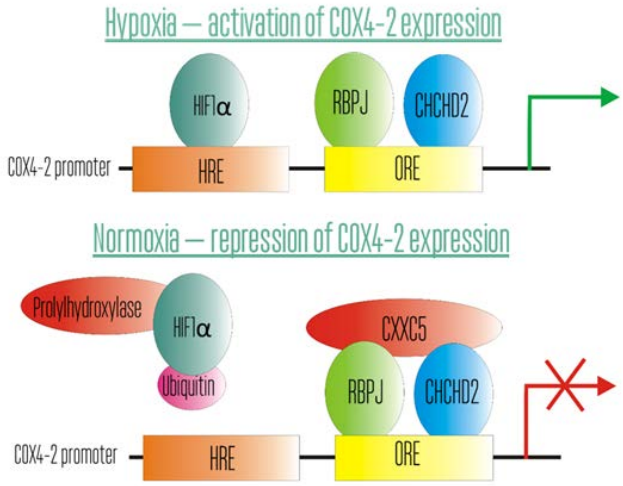

Figure 1.10: Regulation of Cox4i2 isoform expression under the hypoxia.

First hypothesis proposed that expression of Cox4 isoforms in mammals is regulated under the hypoxia by hypoxia inducible factor-1, HIF-1 (Fukuda *et al.*, 2007). HIF-1 is a transcription activator which regulates oxygen homeostasis in animals. Under hypoxia, HIF-1 activates genes of glycolytic pathway and supports anaerobic ATP production (Seagroves *et al.*, 2001). In human Cox4i2 gene promoter HIF-1 targeted consensus sequences - HREs (hypoxia-response elements), HRE1 on 5'end and HRE2 in intron 1, were identified. Therefore, HIF-1 can bind these sequences and activate transcription of Cox4i2 isoform under hypoxia. Simultaneously, HIF-1-dependent degradation of Cox4i1 isoform by mitochondrial LON protease is proposed, as HIF-1 also induces LON expression (Fukuda *et al.*, 2007). Moreover, increase of Cox4i2 isoform during HIF-1 signaling was found in heart of acclimated rat and it was coupled to LON upregulation (Alexander-Shani *et al.*, 2017).

Concurrently, another research group discovered 24-bp conserved sequence (ORE - oxygen responsive element, 13-bp) in proximal promoter sequence of Cox4i2 gene in mouse, rat, beef and human (Hüttemann *et al.*, 2007). Analysis of human promoter also revealed three Sp1-like elements ($Sp1_A$, $Sp1_B$, $Sp1_C$) necessary for maximal promoter activity, whereas one of them ($Sp1_A$) is in conserved region (Hüttemann *et al.*, 2007).

Later, candidate factors binding ORE (OREFs) were found by electrophoretic mobility shift assay (EMSA) in HEK293 cells. As activators of transcription were identified RBPJ (recombination signal sequence binding protein J_κ), whose main role is in evolutionarily conserved NOTCH signaling pathway, and CHCHD2 (coiled-coil-helix-coiled-coil-helix domain 2, alternatively MNRR1), whose gene is co-expressed with other OXPHOS

genes. These factors (RBPJ, CHCHD2) together allow hypoxic activation of Cox4i2 promoter. Knockdown of RBPJ (HEK293-RBPJ-KD) decreases hypoxic answer mediated by CHCHD2 factor, therefore both are necessary for optimal regulation of promoter. CXXC5 (CXXC finger protein 5) was found to repress transcription of Cox4i2 gene, mainly under normoxia. That suggests negative regulation of ORE by this factor. Interactions between RBPJ-CXXC5 and RBPJ-CHCHD2 were showed by co-immunoprecipitation. Meanwhile, this regulation is not dependent on HIF-1α. If CHCHD2 is overexpressed, it suppresses the repression by CXXC5 factor. The greatest increase of CHCHD2 mRNA and protein was shown at 4% oxygen concentration, when COX4i2 promoter is also maximally active (Aras *et al.*, 2013). MNRR1 overexpression in HEK293 cells showed increased expression of endogenous, but also transfected MNRR1 gene. This suggests self-activation of MNRR1 expression (Aras et al. 2015). Consistent results were obtained by experiments with primary lung cells from rat with endogenous expression of Cox4i2 isoform (Aras *et al.*, 2013).

Other study showed screen of mRNA expression (qPCR) of nuclear-encoded genes in mice embryonal fibroblasts (MEFs). It compared expression of HIF1-α-WT and HIF1-α-KO cells under hypoxia (1% oxygen concentration) and under control conditions. Cox4i2 had higher expression under hypoxia in HIF1-α-KO cells compared to HIF1-α-WT cells (Hwang *et al.*, 2015). These data suggest that HIF-1 is not the main factor regulating hypoxic expression of Cox4i2. Another disproof of HIF-1 hypoxic regulation of Cox4 isoforms expression may be the measurement of reporter gene activity with Cox4i2 promoter in H460 cells under different conditions (oxygen concentration range from anoxia to normoxia). The highest activity was determined at 4% oxygen concentration, while the highest activity of HRE reporter corresponds to anoxia (see Figure 1.11). Thus, HIF-1 regulation may not be relevant under physiological conditions but it can still be applicable under pathological conditions (Hüttemann *et al.*, 2007).

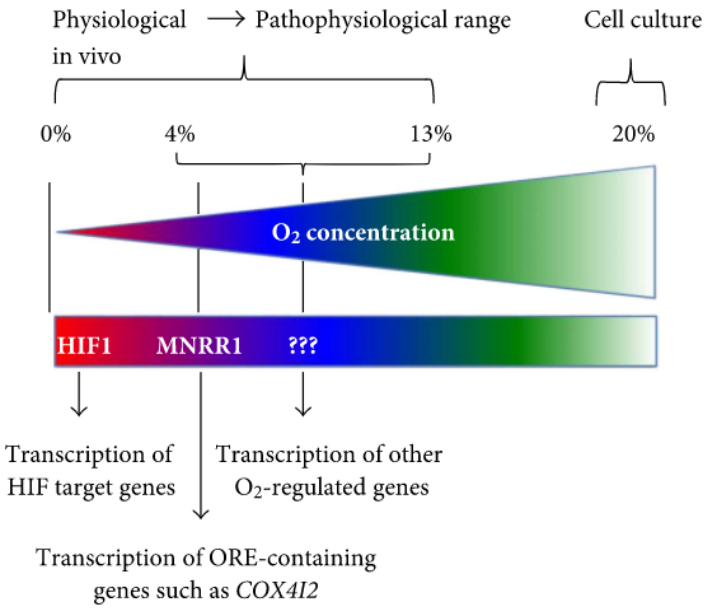

Figure 1.11: HIF1 vs MNRR1 regulation (Grossman *et al.*, 2017).

1.5.5. Evolution of oxygen sensitivity

Prokaryotes have ability of adaptation to the environment by their diverse metabolic pathways. They are able to use one of various terminal oxidases according to the current situation and thus regulate effectivity of OXPHOS under normoxia or hypoxia. Similar mechanism of regulation by oxygen concentration is also present in plants, which are using alternative terminal oxidases (AOX). The main function of AOX is prevention of excessive reduction of ubiquinone pool under hypoxia (as a terminal acceptor of electrons), thereby protection against ROS formation (Gupta, Zabalza and Dongen, 2009). AOX were found in some animal phyla (*Cnidaria, Annelida, Mollusca, Nematoda, Chordata*), which suggests potential role of AOX in evolution of electron-transport chain (McDonald et al. 2009). As no AOX was identified in vertebrates, its secondary loss was proposed (McDonald, Vanlerberghe and Staples, 2009). Presumably, secondary loss was accompanied by whole genome duplication and by origin of isoform pairs of nuclear-encoded subunits, including Cox4 subunit isoforms (Little *et al.*, 2010). Expression of Cox4 subunit isoforms has similar effect on the cell as expression of AOX, it is an alternative way to decrease ROS production under hypoxia (Fukuda *et al.*, 2007).

Saccharomyces cerevisiae, which has pair of isoforms of Cox5 subunit (Cox5a and Cox5b) that is homologous to Cox4 subunit in mammals, also lost AOX (McDonald, Vanlerberghe and Staples, 2009). Interestingly, presence of these isoform pairs is a result of convergent evolution, because gene duplication occurred independently in both

lineages, as indicated by low homology of promoters and amino acid sequences (Pierron *et al.*, 2012). Moreover, "hypoxic" isoform is constantly expressed in highly oxygenated lung tissue in mammals, which suggests primary adaptation of this isoform to the environment with high oxygen concentration (Hüttemann *et al.*, 2007). To the contrary, yeast's hypoxic isoform is expressed exclusively after induction by hypoxia (Kwast, Burke and Poyton, 1998).

On the other hand, studies of fish, reptiles and amphibians showed no evidence of Cox4 isoforms expression dependence on oxygen availability (see Figure 1.12). Thus, subfunctionalization of Cox4 isoforms differs between mammals and these taxa, while Cox4 isoforms genes are orthologous among vertebrates (Porplycia *et al.*, 2017). Moreover, cysteine residues found in mammalian Cox4i2 isoform are specific for that lineage and are not present in fish Cox4i2 (Kocha *et al.*, 2014). Interestingly, fish Cox4i2 isoform enriched red muscle showed increased COX activity versus Cox4i1 enriched gill (Porplycia *et al.*, 2017).

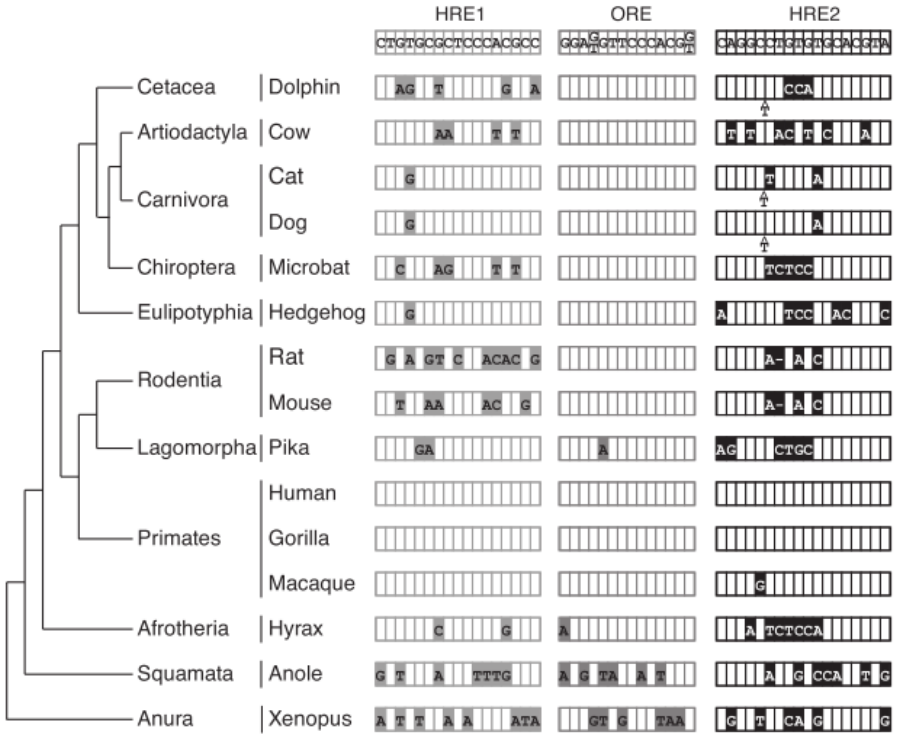

Figure 1.12: Conservation of Cox4i2 elements across vertebrates (Kocha *et al.*, 2014). Alignment of Cox4i2 promotor sequences depicting changes in nucleotide sequences during vertebrate evolution. Empty boxes indicate identical base pairs as in human sequence.

2. Aims of the study

The overall aim of the present thesis was preparation of unique HEK293 cell line-based knock-out models for COX4i1, COX4i2 and COX4i1/4i2 double knockout and their functional characterisation. The COX4i1/4i2 KO model established in this study will later be utilized for knock-in of either Cox4i1 or Cox4i2 isoform to clarify functional differences between Cox4i1 or Cox4i2 isoform containing enzyme.

The specific aims of the thesis were:

1. To prepare HEK293 cell line-based COX4i1, COX4i2 and COX4i1/4i2 knock-out (KO) models by CRISPR technology
2. To characterize the impact of Cox4 isoforms knock-outs on biogenesis and function of COX
3. To examine the consequences of COX4 knock-out on other OXPHOS enzyme complexes

3. Materials and methods

3.1. Materials

3.1.1. List of chemicals

L-methionine	Sigma-Aldrich (USA)
L-cysteine	Calbiochem (USA)
Anisomycin	Sigma-Aldrich (USA)
EXPRE35S35S Protein Labeling Mix	Perkin Elmer (USA)
6-Aminocaproic acid	Sigma-Aldrich (USA)
ADP	Sigma-Aldrich (USA)
Agarose	Sigma-Aldrich (USA)
Acrylamide	SERVA (Germany)
Ammonium peroxodisulphate	Bio-Rad (USA)
Ascorbate	Sigma-Aldrich (USA)
Ampicillin	Sigma-Aldrich (USA)
Bradford reagents	Bio-Rad (USA)
Bis-Tris	Sigma-Aldrich (USA)
BSA (bovine serum albumin)	Sigma-Aldrich (USA)
Coomassie Brilliant Blue R-250	SERVA (Germany)
Coomassie Brilliant Blue G-250	SERVA (Germany)
Digitonin	Sigma-Aldrich (USA)
DMM	Sigma-Aldrich (USA)
DMSO	Sigma-Aldrich (USA)
DMEM-M-C (Cat. n. 21013024)	Thermo Fisher Scientific (USA)
DMEM + GlutaMaxTM (Cat. n. 31966-021)	Thermo Fisher Scientific (USA)
DMEM/F12 + GlutamaxTM (Cat. n. 31331-028)	Thermo Fisher Scientific (USA)
EDTA	Sigma-Aldrich (USA)
EGTA	Sigma-Aldrich (USA)
Ethanol	Penta (Czech Republic)
FBS (fetal bovine serum)	Thermo Fisher Scientific (USA)
FCCP	Sigma-Aldrich (USA)
FluoroBrite DMEM Media	Thermo Fisher Scientific (USA)
Glucose	Sigma-Aldrich (USA)
Hoechst 3342	Thermo Fisher Scientific (USA)
Sodium glutamate	Sigma-Aldrich (USA)
Glycerol	Sigma-Aldrich (USA)
HEPES	Sigma-Aldrich (USA)
Chloroform	Sigma-Aldrich (USA)
Imidazole	Sigma-Aldrich (USA)
IPTG	Sigma-Aldrich (USA)
Isopropanol	Sigma-Aldrich (USA)
Kanamycin	Sigma-Aldrich (USA)
KCN	Sigma-Aldrich (USA)
poly-L-lysine	Sigma-Aldrich (USA)

Malonate	Sigma-Aldrich (USA)
2-Mercaptoethanol	Sigma-Aldrich (USA)
METAFECTENE PRO	Biontex (Germany)
Methanol	Penta (Czech Republic)
Myxothiazol	Sigma-Aldrich (USA)
NativeMark Unstained Protein Standard	Themo Fisher Scientific
Laktino dry milk	ARTIFEX Instant (Czech Republic)
LB Agar	Thermo Fisher Scientific (USA)
LB broth	Affymetrix (USA)
N,N'-Methylenebisacrylamide	SERVA (Germany)
Oligomycin	Sigma-Aldrich (USA)
PageRulerTM Prestained Protein Ladder	Thermo Fisher Scientific (USA)
Penicillin/streptomycin	Sigma-Aldrich (USA)
Poly-L-lysine	Sigma-Aldrich (USA)
Ponceau S	Sigma-Aldrich (USA)
PPP Master mix	Top-Bio (Czech Republic)
Protease Inhibitor Cocktail P8340	Sigma-Aldrich (USA)
Proteinase K	Roche (Switzerland)
Puromycin	Sigma-Aldrich (USA)
RNaseZap	Sigma-Aldrich (USA)
Rotenone	Sigma-Aldrich (USA)
SDS	SERVA (Germany)
Serva Blue G	SERVA (Germany)
Sodium malate	Sigma-Aldrich (USA)
Sodium succinate	Sigma-Aldrich (USA)
TEMED	SERVA (Germany)
TMPD	Sigma-Aldrich (USA)
Tris	Sigma-Aldrich (USA)
Tricine	Sigma-Aldrich (USA)
TRIzol reagent	Thermo Fisher Scientific (USA)
Trypsin	Sigma-Aldrich (USA)
Tween-20	Sigma-Aldrich (USA)
X-Gal	Sigma-Aldrich (USA)

3.1.2. List of kits

DNA-free DNA Removal Kit	Thermo Fisher Scientific (USA)
EndoFree Plasmid Maxi Kit	QIAGEN (USA)
QIAamp DNA mini kit	QIAGEN (USA)
QIAprep Spin Miniprep Kit	QIAGEN (USA)
QIAquick PCR Purification kit	QIAGEN (USA)
pGEM-T Easy Vector System	Promega Corporation (USA)
SCRIPT cDNA Synthesis kit	Jena Bioscience (Germany)
SURVEYOR Mutation Detection Kit	Integrated DNA Technologies (USA)

3.2. Methods

3.2.1. Cultivation of HEK293 cells

As a cellular model, HEK293 (human embryonic kidney) cell line was chosen for preparation of COX4i1 and COX4i2 knock-out clones. Cells were initially cultivated in DMEM medium (Dulbecco's Modified Eagles Medium) + GlutaMax™ supplemented with 10% (v/v) FBS, 20 mM HEPES and antibiotics (penicillin (10 U/mL) and streptomycin (10 μg/mL)). After construction of COX4 knock-out cellular models, cultivation was switched into more nutrient-rich DMEM/F-12 + GlutaMax™, concentration of HEPES buffer was doubled to 40 mM, and additional nutrient supplement, 50 μM uridine, was used to facilitate growth of highly glycolytic knock-out cells. Cultivation went on 100 cm^2 (Ø 10 cm) cultivation dishes (TPP) in 12 mL of medium, at 37 °C and 5% CO_2 atmosphere.

Cell passage was performed at 80-100% confluence of the cells in sterile laminar box. As a first step, medium was removed and 5 mL of room tempered PBS (phosphate buffer saline, 140 mM NaCl, 5 mM KCl, 8 mM Na_2HPO_4, 1,5 mM KH_2PO_4, pH 7,2 – 7,3) was added to wash away medium traces. Thereafter, 1,5 mL of T+E (0,05% trypsin + 0,02% EDTA in PBS) warmed to 37 °C was added for 3-5 minutes for dissociation of attached cells from the dish bottom. Then, 5 mL of cultivation medium was added for trypsin inhibition and cells were seeded in requested dilution on a new dish with medium.

Harvesting of cells for biochemical analyses proceeded on ice (4 °C), out of sterile laminar box. Medium was removed, dish was washed with 5 mL of PBS and then 1,5 mL of T+E was added for trypsinization (3-5 minutes). Later, medium was added to final volume 10 mL and homogenous cellular suspension was transferred into 15 mL sterile tube. Cells were centrifuged for 5 minutes at 300 g using Sigma 3-K18 centrifuge (Sigma Laborzentrifugen GmbH, Germany) with rotors SIGMA 11 133 or 12 131. Pellet was resuspended in a small volume of PBS and after addition of PBS to final volume of 10 mL, cells were centrifuged again at the same conditions as in the first centrifugation step. After second PBS washing step, cellular pellet was either frozen for later analyses or resuspended in 150-300 μL of PBS for respiration measurements.

3.2.2. Preparation of HEK293 cellular knock-out models

COX4i1 and COX4i2 gene knock-out was introduced into HEK293 cells by CRISPR knock-out technology (Ran *et al.*, 2014). System of Cas9-D10A paired nickase with two chimeric RNA duplexes was used for its higher specificity for targeted sequence thanks to recognition of two different gRNAs by two endonucleases, which work simultaneously (represented in Figure 3.1). Cas9 endonuclease modified by one amino acid substitution (D10A) has inhibited nuclease activity and activated nickase activity. Thus, after recognition of targeted sequence by gRNAs (one gRNA recognises sense strand of DNA, second recognises antisense strand), two Cas9-D10A nickases are activated by binding of gRNA and it leads to single strand breaks (nicks) in targeted sequence. Resulting 5‘-end overhangs on both strands are mostly repaired by non-homologous end joining, which most often leads to insertion/deletion mutations.

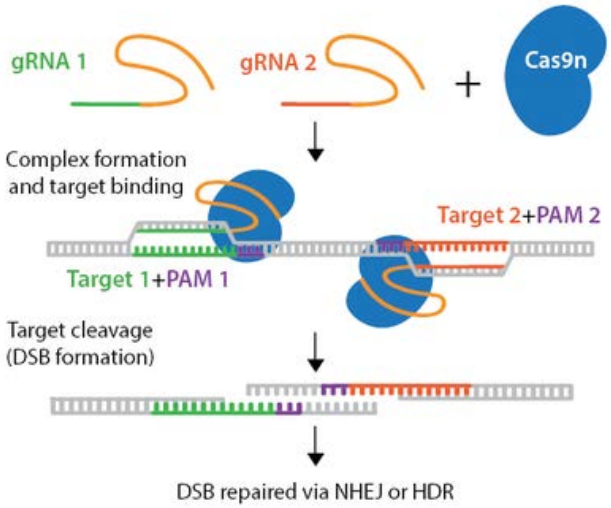

Figure 3.1: Knock-out mechanism of Cas9-D10A paired nickase (Cas9n). Pair of gRNAs is recognized by two Cas9n and target specific sequence. Then, two single strand nicks are proceeded by Cas9n, which lead to non-homologous end joining (Addgene, 2018).

Commercial library of gRNAs targeting human genes (Sigma-Aldrich, USA) was used for choosing gRNAs for COX4i1 and COX4i2 knock-out preparation. Chosen gRNAs (listed in Table 3.1) were received in form of expression plasmid (U6-gRNA, expressed by U6 promoter), along with expression plasmid for Cas9-D10A nickase fused with GFP (Sigma-Aldrich, USA). All the plasmids contain kanamycin resistance gene, thus selection of transformed bacteria can be performed using selection LB agar plate with kanamycin.

Target gene	gRNA	gRNA ID	Target Exon	gRNA sequence
COX4i1	1	HSL0001377215	3	ACGCCGATCCATATAAGCTGGG
COX4i1	2	HSL0001377220	3	GGCCACCTCCGGCAAGGGGTGG
COX4i1	3	HSR0001377224	3	CACCTGTCTGCCAGCCAGAAGG
COX4i1	4	HSR0001377226	3	GCCAGCCAGAAGGCATTGAAGG
COX4i2	5	HSR0002687616	2	AAGGTGGAGGTGGAAGACGAGG
COX4i2	6	HSR0002687617	2	AGGTGGAGGTGGAAGACGAGGG
COX4i2	7	HSL0002687619	2	CAAGCTCCAGGCAGCTCTGGGG
COX4i2	8	HSL0002687620	2	ACCAAGCTCCAGGCAGCTCTGG

Table 3.1: List of gRNA sequences tested for efficiency of mutagenesis.

Received plasmids were amplified in competent DH5α *Escherichia coli* strain (Thermofisher, USA). 1 µL of plasmid DNA (1 ng) was mixed with 50 µL of *E. coli* culture in 1,5 mL sterile tubes on ice. After 30 min incubation on ice, 20 s heat shock in 42 °C bath was performed to transform bacteria. Then, cells were cooled on ice for 2 min, suspended in 950 µL of preheated LB broth incubated for 1 hour at constant shaking (225 rpm) on shake pad at 37 °C. Afterwards, aliquots of bacterial cultures were streaked onto selection 1,5% LB agar plate with kanamycin (50 µg/mL) and incubated at 37 °C overnight.

Single cell colonies were picked out of the plate and inoculated into 3 mL of LB broth with kanamycin (50 µg/mL). Starter cultures were incubated for 8 hours at 300 rpm, 37 °C. Then, 200 µL of culture was inoculated into 100 mL of selection LB broth and incubated for 14 hours at 300 rpm at 37 °C. After incubation, grown bacterial cultures were centrifuged at 6000 g/4 °C for 15 min. Bacterial pellets were used for plasmid isolation using EndoFree Plasmid Maxi Kit (QIAGEN, USA) according to manufacturer's manual. Plasmid DNA concentration was measured at wavelength 260 nm using NanoDrop Spectrophotometer ND-1000 (Thermofisher, USA).

Isolated plasmids were transfected into HEK293 cells using METAFECTENE PRO reagent (Biontex, Germany), which forms liposomes around plasmid DNA, thus allowing plasmid entry into the cell. At first, working solutions (500 ng/µL DNA) of plasmid stocks were prepared. Mixture of 44 µL of DMEM medium with 2 µL (1 µg DNA) of each sense gRNA, antisense gRNA and Cas9n plasmids was prepared in 500 µL tube. Then, second

solution containing 6 µL of METAFECTENE PRO in 44 µL DMEM was prepared. Solution of METAFECTEN PRO was immediately added into plasmid DNA solution, thus liposomes could be formed. Transfection solution was incubated at room temperature for 20 min. After incubation, HEK293 cells grown at 70 % confluency on 12-well plates (in 1 mL of complete DMEM medium without antibiotics) chosen for transfection were dropped by transfection solution. Plate was then incubated in thermostat at 37 °C and 5 % CO_2 atmosphere. After 4 hours, medium with transfection solution was removed and replaced by complete DMEM medium with antibiotics (penicillin and streptomycin).

Preparation of knock-out HEK293 clones was preceded by selection of the most efficient gRNAs pair. For this purpose, cells were transfected with all possible plasmid combinations (COX4i1 gene gRNAs: 1+2, 1+4, 3+2, 3+4). Cells were harvested after 72 hours after transfection for detection of mutagenesis efficiency of different gRNAs pairs by SURVEYOR Mutation Detection Kit (Integrated DNA Technologies, USA). The requirement of this method is formation of heteroduplexes between mutated and wild-type sequences amplified from the gRNA-targeted locus. These mismatches are non-specifically recognized and cleaved by Surveyor nuclease. Efficient mutagenesis is detected by agarose gel electrophoresis displaying pattern of multiple bands representing heterogeneously modified sequences, instead of single amplicon band in case of non-mutated sample. At first, DNA was isolated from HEK293 cellular pellets by QIAamp DNA mini kit (QIAGEN, USA) according to manufacturer's protocol. Concentration of isolated DNA was measured by NanoDrop. Samples were diluted on concentration 100 ng/µL in PCR clean water. Then, relevant sequences of COX4i1 and COX4i2 genes were amplified using PPP Master Mix (Top-Bio, s.r.o., Czech Republic). Methodology is described in Chapter 3.2.3. Primers used for that purpose are shown in Figure 3.2. PCR product was purified by QIAquick PCR Purification Kit (QIAGEN, USA) and concentration was measured by NanoDrop. Sample was diluted in PCR clean water to 50 ng/µL. SURVEYOR analysis was then performed according to manufacturer's manual. Eppendorf MasterCycler Gradient (Eppendorf, Germany) was used for hybridization. After this procedure, samples were analysed using 1,5% agarose gel electrophoresis.

COX4i1 primers (exon 3)

NCBI Gene ID: 1327

PCR product length: 423 bp

Forward primer: $_{5231}$TAAACAGTGGCTGTGACCCC$_{5250}$

Reverse primer: $_{5653}$AACCCTCCTGTGCAAGACTG$_{5634}$

Annealing temperature: 61 °C

COX4i2 primers (exon 2)

NCBI Gene ID: 84701

PCR product length: 511 bp

Forward primer: $_{1013}$GAAGGGTCAAGGGCATGAGG$_{1032}$

Reverse primer: $_{1523}$TCAGCATCCTCCACCTCAGA$_{1504}$

Annealing temperature: 60 °C

Figure 3.2: Primers used for PCR amplification of COX4i1 gene's exon 3 sequence or COX4i2 gene's exon 2 sequence. Numbers represent position of nucleotide in whole-gene sequence.

After choosing of the most efficient pair of gRNAs, HEK293 cells were transfected by relevant plasmids, incubated for 72 hours and then trypsinized, counted by Scepter counter (Millipore, USA) and diluted to concentration of 20 cells/mL. This suspension was aliquoted by 100 μL onto 96-well plates. Wells containing single cell colonies were identified and further cultivated. Confluent cells in 6-well plates were harvested and used for selection of mutant clones by sequencing or SDS-PAGE.

3.2.3. Polymerase chain reaction

For purpose of sample preparation for sequencing of COX4 KO clones, amplification of targeted sequences was performed using PPP Master Mix (Top-Bio, s.r.o., Czech Republic). Reagents of reaction are shown in Table 3.2. Primers, represented in Figure 3.3, were obtained from Generi Biotech s.r.o. (Czech Republic).

Reagent	Volume (µL)	Stock concentration
PPP Master Mix	12.5	-
Forward primer	1	1 µM
Reverse primer	1	1 µM
Template DNA	1	20 ng/µL
PCR H2O	9.5	-

Table 3.2: PPP Master Mix reagents are shown in the table. Final volume of a reaction is 25 µL

COX4i1 primers (exon 3)

PCR product length: 850 bp

Forward primer 1: $_{5103}$TTAATGTAGGAAGTGCTGCCTCTG$_{5126}$
Reverse primer 1: $_{5952}$AGTTCGCTTCAGGTGCAAAT$_{5933}$

Annealing temperature: 58 °C

PCR product length: 821 bp

Forward primer 2: $_{5138}$CCCAGGGTTCATTAGCAGTT$_{5157}$

Reverse primer 2: $_{5958}$GCATACAGTTCGCTTCAGGT$_{5939}$

Annealing temperature: 58 °C

COX4i2 primers (exon 2)

PCR product length: 511 bp

Forward primer: $_{1013}$GAAGGGTCAAGGGCATGAGG$_{1032}$

Reverse primer: $_{1523}$TCAGCATCCTCCACCTCAGA$_{1504}$

Annealing temperature: 60 °C

Figure 3.3: Primers used for PCR and sequencing of COX4i1 gene's exon 3 sequence or COX4i2 gene's exon 2 sequence. Numbers represent position of nucleotide in whole-gene sequence.

All reagents (except template DNA) of reaction were pipetted on ice in sterile flow box. After addition of template DNA, reaction in 0,2 mL PCR tube was gently mixed and centrifuged. Then, PCR reaction was initiated on cycler Eppendorf MasterCycler Gradient (Eppendorf, Germany) according to the protocol shown in Table 3.3.

	Temperature	Time	Number of cycles
Initial denaturation	94 °C	1 min	1
Denaturation	94 °C	15 s	35
Annealing	*	15 s	
Extension	72 °C	1 min	
Final extension	72 °C	7 min	1
Cooling	22 °C	-	-

Table 3.3: In the table, PCR cycles protocol is represented. *Annealing temperature vary according to primers used in the reaction. Temperatures are given in Figure 3.3.

Thanks to properties of PPP Master mix, PCR product can be directly loaded into agarose gel for electrophoresis without mixing with loading buffer. After electrophoresis, PCR product was purified by QIAquick PCR Purification Kit (QIAGEN, USA).

3.2.4. Agarose electrophoresis

Agarose electrophoresis was used to detect PCR product quality and size. Agarose gel contained 1% or 1,5% agarose in TBE Buffer (Tris-borate-EDTA, 89 mM Tris-borate and 2 mM EDTA, pH 8.3) according to the size of separated sequences. Constant voltage employed in electrophoresis was 5–10 V/cm.

3.2.5. TA cloning

Method of TA cloning was performed to reveal different allelic variants of COX4i1 gene, because sequencing of multiple overlapping sequences gave undecipherable results.

First day, PCR (PPP master mix) of isolated DNA samples (QIAamp DNA mini kit, QIAGEN, USA) was performed with Taq Purple DNA polymerase, which produces PCR products with adenine added on the 5' terminal end of the sequence (method is described in Chapter 3.2.3.). After that, PCR product was purified by QIAquick PCR Purification Kit (QIAGEN, USA), checked by agarose electrophoresis (Chapter 3.2.4.), and concentration of sample was measured by NanoDrop Spectrophotometer ND-1000 (Thermofisher, USA). Also, plates enabling blue/white selection (selection LB agar plates with 100 μg/mL ampicillin, 0,5 mM IPTG and 80 μg/mL X-Gal) and LB broth solution were prepared for bacteria cultivation.

Second day, ligation of PCR product into plasmid with 3' end thymine overhang was performed employing pGEM -T Easy Vector System (Promega Corporation, USA). Template to vector ratio was 5:1 and procedure was done by manufacturer's manual. After ligation, JM109 Competent cells (provided within the kit) were transformed according to manufacturer's protocol, which was modified by decrease of used volume of competent cells to 25 μL and SOC medium (2% tryptone, 0.5% yeast extract, 10 mM NaCl, 2.5 mM KCl, 10 mM $MgCl_2$, 10 mM $MgSO_4$, and 20 mM glucose) to 475 μL. Transformation allows each bacteria cell to gain only one of the various plasmids from the mix of plasmids with different inserts, therefore only one allelic variant. Then, 70 μL of transformed culture was plated on blue/white selection LB plate.

Third day, thanks to blue/white selection, transformed (white) single cell bacterial colonies were picked out of the plate and starter culture was prepared by adding pipette tip with picked bacterial colony into 14 mL Falcon Round-Bottom Polystyrene Tubes (Thermofisher, USA) filled by 6 mL of LB broth with ampicillin (final concentration 100 μg/ml). Starter culture was incubated at constant shaking at 37 °C overnight.

Fourth day, grown starter culture was centrifuged (10 000 g/10 min/4 °C) and obtained bacterial pellet was further used for isolation of amplified plasmid using QIAprep Spin Miniprep Kit (QIAGEN, USA). Isolated plasmid was restricted by restriction enzyme Eco RI (Fermentas, Thermo Fisher Scientific, USA), thus inserted sequence was released out of the plasmid, as depicted in Figure 3.4. Prepared reaction mix was incubated 1-2 hours at 37 °C, composition of reaction is showed in Table 3.4. Restricted plasmids were analysed by agarose electrophoresis and plasmids with different insert length were chosen and sent to sequencing service (GATC Biotech AG, Cologne, Germany). Primers used for sequencing are listed in Figure 3.5.

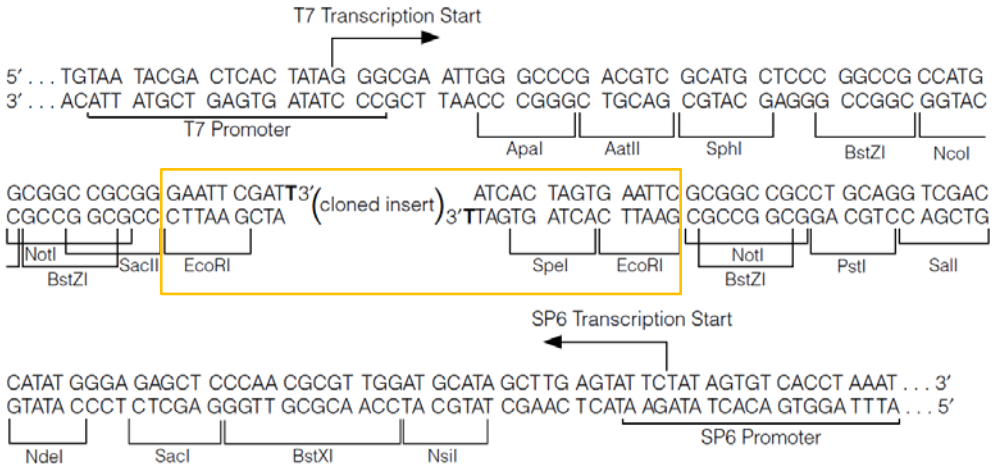

Figure 3.4: Multiple cloning sequence of the pGEM -T Easy Vector – EcoRI cleavage in EcoRI restriction sites release cloned insert sequence (modified from pGEM -T and pGEM -T Easy Vector Sysems Technical Manual TM042).

Component	Volume (µL)
10x Buffer EcoRI	1
EcoRI enzyme	1
Plasmid DNA (1 µg)	5
dH2O	3

Table 3.4: Composition of restriction reaction using EcoRI enzyme.

Primer for insert sequencing and its binding site

pUC/M13 Forward Primer (24mer):

5´-d(CGCCAGGGTTTTCCCAGTCACGAC)-3´

+ pUC/M13 Forward Sequencing Primer binding site 2949–2972

pUC/M13 Reverse Primer (22mer):

5´-d(TCACACAGGAAACAGCTATGAC)-3´

+ pUC/M13 Reverse Sequencing Primer binding site 176–197

Figure 3.5: Figure shows primers used for insert's sequencing with their binding sites on plasmid. Numbers represent base pair position within 3015 bp plasmid sequence. Primers were synthetised by Generi Biotech s.r.o. (Czech Republic).

3.2.6. Bradford protein assay

Bradford protein assay was used for determination of protein concentration of cellular pellet samples resuspended in PBS. Samples were diluted in distilled water (dH_2O) in 1:10 ratio, vortexed and sonicated. 10 µL of sample was diluted in 990 µL dH_2O, vortexed

and 250 μL of Bradford reagent (Bio-Rad, USA) was added. After 2 min incubation in room temperature with occasional vortex, sample was transferred into 1 cm wide polystyrene cell and absorbance was measured at wavelength of 595 nm by spectrophotometer BioPhotometer (Eppendorf, Germany). Calibration curve needed for determination of protein concentration was prepared using stock solution of bovine serum albumin (BSA) (concentration 0,2 mg/mL). BSA was diluted in 1 mL of H_2O in a scale – 0, 4, 8, 16, 20 ug of BSA.

3.2.7. Isolation of mitochondria

Mitochondria from HEK293 were released by hypotonic shock and isolated using differential centrifugation as described (Bentlage *et al.*, 1996). Cellular pellets were diluted in PBS and centrifuged at 600 g (10 min, 4° C). Supernatant was removed, pellet was weighed and resuspended 10:1 (v/w) in hypotonic solution of 10 mM Tris pH 7.6, supplemented with protease inhibitor cocktail (PIC, 1:500). Immediately, suspension was homogenized with Teflon pestle and glass grinding vessel (20-times, 600 rpm). After homogenization, sucrose was added to the homogenate from 1,5 M stock solution supplemented with PIC (1:500) to reach final concentration 250 mM. Non-disrupted cells and nuclei were removed by centrifugation at 600 g (10 min, 4°C). Supernatant was recovered into clean tube and pellet was resuspended in SEKT (250 mM sucrose, 40 mM KCl, 20 mM Tris-HCl, 2mM EGTA, pH 7,6) with PIC, rehomogenized (5-times, 800 rpm) and centrifuged at 600 g (10 min, 4°C). Combined supernatants were centrifuged at 10 000g (10 min, 4°C), pelleted mitochondria were resuspended in 500 uL of SEKT with PIC and centrifuged again at 10 000g (10 min, 4°C). Final pellet, mitochondrial fraction, was resuspended in SEKT to measure protein concentration. Mitochondria were then stored as dry pellets at -80°C.

3.2.8. SDS-PAGE

Sodium dodecyl sulphate polyacrylamide gel electrophoresis (SDS-PAGE), specifically tricine-SDS-PAGE, was used as a method for separation of proteins based on their different molecular weight under denaturing conditions. Sodium dodecyl sulphate (SDS) is anionic detergent which disrupts noncovalent bonds of higher protein

organisations by forming of complexes with proteins and gives them uniform negative charge (Schägger and von Jagow, 1987; Schägger, 2006).

SDS-PAGE samples were prepared from frozen aliquots of harvested cellular pellets. As a first step, samples were lysed by SLB buffer (sample lysis buffer; 2% (v/v) 2-mercaptoethanol, 4% (w/v) SDS, 50 mM Tris (pH 7,0), 10% (v/v) glycerol, 0,02% Coomassie Brilliant Blue R-250) to final concentration 2-5 mg protein/mL. Then, samples were sonicated for 3 min by sonicator BANDELIN SONOPULS and incubated for 20 min in 40 °C.

Stacking gel and separating gel were prepared on ice according to protocol, which is shown in Table 3.5. Then, approximately 4,5 mL of separating gel was applied into vertical electrophoretic system Mini-PROTEAN III (1 mm wide gel, Bio-Rad, USA) and the top was covered by water to prevent inhibition of polymerization. After polymerization, water was removed and 1,5 mL of stacking gel was applied with a comb for sample loading.

	Stacking gel 4%	**Separating gel 12%**
Final volume	2,5 mL	5 mL
AB	0,20 mL	1,20 mL
3×GB	0,60 mL	1,65 mL
Glycerol 87%	0	0,50 mL
dH_2O	1,68 mL	1,60 mL
APS	20 µL	25 µL
TEMED	2 µL	2 µL

Table 3.5: Components of polyacrylamide stacking and separating gel.

Abbreviations: AB (48% (w/v) acrylamide, 1,5% (w/v) N,N'-Methylenebisacrylamide), 3×GB (gel buffer - 75 mM imidazol, 1,5 mM 6-aminocaproic acid, pH 7,0), APS (10 % (w/v) ammonium peroxodisulfate), TEMED (tetramethylethylenediamine)

Samples (10-50 µg of protein) or 4 µL of molecular weight standard PageRuler Prestained Protein Ladder (Thermo Fisher Scientific, USA) were loaded into the wells. Anode buffer (100 mM Tris-HCl; pH 8,9) was poured into electrophoretic bath and cathode buffer (100 mM Tris-HCl, 100 mM Tricine, 0,1% (w/v) SDS; pH 8,25) was poured between electrophoretic glasses. Initial voltage of electrophoresis was 45 V and

after focusing of samples on stacking and separating gel interface voltage was increased to 100 V.

3.2.9. Native electrophoresis

Blue-native (BNE-PAGE) electrophoresis (Wittig, Braun and Schägger, 2006) was chosen as a method for studying of native protein complexes. For protein complexes solubilization, mild non-ionic detergent digitonin, which prevents dissociation of supercomplexes, was used, thus OXPHOS complexes and their supercomplexes can be detected.

Isolated mitochondrial pellets were resuspended in solubilisation buffer A (50mM NaCl, 50mM imidazole/HCl, 2mM 6-aminocaproic acid, 1mM EDTA; pH 7,0) to reach final protein concentration 10 mg/mL. Digitonin (20% (w/v) stock solution) was added (2 g DIG/1 g of protein) to mitochondrial suspension, and solubilisation proceeded on ice for 10 min. Afterwards, samples were centrifuged at 30 000 g (20 min, 4 °C) and supernatant containing released membrane proteins was transferred into clean tube. Concentration of protein and sample volume were measured. Then, glycerol was added to final 5 % (v/v) concentration and Coomassie Brilliant Blue G-250 (CBB) was supplemented according to detergent/dye ratio 8:1 (w/w).

Polyacrylamide gel was mixed according to the protocol shown in Table 3.6. Gradient gel (2,85 mL of lower concentration gel; 2,35 mL of higher concentration gel) was prepared using peristaltic pump (Cole-Parmer Instruments, USA) and Mini-PROTEAN III (Bio-Rad Laboratories, USA).

Bis-Tris system			
	Stacking gel 4%	**Separating gel 5%**	**Separating gel 16%**
Final volume	2,5 mL	5 mL	5 mL
AB	0,20 mL	0,50 mL	1,60 mL
3×GB	0,82 mL	1,65 mL	1,65 mL
Glycerol 99 %	0	0	0,80 mL
dH_2O	1,45 mL	2,82 mL	0,95 mL
APS	30 µL	30 µL	7 µL
TEMED	3 µL	3 µL	2 µL

Table 3.6: Components of polyacrylamide stacking and separating gels.

Abbreviations: AB (48% (w/v) acrylamide, 1,5% (w/v) N,N'-Methylenebisacrylamide), 3×GB (gel buffer - 75 mM imidazol, 1,5 mM 6-Aminocaproic acid, pH 7,0), APS (10 % (w/v) ammonium peroxodisulfate), TEMED (tetramethylethylenediamine).

Initial voltage of electrophoresis was 45 V. After focusing of samples on stacking and separating gel interface voltage was increased to 120 V. Electrophoresis was performed at 4 °C. Anode buffer (25 mM imidazole; pH 7,0) and cathode buffer B (50 mM tricine, 7,5 mM imidazole, 0,02% (w/v) CBB; pH 7,0) were used. After focusing of samples, cathode buffer B was removed and changed by cathode buffer B/10 (50 mM tricine, 7,5 mM imidazole, 0,002% (w/v) CBB; pH 7,0). As a molecular weight standard, NativeMark Unstained Protein Standard (Thermo Fisher Scientific, USA) was loaded into one well.

3.2.10. Western blot and immunodetection

Proteins separated by electrophoresis were transferred onto PVDF (polyvinylidene difluoride) membrane (Immobilon FL 0,45 µm, Millipore Corporation, USA) by semi-dry electroblotting using Transblot SD apparatus (Bio-Rad Laboratories, USA).

Gel was equilibrated in blotting buffer III (38 mM Tris, 10% (v/v) methanol, 10 mM glycine; pH 8,5) for 15 minutes. Meanwhile, PVDF membrane was activated for 15 s in 100% methanol, washed for 2 min in dH_2O and then incubated for 5 min in blotting buffer II (25 mM Tris, 10% (v/v) methanol; pH 9,0). Six filter papers (Whatman CHR 3mm, GE Healthcare, USA) were incubated in blotting buffer I (0,3 M Tris, 10% (v/v) methanol; pH 10,4) and put on a moistured anode. Then, three filter papers incubated in blotting buffer II, PVDF membrane, equilibrated gel and six filter papers incubated in

blotting buffer III were stacked to complete the semi-dry transfer sandwich. Wet cathode was put on the top and electro-transfer proceeded for 1 hour under a constant current of 0,8 mA/cm^2.

After blotting, PVDF membrane was washed for 5 min in TBS (150 mM Tris-HCl, 10 mM NaCl; pH 7,5) and blocked in 5% (w/v) fat-free dry milk diluted in TBS for 1 hour. Then, membrane was washed 2×10 min in TBST (0,1% (v/v) detergent Tween-20 in TBS) and was prepared for immunodetection of proteins.

For immunodetection, membrane was incubated for 2 hours in primary antibody (diluted in TBST) at room temperature. Then, membrane was washed 3×10 min with TBST and secondary antibody (conjugated with fluorescence tag, diluted in TBST) incubation for 1 hour in dark followed. Afterwards, membrane was washed 3×10 min in TBST and 10 min in TBS. Primary and secondary antibodies used for immunodetection are mentioned in Table 3.7 and Table 3.8. Signal detection was performed using fluorescence scanner Odyssey (LI-COR Biosciences, USA).

Signals detected by scanner were quantified by software AIDA Image Analyzer (Raytest Isotopenmessgeräte GmbH, Germany).

Protein specifity	Catalog number	Provider	Dilution	Type
Cox1	Ab14705	Abcam, UK	1:1000	mo/M
Cox2	Ab110258	Abcam, UK	1:1000	mo/M
Cox3	Ab110259	Abcam, UK	1:250	mo/M
Cox4	11463-1-AP	Proteintech Group, USA	1:1000	rb/P
Cox4i1	Ab14744	Abcam, UK	1:1000	mo/M
Cox4i2	H00084701-M01	Abnova, Taiwan	1:1000	mo/M
Cox5a	Ab110262	Abcam, UK	1:1000	mo/M
Cox6c	Ab110267	Abcam, UK	1:500	mo/M
Ndufa9	Ab14713	Abcam, UK	1:1000	mo/M
SDHA	Ab14715	Abcam, UK	1:10000	mo/M
Core2	Ab14745	Abcam, UK	1:1000	mo/M
$F_1\beta$	Ab14730	Abcam, UK	1:2000	mo/M
F_Oc	Ab18	Abcam, UK	1:1000	rb/P
actin	MAB1501	Merck Millipore, USA	1:60000	mo/M
Citrate synthetase	Ab129095	Abcam, UK	1:1000	rb/M

Table 3.7: Table shows primary antibodies used for immunodetection of proteins on PVDF membrane. Abbreviations: mo - mouse, rb - rabbit, M - monoclonal

Secondary antibodies	Provider	Detection wavelenght	Dilution in TBST
Alexa Fluor 680: goat anti-mouse, donkey anti-goat, goat anti-rabbit IgG	Thermo Fisher Scientific, USA	700 nm	1:3 000
IRDye 800: goat anti-rabbit, anti-mouse IgG	Rockland, USA	800 nm	1:3 000

Table 3.8: Table shows secondary antibodies used for immunodetection of proteins on PVDF membrane.

3.2.11. Mass spectrometry - LFQ analysis

Proteomic analysis was performed on service basis by Proteomics core facility at Biocev Institute. Biological duplicates (COX4i1 KO 1 and 2, COX4i2 KO 1 and 2, COX4i1/4i2 KO 1 and 2) were harvested and MS LFQ analysis was performed in technical duplicates. Briefly (Piherov *et al.*, 2018), cell pellets (100 µg of protein) of wild-type HEK293 cell line, COX4i1, COX4i2 and COX4i1/4i2 KO clones were solubilized by sodium deoxycholate (final concentration 1% (w/v)), reduced with TCEP [tris(2-carboxyethyl)phosphine], alkylated with MMTS (S-methyl methanethiosulfonate),

digested sequentially with Lys-C and trypsin and extracted with ethylacetate saturated with water as described. Samples were desalted on Empore C18 columns, dried in Speedvac and dissolved in 0.1% TFA + 2% acetonitrile. About 1 µg of peptide digests were separated on 50 cm C18 column using 2.5 h elution gradient and analyzed in a DDA mode on a Orbitrap Fusion Tribrid (Thermo Scientific) mass spectrometer. Resulting raw files were processed in MaxQuant (v. 1.5.3.28) with label-free quantification (LFQ) algorithm MaxLFQ. Downstream analysis and visualization was performed in Perseus (v. 1.5.3.1).

3.2.12. Pulse-chase analysis

To study proteosynthesis and turnover of mtDNA-encoded proteins, the method of *in-vivo* metabolic pulse-chase protein labelling by ^{35}S-methionine + ^{35}S-cysteine was employed as described (McKenzie, Lazarou and Ryan, 2009), using Express Protein Labelling Mix, [^{35}S] (PerkinElmer, USA).

As a first step, cells cultivated in 1 mL of complete DMEM medium on a 6-well plate were washed with prewarmed PBS and incubated in DMEM medium without methionine and cysteine (DMEM-M-C, 0,11 mg/mL sodium pyruvate, 2 mM Glutamine, 5% dialysed FBS, 10 mL/500 mL HEPES) at 37 °C and 5% CO_2 atmosphere for 15 min. After 15 min, 100 µL of 1,2 mg/mL anisomycin in DMEM-M-C was added for cytosolic translation inhibition. Cells were then incubated for 15 min in thermostat. Afterwards, cells were labelled in DMEM-M-C with 100 µg/mL of anisomycin and the radioactive labelling mix with 100 µCi/mL 37 °C and 5% atmosphere for 3 hours. After 3 hours, 20 µL of the mixture of "cold" methionine and cysteine (non-labelled Met and Cys) was added into each well (final concentration 250 µM) and incubated at 37 °C and 5% CO_2 atmosphere for 15 min. Then, cells were washed two-times with PBS containing 250 µM cold methionine and 250 µM cold cysteine.

One aliquot of labelled cells was immediately harvested ("pulse" sample). Last centrifugation step was performed for 10 min in pre-weighted 2 mL tubes. The pellet was then weighed and flash frozen at -80 °C until used.

Two other labelled cells aliquots ("chase" samples) were further incubated in complete non-labelling DMEM medium for 4 or 24 hours. Then, they were harvested the same way as in case of "pulse" samples.

Cellular pellets were later used for SDS-PAGE analysis (as described in Chapter 3.2.8) using large format Hoefer™ SE 600 Chroma Vertical Electrophoresis System (Thermofisher, USA). 70 µg protein-aliquots of each sample were separated by 16 % gel. Following the electrophoretic run, gel was fixed in CBB staining solution (40 % (v/v) methanol, 8 % (v/v) acetic acid, 0.05 % (w/w) Coommasie Brilliant Blue R-250) and dried onto Whatmann CHR 3 mm paper. Radioactivity was detected by exposing the gel to Storage Phosphor Screen BAS-IP SR 2025 E for 14 days (GE Healthcare), which was then scanned by FX Molecular Imager (Bio-Rad Laboratories, USA). Signals detected by scanner were quantified by software AIDA Image Analyzer (Raytest Isotopenmessgeräte GmbH, Germany).

3.2.13. RNA isolation

First step of RNA isolation was harvesting of confluently grown cells on six-well plate by 1 mL of TRIzol reagent (Thermo Fisher Scientific, USA) and transfer of the samples into 1,5 mL sterile tubes. Then, 200 µL of chloroform was added, tubes were vortexed and incubated in room temperature for 10 min. After incubation, samples were centrifuged (12 000 g/15 min/ 4 °C) and liquid RNA phase on the top was transferred into new sterile 1,5 mL tube. 500 µL of isopropanol was added into RNA phase and after vortexing and room temperature incubation, samples were centrifuged again (12 000 g/10 min/ 4 °C). Supernatant was removed and 75% (v/v) ethanol chilled to 4 °C was added to RNA pellet. Sample was centrifuged again (7 500 g/10 min/4 °C), supernatant was removed and pellet was dried out. Dried pellets were resuspended in 15 µL of RNase-free H_2O.

RNaseZap (Sigma) was used for cleaning of workspace to prevent degradation of RNA.

3.2.14. Removal of genomic DNA

In case of using RNA for quantification of mitochondrial genes expression, it was necessary to remove residual DNA from RNA samples. DNA-*free* DNA Removal Kit (Thermo Fisher Scientific, USA) was used for that purpose according to the manufacturer's guidelines. RNA concentration was measured by NanoDrop instrument and RNA was stored at -80 °C.

3.2.15. Reverse transcription

SCRIPT cDNA Synthesis kit (Jena Bioscience, Germany) was used, according to instructions, for reverse transcription of isolated and purified RNA. Reaction proceeded on cycler Eppendorf MasterCycler Gradient (Eppendorf, Germany).

3.2.16. Quantitative PCR

Quantitative PCR (qPCR) was chosen as a method for studying of gene expression and for mitochondrial DNA (mtDNA) quantification.

For gene expression analysis, selected genes (see Table 3.9) were analysed in biological hexaplicates (technical duplicates) using TaqMan Gene Expression Assays (Thermo Fisher Scientific, USA) and 5x HOT FIREPol Probe qPCR Mix (Solis BioDyne, Estonia). Primers used for mtDNA quantification are shown in Table 3.10. 5x HOT FIREPol EvaGreen qPCR Mix (Solis BioDyne, Estonia) was used in the reaction. Biological triplicates (technical triplicates) were analysed. Measurement was performed using cycler ViiA7 (Thermo Fisher Scientific, USA).

Gene	Assay ID	Protein	Enzyme	Origin
COX1	Hs02596864_g1	Cox1	COX	mtDNA
COX3	Hs02596866_g1	Cox3	COX	mtDNA
COX4i1	Hs00971639_m1	Cox4i1	COX	nDNA
COX4i2	Hs01025454_m1	Cox4i2	COX	nDNA
ND1	Hs02596873_s1	ND1	Complex I	mtDNA
ND2	Hs02596874_g1	ND2	Complex I	mtDNA
ND6	Hs02596879_g1	ND6	Complex I	mtDNA
SDHB	Hs01042482_m1	SDHB	Complex II	nDNA
CYTB	Hs02596867_s1	Cytochrome b	Complex III	mtDNA
ATP6	Hs02596862_g1	Fo-a	Complex V	mtDNA
B2M	Hs00984230_m1	B2M	Reference gene (nDNA)	
HPRT1	Hs02800695_m1	HPRT1	Reference gene (nDNA)	

Table 3.9: TaqMan Gene Expression Assay's targeted genes.

Gene	Primer	
GAPDH	F: TTCAACAGCGACACCCACT R: CCAGCCACTACCAGGAAAT	Reference gene (nDNA)
D-loop	F: CACCATCCTCCGTGAAATCAA R: GCGAGGAGAGTAGCACTCTTGTG	Reference gene (mtDNA)

Table 3.10: Primers used for mtDNA quantification. F: forward primer, R: reverse primer.

Before measurement itself, Master Mix was prepared on ice in flow box according to the protocol shown in Table 3.11. Then, Master Mix was pipetted by 9 µL into MicroAmp Fast Optical 96-Well Reaction Plate (Thermo Fisher Scientific). As a last step, 1 µL of cDNA was pipetted into wells and measurement according to protocol described in Table 3.12 was started. Five-points calibration curve was diluted from wild-type HEK293 sample (1 x, 0.5 x, 0.1 x, 0.05 x, 0.01 x concentrated). Results were evaluated by ViiA7 Software (Thermo Fisher Scientific, USA).

Reagent – Probe assay	Final concentration	Volume [µL]
5x HOT FIREPol Probe qPCR Mix	1×	2
Primer mix 20×	1×	0,5
PCR clean H_2O	-	6,5

Reagent – SYBR green assay	Final concentration	Volume [µL]
5x HOT FIREPol EvaGreen qPCR Mix	1×	2
Forward primer (100 µM)	1×	0,05
Reverse primer (100 µM)	1×	0,05
PCR clean H_2O	-	6,9

Table 3.11: Composition of Master Mix for qPCR.

	Temperature	Time	Number of cycles
Viia7	95 °C	15 min	
	95 °C	20 s	40
	60 °C	1 min	
LightCycler 480	**Temperature**	**Time**	**Number of cycles**
	95 °C	15 min	
	95 °C	20 s	40
	60 °C	1 min	

Table 3.12: Protocol of qPCR measurement using Viia7.

3.2.17. Seahorse measurement

For functional characterization of knock-out clones, parallel measurement of mitochondrial respiration and glycolytic capacity was performed. Seahorse Extracellular Flux (XF) Analyzer (Agilent Technologies, USA) detects oxygen concentration and pH in medium in real time in high-throughput manner in multi-well plates, using cartridge with separate sensor head with oxygen and pH sensitive fluorofores for each well. In this project, Seahorse XFe24 was used, data acquisition and analysis were performed by Wave Desktop software (Agilent Technologies, USA), yielding oxygen consumption rate (OCR) and extracellular acidification rate (ECAR) parameters representing mitochondrial respiration and glycolytic rate, respectively, thus providing cellular bioenergetic phenotype.

Preparation of plates for measurement was done under sterile conditions in laminar box. One day before measurement, each well of Seahorse XFe24 cell culture microplate was treated with 50 μL of poly-L-lysine (1:10 (v/v) in dH_2O) for improved cell's adhesion and after 10 min incubation washed with PBS. Harvested cells were counted by Scepter counter (Millipore, USA) and diluted in complete DMEM medium to density of 8.10^5/mL. Then, 50 μL of cellular suspension was pipetted into a well (40 000 cells/well) and microplate was incubated in thermostat, allowing cells to attach to well bottom. After 2 hours, medium was added to final volume of 200 μL per well. Four wells were always prepared without cells to serve for calibration of background signals. Microplate was then incubated overnight in thermostat. Hydration of XF24 Sensor Cartridge by XF Calibrant solution (pH 7,4; Agilent Technologies, USA) was also carried out overnight at 37 °C.

Day after, microplate was washed with 1 mL of XF Assay Medium Modified DMEM (pH 7,4, 37 °C), 500 μL of the same medium with 0,2% BSA was pipetted and microplate was incubated at 37 °C for 30 min. Meanwhile, XFe24 Sensor Cartridge was prepared by injection of different substrates and inhibitors into ports according to the experiment.

Before measurement itself, it was necessary to calibrate XFe24 Sensor Cartridge on Seahorse XFe24, and after that sensors plate was exchanged by microplate and experiment begins. Assay chosen for measurement combined Mito (Agilent, 2018a) and Glycolysis (Agilent, 2018b) Stress assays in one run to characterize cellular metabolic phenotype in one experiment. Protocol of individual additions during experiment is shown in Table 3.13.

Addition	Reagent	Volume (µL)	Final concentration
1	oligomycin	55	1 µM
2	FCCP	60	2 µM
3	rotenon antimycine A 2-DG	68	1 µM 1µg/ml (in 2-DG)

Table 3.13: Protocol of inhibitors addition during Seahorse measurement.

Data from measurement had to be normalized to number of cells in each well of microplate to correct for different proliferation rate of the cell lines with different phenotype. For that purpose, immediately after Seahorse run, cell nuclei were labelled by Hoechst stain (final concentration 5 µg/mL, diluted in FluoroBrite DMEM Media), which binds to the minor groove of double-stranded DNA. Images of whole wells were acquired by Cytation 3 Cell Imaging Reader (BioTek, USA) and analysed using software Gen5 (automated protocol) to obtain cell counts for each well.

3.2.18. High-resolution respirometry

High resolution respirometry employing OROBOROS Oxygraph-2k (OROBOROS INSTRUMENTS, Austria) was chosen as an alternative method for detection of respiration rate of intact cells.

OROBOROS enables measurement of oxygen consumption (thanks to polarographic Clark electrodes) with high resolution in intact cells, permeabilized cells, isolated mitochondria and even in tissue. Using intact cells, it is possible to determine respiration parameters, while measurement of permeabilized cells enables evaluation of individual complexes capacity thanks to saturating concentration of substrates or inhibitors (Gnaiger, 2014).

For characterization of cells, individual respiratory states (routine respiration, leak, electron transport system capacity, residual oxygen consumption) were established in intact cells during measurement using corresponding substrates and inhibitors. This protocol principally matched the conditions during Seahorse measurement.

At first, routine respiration without any addition was measured, which refers to oxidation of endogenous substrates. Then, addition of CV inhibitor oligomycin (binding

the interface between proton channel and c-ring in F_o domain) was titrated to block oxidative phosphorylation, in order to measure oxygen consumption rate compensating for non-specific proton leak at inner mitochondrial membrane. After that, maximal ETS (electron transport system) capacity was measured after titration of chemical uncoupler FCCP (Carbonyl cyanide-p-trifluoromethoxyphenylhydrazone), discharging the proton gradient to relieve respiratory control. As a last step, inhibitor of CI (rotenone) with CIII inhibitor (antimycin A) or KCN, as an inhibitor of COX, were added to evaluate residual oxygen consumption.

Measurement proceeded in 2 mL chambers, at 30 °C and with constant stirring at 750 rpm. At first, protein concentration of harvested cells was measured and volume for final concentration 0,25 mg/mL was pipetted into the cell with medium MIRO5 (110 mM sucrose, 60 mM K+-lactobionate, 0.5 mM EGTA, 3 mM $MgCl_2$, 20 mM taurine, 10 mM KH_2PO_4, 20 mM HEPES, pH 7.1), optimal for measurement of oxygen consumption of intact cells. Then, addition of substrates and inhibitors followed according to protocol showed in Table 3.14. Substrates and inhibitors were added by Hamilton syringes (Hamilton, USA) at steady state level, when oxygen flux was stable. Results were analyzed using DatLab5 software (Oxygraph-2k, OROBOROS INSTRUMENTS, Austria).

Substrate	Final concentration
FCCP	0,5 µM
rotenone	1 µM
oligomycin	0,5 µM
antimycin A	0,25 µM
KCN	0,5 mM

Table 3.14: Inhibitors and substrates used in high resolution respirometry measurement.

4. Results

4.1. COX4i1 and COX4i2 gene knock-out

For investigation of Cox4 subunit isoforms function, unique HEK293 cell line based knock-out (KO) models were prepared using Cas9-D10A paired nickase (CRISPR) system.

4.1.1. Analysis of gRNA pairs efficiency

Efficiency of different combinations of gRNA pairs for Cas9-D10A nickase system was determined by SURVEYOR assay. For both, COX4i1 and COX4i2 gene KO preparation, relevant combinations of two gRNAs binding sense strand, and two gRNAs binding antisense strand were transfected into HEK293. The target region was amplified, subjected to the assay and analyzed by gel electrophoresis. For COX4i1 KO, HSL0001377215 (1)/ HSR0001377224 (3) gRNA pair displayed the most prominent band pattern (see yellow box in Figure 4.1) representing cleaved heteroduplexes of wild-type and mutated gene region. This pair was therefore chosen for subsequent work. Analogously, HSR0002687616 (5) / HSL0002687619 (7) gRNA pair was chosen in case of the COX4i2 gene KO (not shown).

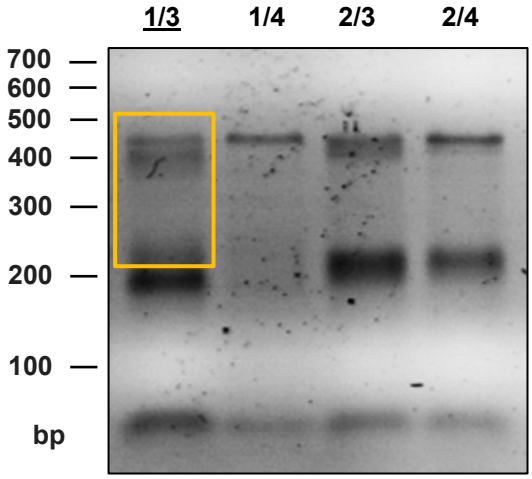

Figure 4.1: SURVEYOR assay analysis of COX4i1 targeted gRNA pairs. Representative 1,5 % agarose gel electrophoresis.

4.1.2. Selection of COX4i2 knock-out clones

30 single cell clones were isolated following transfection with CRISPR gRNAs. These clones were screened for putative COX4i2 KO by sequencing PCR-amplified gRNA-targeted exon 2 of COX4i2 gene. Out of these, two clones displayed homozygous deletions resulting in aberrant protein predicted for loss of function. Image of exon 2 amplicons and obtained sequences of these homozygous COX4i2 KO clones are presented in Figure 4.2. Selected clones, denoted as COX4i2 KO 1 and COX4i2 KO 2, were used for biochemical analyses of the impact of COX4i2 KO, as well as for subsequent transfection with COX4i1 CRISPR gRNAs to produce cells with double knockout of both COX4 isoforms.

a)

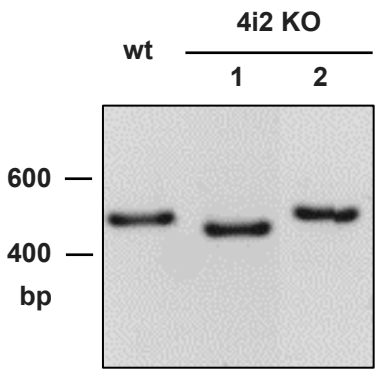

b)

4i2 KO	Sequence (exon 2)	Mutation	Result
wt	ATGCTCCCCAGAGCTGCCTGGAGCTTGGT GCTGAGGAAAGGTGGAGGTGGAAGACGA GGGATGCACAGCTCAGAAGGCACCA	-	-
1	ATGCTCCCCAGAGCTGCCTGGAGCTTGGT GCTGAGGAAAGGTGGAGGTGGAAGACGA GGGATGCACAGCTCAGAAGGCACCA	30 bp deletion	In-frame deletion of 10 aminoacids
2	ATGCTCCCCAGAGCTGCCTGGAGCTTGGT GCTGAGGAAAGGTGGAGGTGGAAGACGA GGGATGCACAGCTCAGAAGGCACCA	7 bp deletion	Premature STOP codon at position 9

Figure 4.2: a) Agarose gel electrophoresis of PCR products of CRISPR targeted exon 2 of COX4i2 gene. Single band pattern indicates that selected COX4i2 KO 1 (4i2 KO 1) and COX4i2 KO 2 (4i2 KO 2) are homozygotes. PCR product length of these KO clones differs from wild-type HEK293 cell line (wt). **b) Sequences of COX4i2 KO clones.** Characterized mutations in exon 2 of COX4i2 gene lead to aberrant Cox4i2 protein with loss of function.

4.1.3. Selection of COX4i1 and COX4i1/4i2 knock-out clones

In order, to construct COX4i1 knock-out, plasmids encoding the selected pair of gRNAs and Cas9-D10A were transfected into HEK293 wt cells to obtain COX4i1 single KO, as well as into COX4i2 KO 1 and COX4i2 KO 2 to produce COX4i1/2 double knock-out HEK293 cells. Roughly 100 isolated single cell clones from each group (see Table 4.1 for exact counts) were subjected to sequencing screen. Unfortunately, COX4i1 exon 3 PCR products displayed more complex patterns with as many as three bands from single clone (Figure 4.3), resulting in undecipherable overlapping nucleotide sequences.

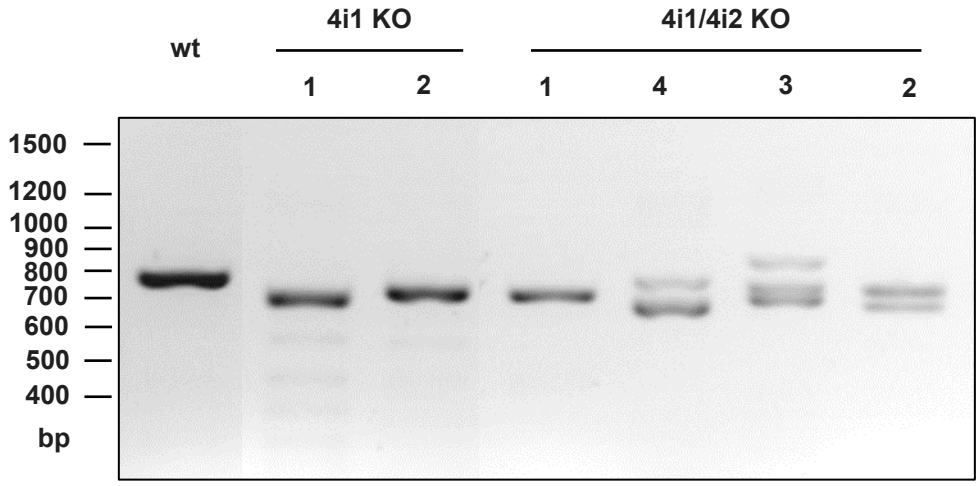

Figure 4.3: Agarose gel electrophoresis of CRISPR targeted exon 3 of COX4i1 gene PCR products. Figure shows, that some clones (COX4i1/4i2 KO 2, 3, 4) are heterozygotes and have two or three variants of incriminated sequence targeted by CRISPR, while length of PCR products differs against wild-type HEK293 cells.

Therefore, COX4i1 KO clones were in parallel screened by Western blot analysis, using immunodetection of Cox4i1 protein in whole cell lysates of single cell clones. While direct protein absence detection is not the typical method of choice for knockout screening, its utility has been proven before in our laboratory, e.g. during the preparation of MLQ or TMEM70 cell knockouts. Analysis revealed wide range of Cox4i1 protein variants in individual clones submitted to mutagenesis. Except KO clones with undetectable levels of Cox4i1 protein, heterozygous clones and clones with changed Cox4i1 migration in SDS-PAGE were also detected (see Figure 4.4). Immunodetection of Cox4i1 protein revealed changes in protein of different selected clones (2-8) against wild-type HEK293 cell line (wt). Total absence of Cox4i1 is observed (1, 2) as well as migration shift of Cox4i1 protein (3, 7, 8) and heterozygous phenotype (4, 5, 6).

Moreover, altered Cox4i1 content or migration shift was coupled with decreased content of catalytic COX subunit Cox2 (1, 2, 3, 8). For further analysis, only clones with undetected Cox4i1 protein were used.

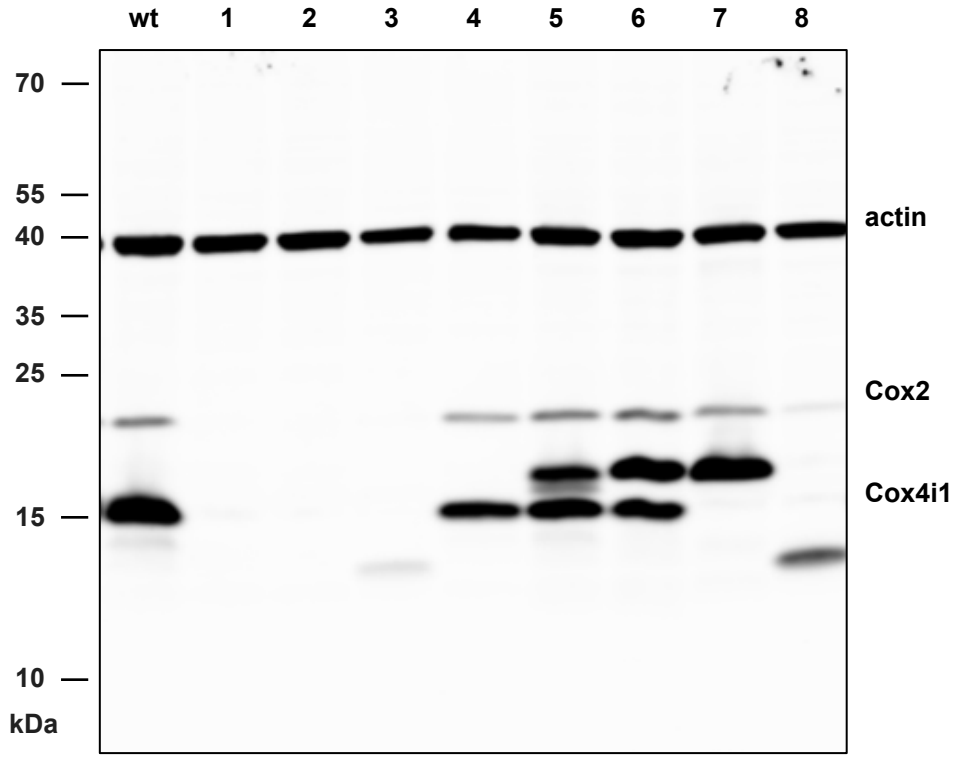

Figure 4.4: Western blot analysis screening of COX4i1 KO clones. Whole cell lysates (30 µg of protein) of single cell clones were subjected to SDS-PAGE. Cox4i1 antibody (Abcam, Ab14744) and Cox2 antibody (Abcam, Ab110258) were used. Actin antibody (Merck Millipore, MAB1501) was used as a loading control.

COX4i1 gene KO was introduced into HEK293 cell line (wt) and into prepared COX4i2 KO clones. Thus, COX4i1 KO and COX4i1/4i2 double KO models were acquired for further studies (for statistics of screened clones see Table 4.1). COX4i2 KO 1 gave a rise to COX4i1/4i2 KO 1, COX4i2 KO 2 to COX4i1/4i2 KO 2.

	No. Screened clones	Complete loss of Cox4	Cox4 migration shift	Cox4 multiple bands
wt	85	7	7	8
4i2 KO 1	109	5	5	1
4i2 KO 2	103	6	6	4

Table 4.1: Various clones obtained by COX4i1 gene knock-out on wild-type or COX4i2 KO background.

4.1.4. COX4i1 and COX4i1/4i2 KO sequences

To verify alterations of COX4i1 gene, TA cloning was performed to analyze different variants of COX4i1 gene CRISPR targeted sequence (shown in Figure 4.3) separately. Plasmids containing inserts of different size (PCR amplified COX4i1 targeted sequence) were chosen and examined by sequencing (see Figure 4.5). Resulting sequences of COX4i1 and COX4i1/4i2 KO clones are presented in Figure 4.6.

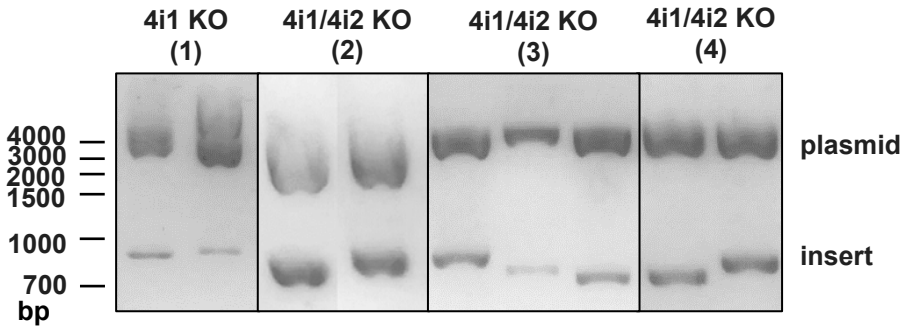

Figure 4.5: Agarose gel electrophoresis of EcoRI restricted plasmid releasing COX4i1 PCR product insert. Figure shows length differences between variants of COX4i1 gene of individual clones. As these plasmids contained only one variant out of two or three present in single cell clone, they were suitable for sequencing.

4i1 KO	Sequence (exon 3)	Mutation	Result
wt	AAAGTGTTGTGAAGAGCGAAGACTTTTCG CTCCCAGCTTATATGGATCGGCGTGACCA CCCCTTGCCGGAGGTGGCCCATGTCAAG CACCTGTCTGCCAGCCAGAAGGCACTGAA GGAGAAGGAGAAGGCCTCCTGGAGCAGC CTCTCCATGGATGAGAAAGTCGAGT	-	-
1.a	AAAGTGTTGTGAAGAGCGAAGACTTTTCG CTCCCAGCTTATATGGATCGGCGTGACCA CCCCTTGCCGGAGGTGGCCCATGTCAAG CACCTGTCTGCCAGCCAGAAGGCACTGAA GGAGAAGGAGAAGGCCTCCTGGAGCAGC CTCTCCATGGATGAGAAAGTCGAGT	76 bp deletion	Frameshift from position 33, premature STOP codon at position 37
1.b	AAAGTGTTGTGAAGAGCGAAGACTTTTCG CTCCCAGCTTATATGGATCGGCGTGACCA CCCCTTGCCGGAGGTGGCCCATGTCAAG CACCTGTCTGCCAGCCAGAAGGCACTGAA GGAGAAGGAGAAGGCCTCCTGGAGCAGC CTCTCCATGGATGAGAAAGTCGAGT	64 bp deletion	Frameshift on position 38, premature STOP codon at position 41
2	AAAGTGTTGTGAAGAGCGAAGACTTTTCG CTCCCAGCTTATATGGATCGGCGTGACCA CCCCTTGCCGGAGGTGGCCCACGTCAAG CACCTGTCTGCCAGCCAGAAGGCACTGAA GGAGAAGGAGAAGGCCTCCTGGAGCAGC, CTCTCCATGGATGAGAAAGTCGAGT	31 bp deletion 1 bp substitution	Premature STOP codon at position 52

Deletion, Insertion, Substitution

4i1/4i2 KO	Sequence (exon 3)	Mutation	Result
wt	AAAGTGTTGTGAAGAGCGAAGACTTTTCG CTCCCAGCTTATATGGATCGGCTGACCAC CCCTTGCCGGAGGTGGCCCATGTCAAGCA CCTGTCTGCCAGCCAAAGGCACTGAGGAG AAGGAGAAGGCCTCCTGGAGCAGCCTCTC CATGGATGAGAAAGTCGAGT	-	-
1	AAAGTGTTGTGAAGAGCGAAGACTTTTCG CTCCCAAAATAAAAGGATCGGCTGACACC TATTTTCTGAGGTGGCCCATGTCAAGAAAT TGTCAGCCAGCCAGAAGGCACTGAAGGAG AAGGAGAAGGCCTCCTGGAGCAGCCTCTC CATGGATGAGAAAGTCGAGT	37 bp deletion 31 bp insertion 1 bp substitution	Frameshift from position 33, premature STOP codon at position 35
2.a	AAAGTGTTGTGAAGAGCGAAGACTTTTCG CTCCCAGCTTATATGGATCGGCTGACCAC CCCTTGCCGGAGGTGGCCCATGTCAAGCA CCTGTCTGCCAGCCAGAAGGCACTGAAGA AGAAGGAGAAGGCCTCCTGGAGCAGCCTC TCCATGGATGAGAAAGTCGAGT	65 bp deletion 1 bp substitution	Frameshift from position 36, premature STOP codon at position 55
2.b	AAAGTGTTGTGAAGAGCGAAGACTTGGTG CTCCCAGCTTATATGGATCGGCTGACCAC CCCTTGCCGGAGGTGGCCCATGTCAAGCA CCTGTCTGCCAGCCAGAAGGCACTGAAGG AGAAGGAGAAGGCCTCCTGGAGCAGCCTC TCCATGGATGAGAAAGTCGAGT	8 bp deletion 3 bp substitution	Frameshift from position 33, premature STOP codon at position 40
3.a	AAAGTGTTGTGAAGAGCGAAGACTTTTCG CTCCCAGCTTATATGGATCGGCTGACCAC CCCTTGCGCCGGAGGTGGCCCATGTCAAG CACCTGTCTGCCAGCCAGAAGGCACTGAA GGAGAAGGAGAAGACCTCCTGGAGCAGC CTCTCCATGGATGAGAAAGTCGAGT	2 bp deletion 1 bp substitution	Frameshift from position 47, premature STOP codon at position 63
3.b	AAAGTGTTGTGAAGAGCGAAGACTTTTCG CTCCCAGCTTATATGGATCGGCTGACCAC CCCTTGCCGGAGGTGGCCCATGTCAAGCA CCTGTCTGCCAGCCAGAAGGCACTGAAGG AGAAGGAGAAGGCCTCCTGGAG	40 bp deletion 1 bp substitution	Frameshift from position 42, premature STOP codon at position 49
3.c	AAAGTGTTGTGAAGAGCGAAGACTTTTCG CTCCTCATCCTGTCTCTTGATCAGAGCTTG ATCCCCTGCGCCATCAGGAGCACCATGTG GTCGCGGGCCTCGTTGCGGTCCTTGCTGA TCTTGGTCTGAGTGCTCAGGTAGTGGTTG ATGGGGATCAGAACTGTTCGCCAGGCTCA AGGCGAGCATGCCCGACGGCGAGGGGCC TGTCTGCCAGCCAGAAGGCACTGAAGGAG AAGGAGAAGGCCTCCTGGAG	113 bp insertion 15 bp substitution	Frameshift from position 33, premature STOP codon at position 67
4.a	AAAGTGTTTTTCAGAGCGAAGACTTTTCGC TCCCAGCTTATATGGATCGGCGTGACCAC CCCTTGCCGGAGGTGGCCCATGTGAAGCA CCTGTCTGCCAGCCAGAAGGCACTGAAGG AGAAGGAGAAGGCCTCCTGGAGCAGCCTC TCCATGGATGAGAAAGTCGAGT	75 bp deletion 5 bp subsitution	Frameshift from position 26, premature STOP codon at position 32
4.b	AAAGTGTTGTGAAGAGCGAAGACTTTTCG CTCCCCTTGCCGGAGGCGGCCCATGTCAA GCACCTGTCGGCGTGACCACCCCTTGCCG GAGGTGGCCCATGTCAAGCACCTGTCTGC CAGCCAGAAGGCACTGAAGGAGAAGGAG AAGGCCTCCTGGAGCAGCCTCTCCATGGA TGAGAAAGTCGAGT	19 bp insertion 6 bp substitution	Frameshift from position 37, premature STOP codon at position 49

Deletion, Insertion, Substitution

Figure 4.6: Sequences of COX4i1 and COX4i1/4i2 KO clones. Characterized mutations in exon 3 of COX4i1 gene lead to aberrant Cox4i1 protein without function.

4.2. Structural characterization of COX4 knock-out clones

Selected COX4i1, COX4i2 and COX4i1/4i2 KO clones were submitted to structural characterization to determine changes in COX content and subunit steady-state levels, as well as changes in the content and assembly status of other OXPHOS complexes.

4.2.1. Effect of COX4 KO on COX subunits content

The steady-state content of five representative COX subunits (Cox4i1, Cox1, Cox2, Cox5a, and Cox6c) was examined by denaturing SDS-PAGE followed by Western blot analysis and immunodetection in two representative clones of each COX4i2 KO, COX4i1 KO and COX4i1/4i2 KO clones in comparison to wt HEK293. Representative WB images are shown in Figure 4.7 A, displaying apparent general decrease of COX subunits in COX4i1 KO and COX4i1/4i2 KO, while COX4i2 KO showed similar pattern as wt cells. Densitometric quantification revealed that relative levels of studied COX subunits in COX4i2 KO clones ranged between 55 – 120 % of controls with significant decrease of Cox2 content, when data were normalized to actin levels (Figure 4.7 B). However, upon normalization to citrate synthase levels (marker of mitochondrial mass), COX subunits content was unaffected (Figure 4.7 C). These data suggest that COX4i2 KO have decreased amount of mitochondria rather than selectively decreased COX content. COX4i1 KO and COX4i1/4i2 KO cells presented with profound COX deficiency (Figure 4.7 A), loss of Cox4i1 resulted in decrease of Cox2 content below detection limit, while subunits Cox1, Cox5a and Cox6c were detected at residual levels ranging between 5 – 30 % of controls (Figure 4.7 B, C).

In addition to classical electrophoretic approach, relative levels of COX subunits were assessed in high-throughput manner using mass spectrometry label-free quantification (MS LFQ). Analysis of two technical replicates of two representative clones for each COX4i2 KO, COX4i1 KO and COX4i1/4i2 KO yielded reliable data for eight COX subunits. These confirmed our previous findings of generalized COX subunit deficiency in COX4i1 KO and COX4i1/4i2 KO cells, with the most affected subunit being Cox2. COX4i2 KO clones were not significantly changed, as COX subunits content was comparable to wild-type cells (see Figure 4.8).

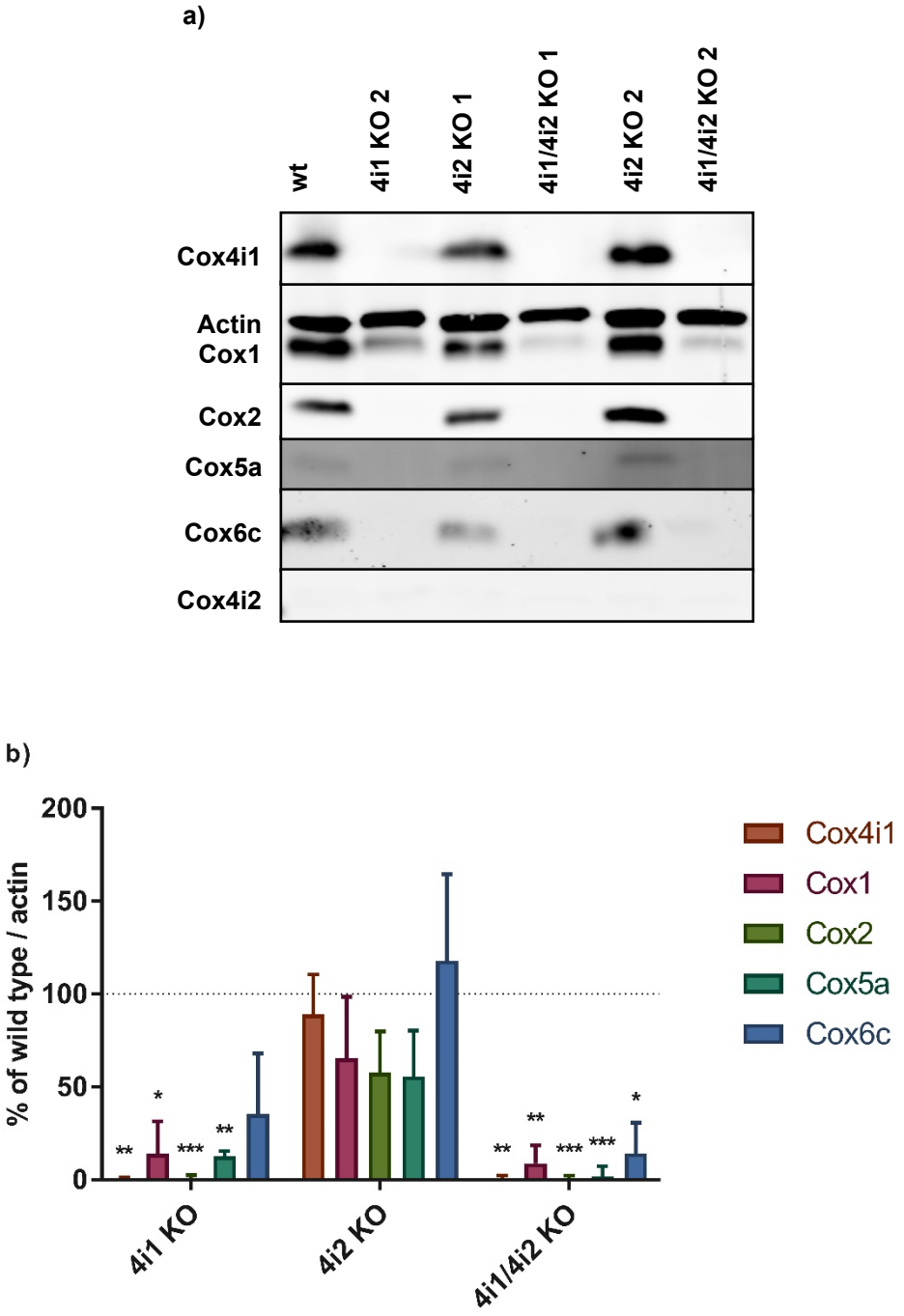
a)
wt
4i1 KO 2
4i2 KO 1
4i1/4i2 KO 1
4i2 KO 2
4i1/4i2 KO 2
Cox4i1
Actin
Cox1
Cox2
Cox5a
Cox6c
Cox4i2
b)
% of wild type / actin
200
150
100
50
0
**
*
***
**
**
***
***
*
4i1 KO
4i2 KO
4i1/4i2 KO
Cox4i1
Cox1
Cox2
Cox5a
Cox6c

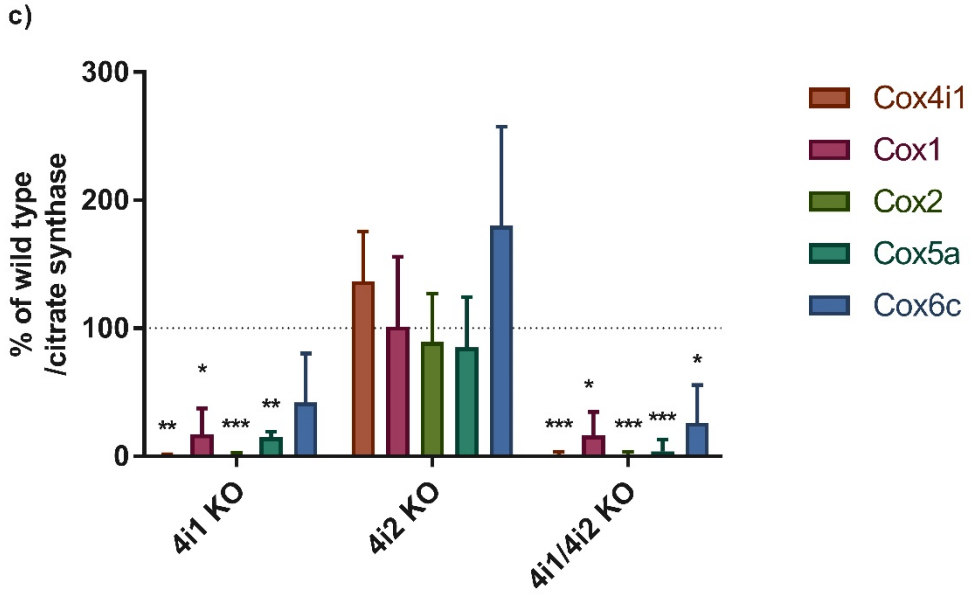

Figure 4.7: a) Representative Western blot analysis of COX subunits in KO clones. Whole cell lysates (30 µg of protein) of COX4i1 KO, COX4i2 KO and COX4i1/4i2 KO clones were subjected to SDS-PAGE. Used antibodies are listed in Chapter 3.2.10. Actin antibody was used as a loading control**. b) Quantification of COX subunits content related to actin.** Plotted values represent mean values relative to wild-type. Asterisks (*) represent p-value: * < 0,05; ** < 0,01; *** < 0,001 (related to wild-type). Error bars represent SD. **c) Quantification of COX subunits content related to citrate synthase.** Plotted values represent mean values relative to wild-type. Asterisks (*) represent p-value: * < 0,05; ** < 0,01; *** < 0,001 (related to wild-type). Error bars represent SD. (n = 2)

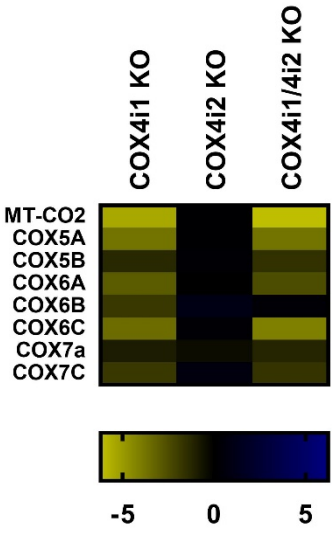

Figure 4.8: Proteomic analysis of relative content of COX subunits using mass spectrometry label-free quantification (MS LFQ). Figure shows decreased content of COX subunits in COX4i1 and COX4i1/COX4i2 KO clones, with Cox2 being the most affected. COX4i2 gene KO do not have deleterious effect on COX subunits level. Data in heat map represent log2 values of quantity fold-changes relative to wild-type, according to colour scale shown below the heat map.

Cox4i2 protein was not detected in any of analyzed samples, neither was it induced after COX4i1 KO (Figure 4.7). To demonstrate that Cox4i2 antibody is functional, detection of Cox4i2 protein in positive control sample, COX4i2 knock-in (4i2 KI) prepared by a colleague in our laboratory using COX4i1/4i2 KO 2 clone, is presented in Figure 4.9.

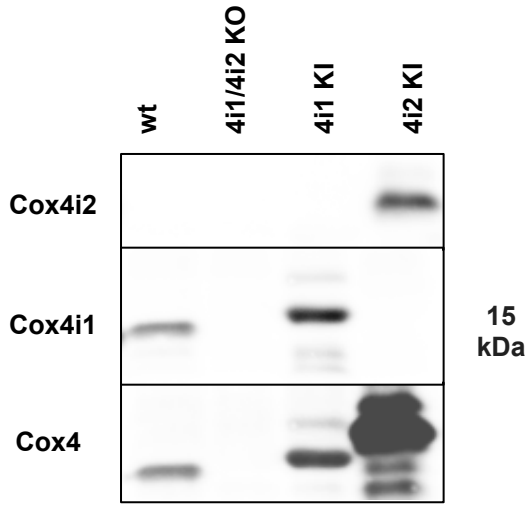

Figure 4.9: Cox4i2 antibody testing. HEK293 cells (wt) show undetectable Cox4i2 protein. On the contrary, Cox4i1 isoform was detected by both, monoclonal (Cox4i1) and polyclonal (Cox4) antibodies. Cox4i2 protein was successfully detected in positive control, COX4i2 knock-in.

4.2.2. Effect of COX4 KO on OXPHOS complexes subunits content

In addition to observed COX subunits content changes in COX4i1 and COX4i1/4i2 KO clones, steady-state levels of representative subunits of OXPHOS complexes were also studied by SDS-PAGE with Western blot immunodetection (see Figure 4.10 A). Specifically, we used the following representative subunits - NDUFA9 of CI, SDHA of CII, Core2 of CIII, and $F_1\alpha$ and F_oc of CV. Change was observed in protein level of NDUFA9, which was decreased in COX4i1, COX4i1/4i2, and COX4i2 KO clones, when data were normalized to actin (Figure 4.10 B). Upon normalization to citrate synthase, NDUFA9 was significantly, approximately 2-fold lower only in the COX4i1 lacking cells (Figure 4.10 C). Core2 subunit was also decreased in COX4i1/4i2 KO, but not in COX4i1 single KO. On the other hand, CII and CV subunit levels were similar or even moderately increased in COX4i1/4i2 and COX4i1 KO cells (Figure 4.10 C).

The electrophoretic data were very well complemented by MS LFQ analysis (heat maps in Figure 4.11), where quantitative data of 32 CI subunits, all four subunits of CII,

seven subunits of CIII, and 13 subunits of CV were obtained. From the perspective of multi-subunit comparison, the decrease of NDUFA9 shown by Western blot analysis was confirmed by LFQ analysis. The levels of CI subunits were between 1.5 – 3-fold decreased in Cox4i1 and COX4i1/4i2 KO clones, while levels of CI subunit in COX4i2 KO were comparable to wild-type. Other OXPHOS complexes (CII, CIII, CV) are comparable to wild-type in Cox4i1 and COX4i1/4i2 KO clones. Consistently, COX4i2 KO clones were not significantly affected.

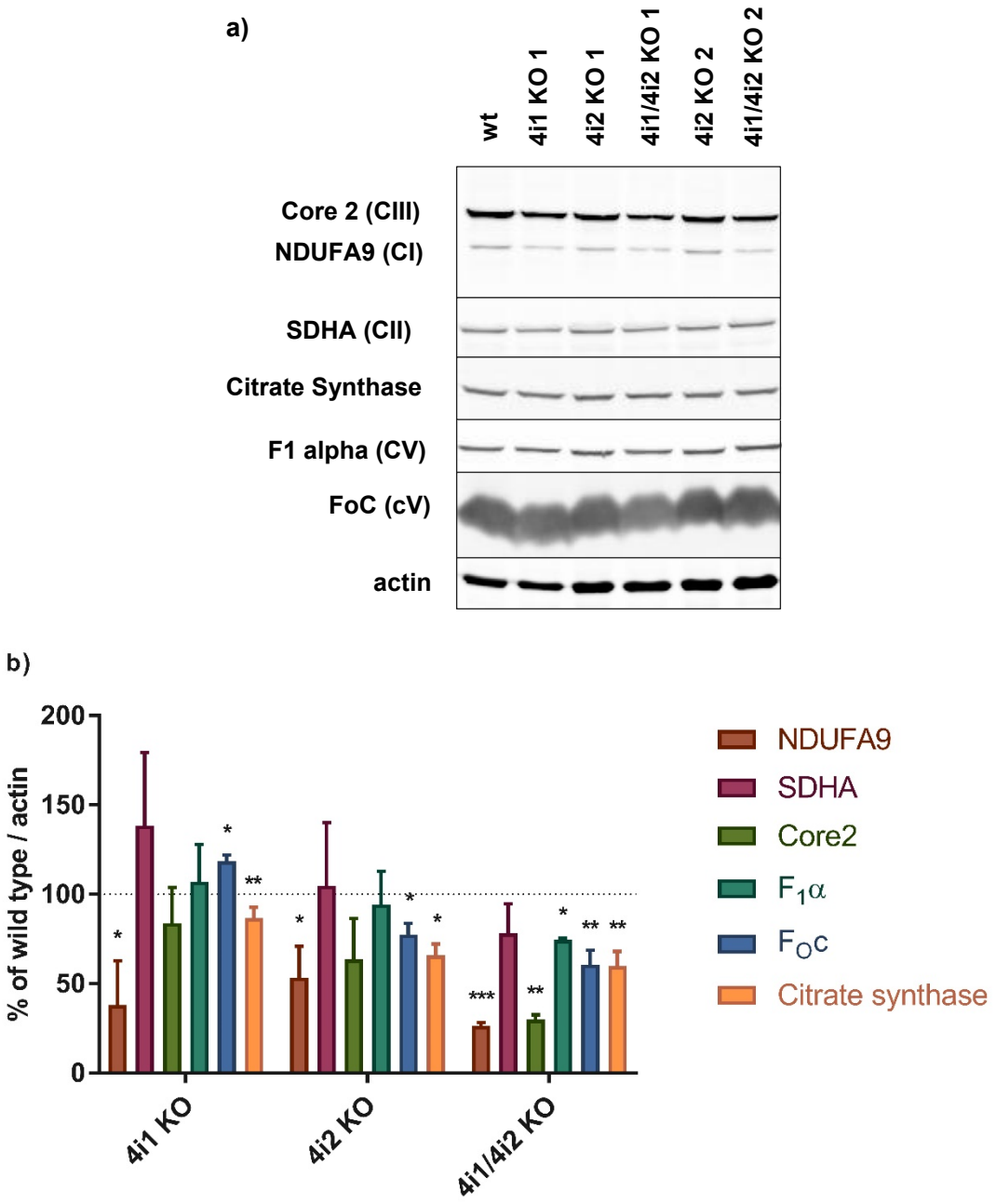

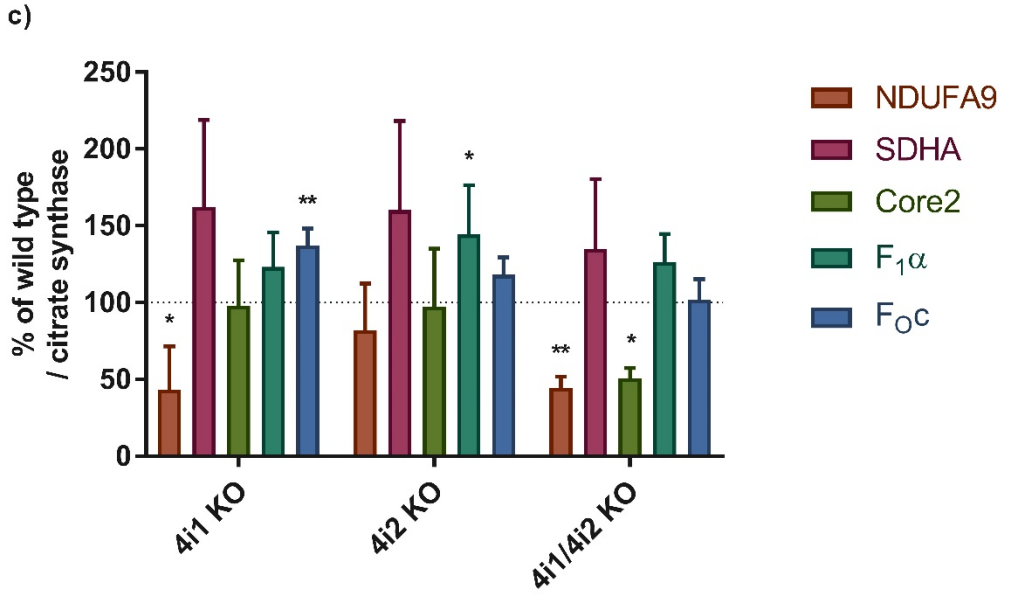

Figure 4.10: a) Representative Western blot analysis of OXPHOS complexes subunits in KO clones. Whole cell lysates (30 µg of protein) of COX4i1 KO, COX4i2 KO and COX4i1/4i2 KO clones were subjected to SDS-PAGE. Used antibodies are listed in Chapter 3.2.10. Actin antibody was used as a loading control. **b) Quantification of OXPHOS subunits content related to actin.** Plotted values represent percentage of wild-type. Asterisks (*) represent p-value: * < 0,05; ** < 0,01; *** < 0,001 (related to wild-type). Error bars represent SD. **c) Quantification of OXPHOS subunits content related to citrate synthase.** Plotted values represent percentage of wild-type. Asterisks (*) represent p-value: * < 0,05; ** < 0,01; *** < 0,001 (related to wild-type). Error bars represent SD. (n = 2)

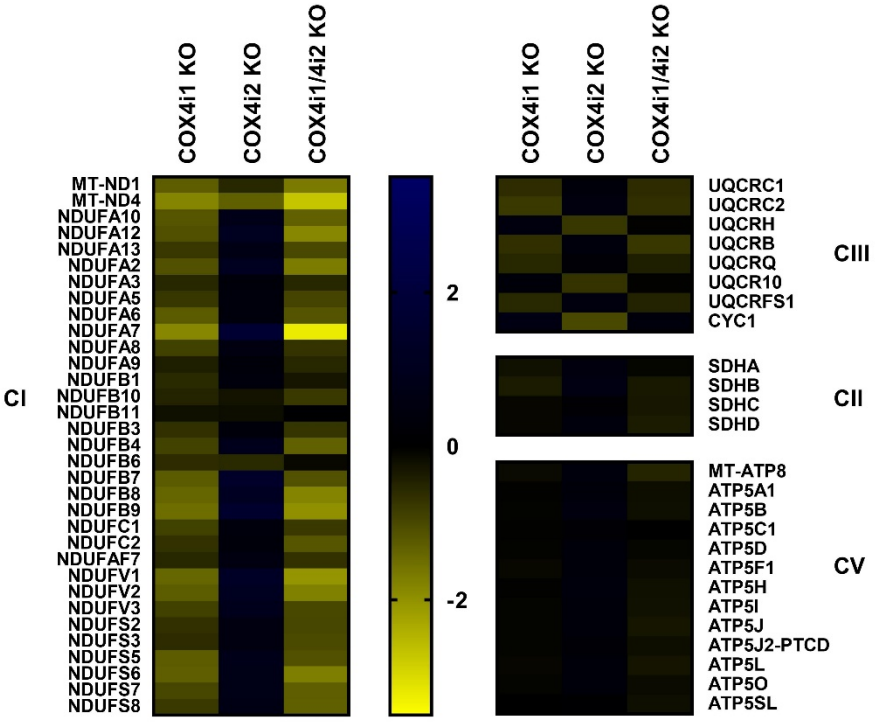

Figure 4.11: Proteomic analysis of OXPHOS complexes subunits using mass spectrometry label-free quantification (MS LFQ). Analysis revealed lower levels for majority of CI subunits in Cox4i1 and COX4i1/4i2 KO clones. To the contrary, CII, CIII and CV are not significantly affected by COX4I1 gene KO. Data in heat map represent log2 values of quantity fold-changes relative to wild-type.

4.2.3. Effect of COX4 KO on OXPHOS complexes content and assembly status

To examine effect of OXPHOS subunit changes caused by COX4I1 gene KO, content and assembly status of OXPHOS complexes in native state was studied by BN-PAGE followed by Western blot immunodetection (see Figure 4.12). Immunodetection with antibody against COX1 subunit revealed total absence of all assembled forms of COX enzyme in Cox4i1 and COX4i1/4i2 KO clones. Residual Cox1 subunit was detected migrating below 100 kDa, likely representing S1 assembly intermediate (see Figure 4.12 A). Early-incorporating subunit COX5a, which also showed residual content in SDS/PAGE experiments, was not detected in association with COX1 in COX4i1 or COX4i1/COX4i2 KO clones. In contrast, COX4i2 KO displayed band pattern and amount of COX-containing complexes comparable to wild-type, including COX monomer, dimer, III_2IV complex and $I_1III_2CIV_X$ supercomplexes (Figure 4.12 A). CI detection using anti NDUFA9 antibody also confirmed findings from SDS/PAGE and MS LFQ, showing profound decrease of CI content in COX4i1 and COX4i1/4i2 KO clones. Moreover, while in wild-type and COX4i2 KO CI was detected mainly in supercomplexes, the remaining CI in COX4i1-lacking clones was present as either free CI or I_1III_2 complex (Figure 4.12 B). CII content was unchanged in Cox4i1, COX4i2, and COX4i1/4i2 KO clones compared to wild-type (Figure 4.12 B). Detection of CIII complexes using antibody against Core2 subunit showed major changes of complex distribution in various assembly forms as a result of COX4i1 absence, rather than changes in enzyme content. While in wild-type and COX4i2 KO cells CIII is detected as CIII dimer, III_2IV and in supercomplexes, lack of COX following COX4i1 gene knock-out shifts almost all CIII to dimer form (Figure 4.12 C). Mild effect of COX absence was also observed in case of CV, detected by $F_1\beta$ antibody, which shows lower amount of CV dimer, and also minor accumulation of F_1 and F_1-c subassemblies in Cox4i1 and COX4i1/4i2 KO clones (Figure 4.12 D).

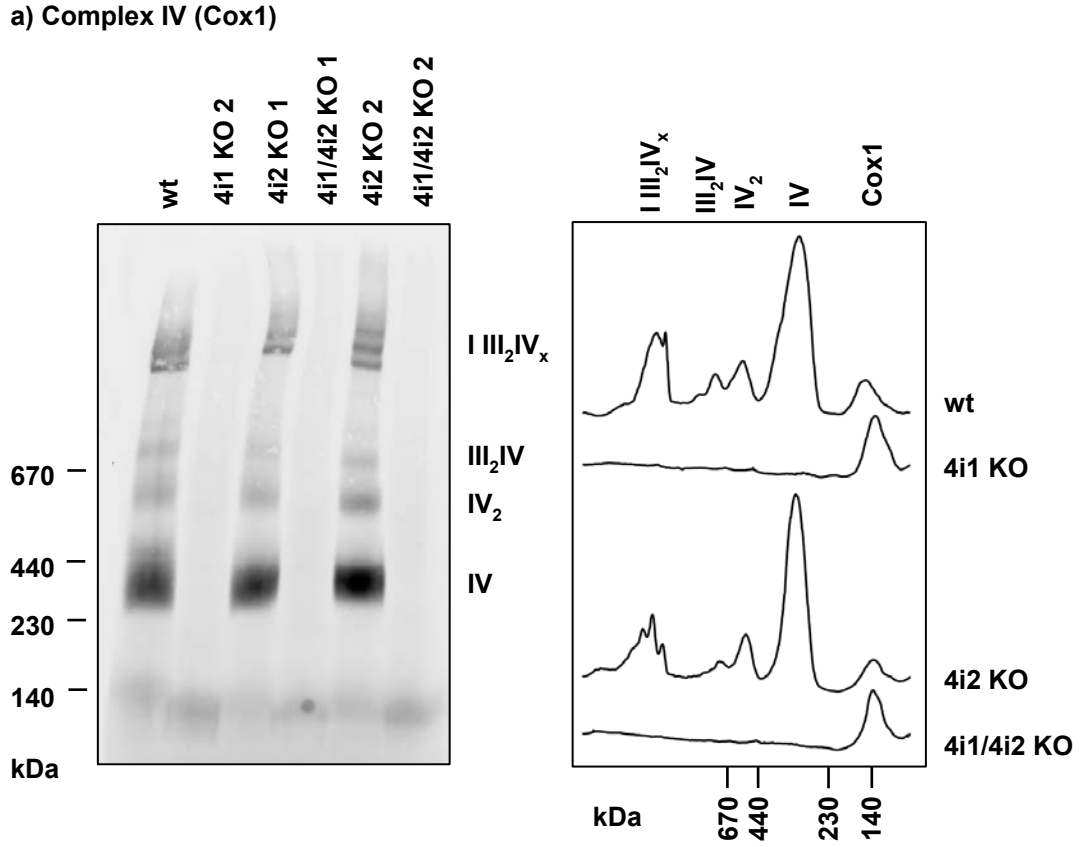
a) Complex IV (Cox1)
wt
4i1 KO 2
4i2 KO 1
4i1/4i2 KO 1
4i2 KO 2
4i1/4i2 KO 2
I III2IVx
III2IV
IV2
IV
670
440
230
140
kDa
I III2IVx
III2IV
IV2
IV
Cox1
wt
4i1 KO
4i2 KO
4i1/4i2 KO
kDa
670
440
230
140

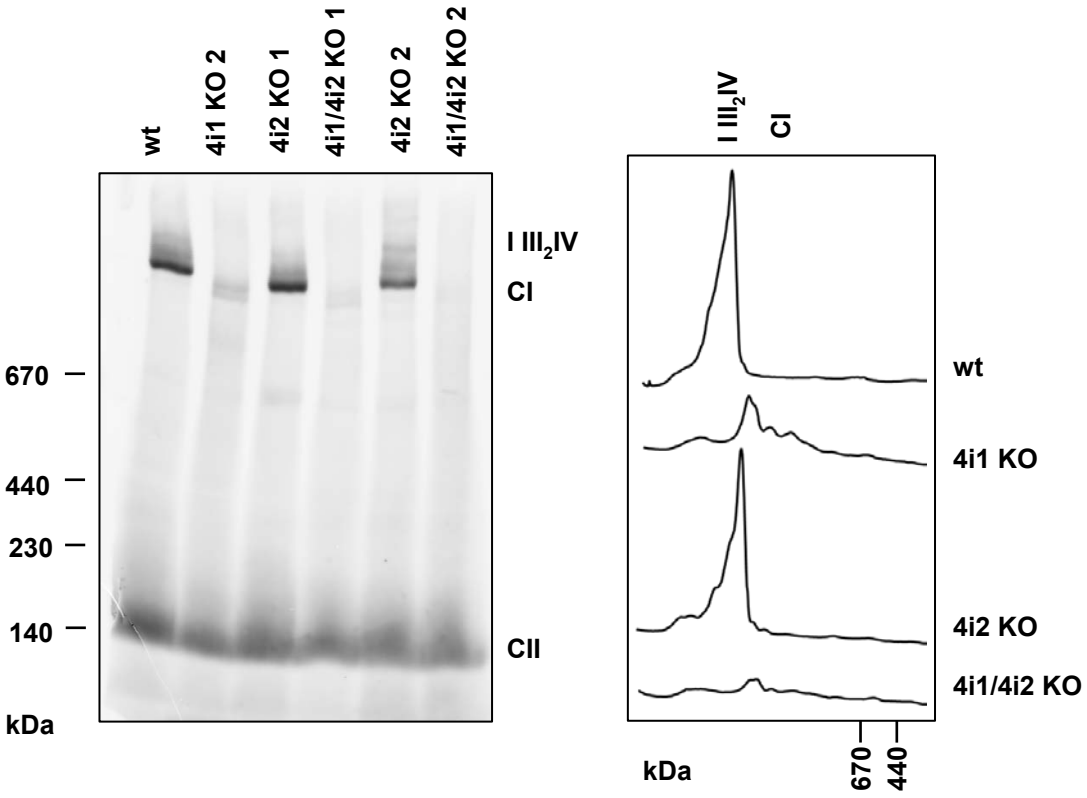
b) Complex I a II (NDUFA9, SDHA)
wt
4i1 KO 2
4i2 KO 1
4i1/4i2 KO 1
4i2 KO 2
4i1/4i2 KO 2
I III2IV
CI
CII
670
440
230
140
kDa
I III2IV
CI
wt
4i1 KO
4i2 KO
4i1/4i2 KO
kDa
670
440

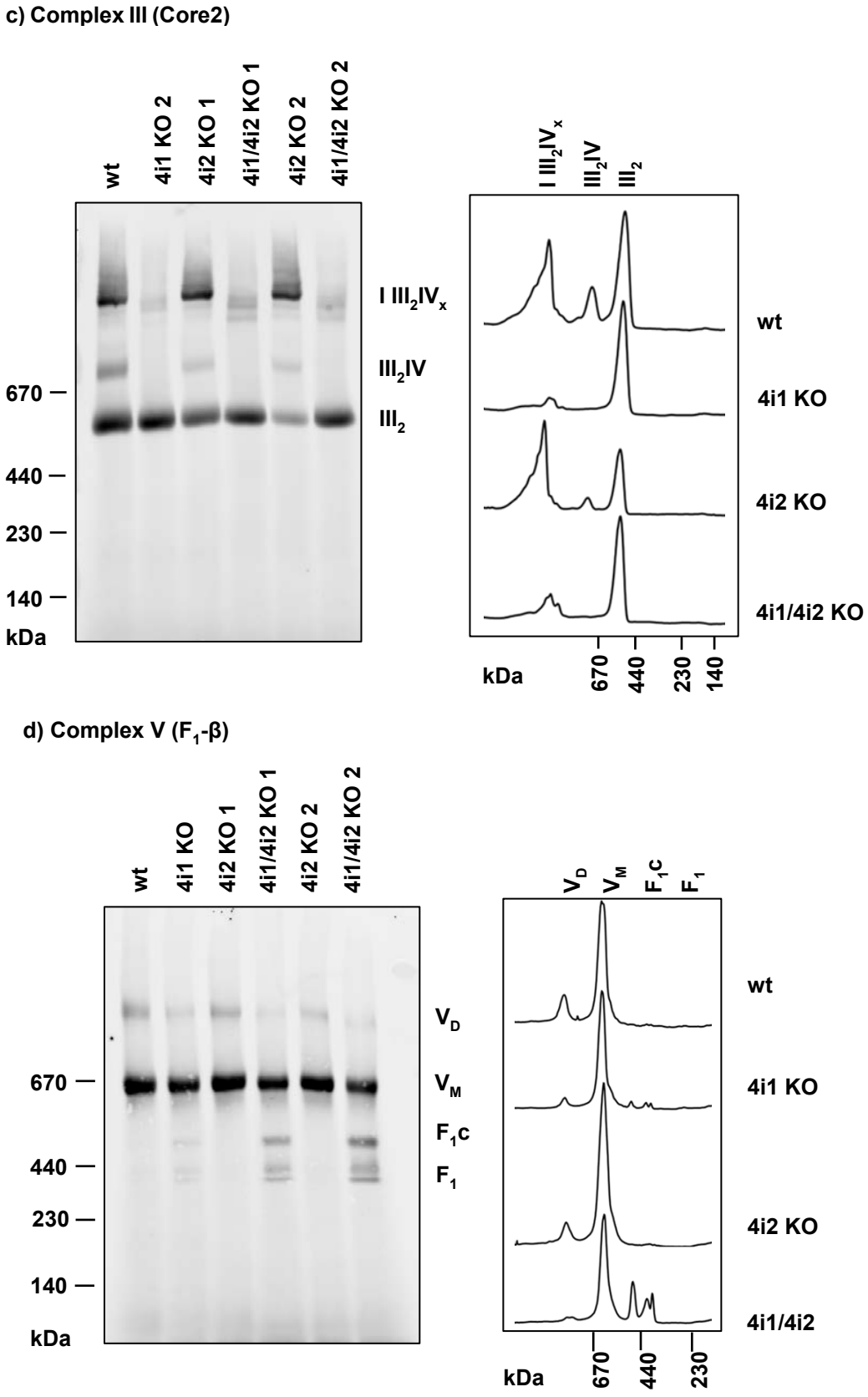

Figure 4.12: Representative Western blot analysis of OXPHOS complexes and supercomplexes with corresponding densitometric profile representation. Digitonin solubilized mitochondria (30 µg of protein) of COX4i1 KO, COX4i2 KO and COX4i1/4i2 KO clones were subjected to BN-PAGE. Used antibodies are listed in Chapter 3.2.10. Densitometric profile representation was prepared using mean values of intensity after Western blot analysis by AIDA Image Analyzer.

4.3. Pulse-chase analysis to elucidate mtDNA-encoded OXPHOS subunits turnover

Pulse-chase *in vivo* ^{35}S Met + Cys metabolic labelling of mtDNA-encoded OXPHOS subunits was performed to decipher, whether COX and CI deficiencies detected in electrophoretic analyses were due to subunit degradation following assembly impairment, or also caused by defect in earlier steps of protein expression. Labelled proteins were separated by SDS-PAGE and detected by phosphor storage screen fluorescence (Figure 4.13 A). Experiments revealed that majority of mtDNA-encoded OXPHOS subunits, with the exception of ATP6 and ATP8 components of CV, in COX4i1 and COX4i1/4i2 KO clones showed lower protein level against wild-type HEK293 cell line in the "pulse" samples, reflecting decreased rate of their proteosynthesis. To the contrary, COX4i2 KO clones were not affected and their pattern was comparable to wild-type. Detection of labelled proteins following the 24h hour chase in non-labelling medium allowed to estimate protein turnover. In general, levels of labelled proteins decreased compared to pulse in all analysed cell lines (Figure 4.13 A). Strikingly, Cox2/Cox3 double band completely disappeared during chase in COX4i1 and COX4i1/4i2 KO clones, while residual levels of Cox1 were still detected (Figure 4.13 B), reflecting their degradation due to inability to assemble, as suggested by previous data. Concerning other OXPHOS complexes, levels of CIII and CV components displayed higher stability than CI and CIV subunits in cells lacking COX4i1 (Figure 4.13 B), in agreement with data on steady-state levels of these complexes. Therefore, COX deficiency caused by COX4I1 gene KO may have deleterious effect on mitochondrial proteostasis, which affects OXPHOS complexes assembly and stability.

Interestingly, mining the MS LFQ data supported the hypothesis of disturbed mitochondrial translation, as content of mitochondrial ribosomal proteins showed mild, approximately 1.5-fold, but generalized decrease in COX4i1 and COX4i1/4i2 KO clones (see Figure 4.14). COX4i2 KO clones did not show such phenotype.

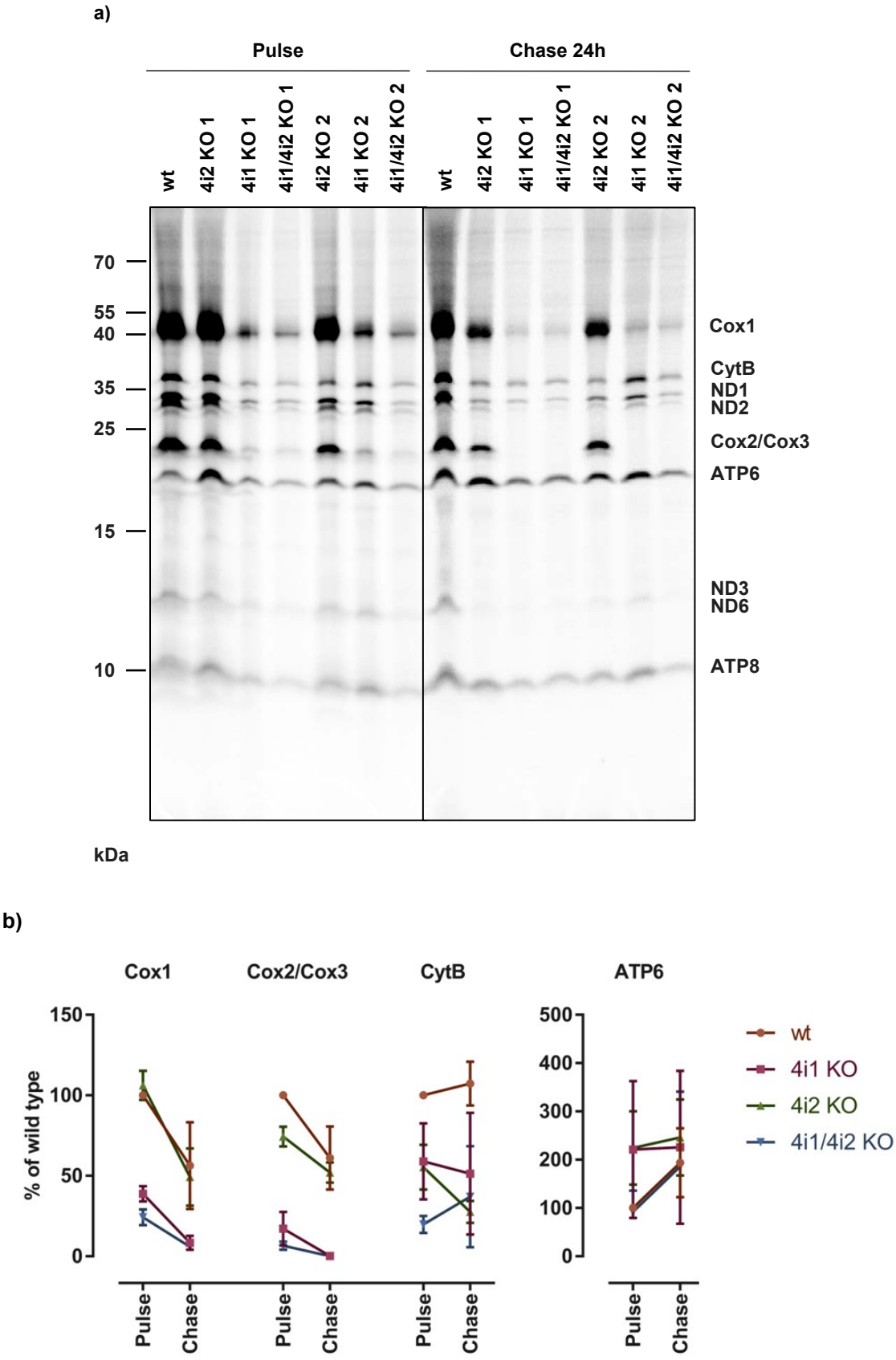

Figure 4.13: ^{35}S *in vivo* labeling of mtDNA-encoded OXPHOS subunits. a) Representative SDS-PAGE uncovers lower "pulse" level of most mtDNA-encoded proteins due to COX4i1 gene KO. **b) Quantitative analysis of pulse-chase experiments.** (n=2)

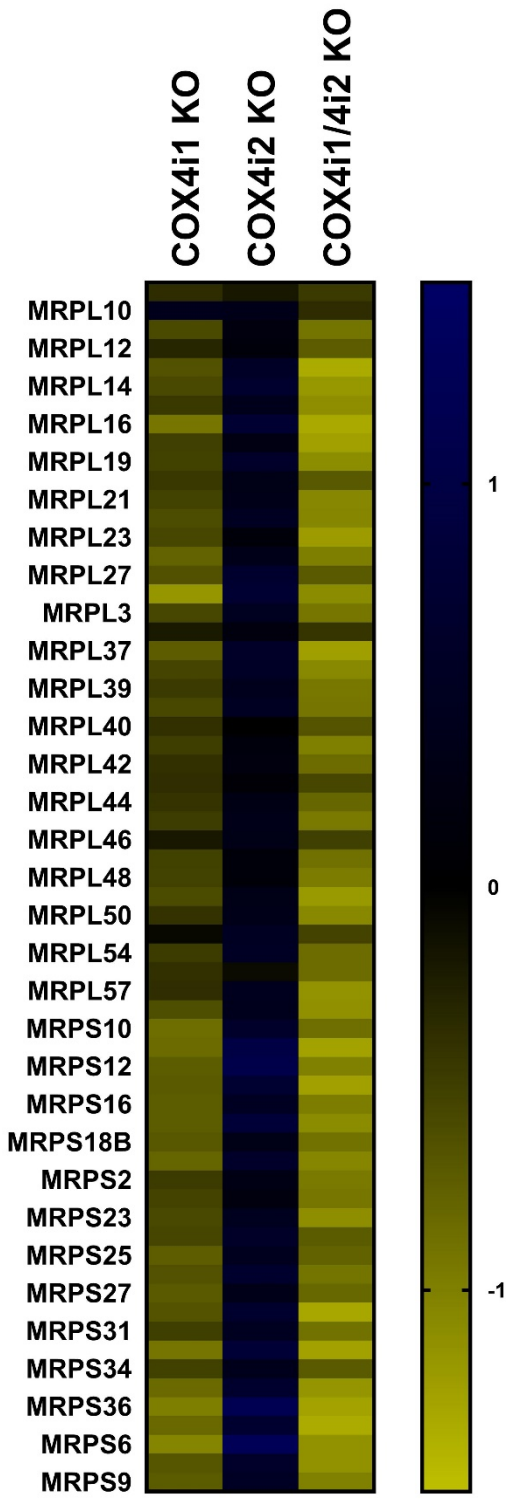

Figure 4.14: MS LFQ analysis reveals lower quantity of mitochondrial ribosomal proteins in Cox4i1 and COX4i1/4i2 KO clones. COX4i2 KO clones are comparable to wild-type HEK293 cell line. Data in heat map represent log2 values of quantity fold-changes relative to wild-type.

4.4. Quantification of mtDNA content

To examine possible effect of mtDNA content decrease on downregulation of mtDNA-encoded proteins, mtDNA quantification of KO clones was performed using GAPDH as a genomic standard gene and D-loop as a mitochondrial standard gene. Results (Figure 4.15) revealed significant decrease of mtDNA content of COX4i2 KO 1 (55% of wild-type) and COX4i1/4i2 KO clones 1 (66% of wild-type) and 2 (52% of wild-type). Observed mtDNA content decrease may alter expression of mtDNA-encoded proteins. However, changes in mtDNA content were not uniform in all KO clones which are, as single cell clones, unique.

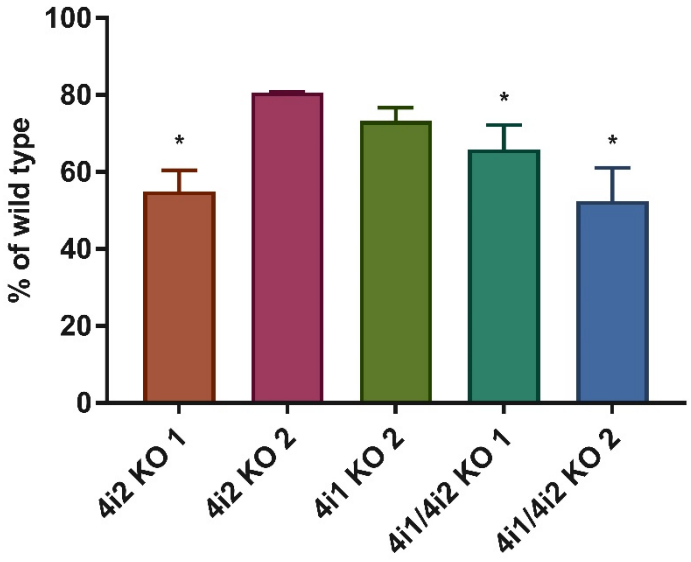

Figure 4.15: Quantification of mtDNA content. For determination of mtDNA content, GAPDH and D-loop genes were used as standard genes for genomic and mitochondrial DNA respectively. Plotted values represent percentage of wild-type firstly calculated as 2^{-dCt}, where dCt = ($Ct_{D\text{-}loop}$ - Ct_{GAPDH}). Asterisk (*) represent p-value < 0,05. Error bars represent SD. (n = 3)

4.5. Effect of COX4 KO on gene expression

OXPHOS subunits expression may also be affected by altered transcript levels. Thus, expression of selected OXPHOS subunits was studied by qPCR technique. Biological hexaplicates of each clone (4i1 KO 1, 4i1 KO 2, 4i2 KO 1, 4i2 KO 2, 4i1/4i2 KO 1, 4i1/4i2 KO 2) were studied as technical duplicates and compared to wild-type HEK 293 cells (biological pentaplicate, technical duplicate). Resulting quantities of each gene were normalized to geometrical mean of two housekeeping genes (B2M, HPRT-1). Results of individual clones were comparable between KO of COX4I1, COX4I2 and

COX4I1/COX4I2 genes, and they were plotted in common graphs as a percentage of wild-type (see Figure 4.16).

Cox1 transcripts did not show any significant changes in all KO clones. On the contrary, significant decrease was revealed in the case of Cox3 (COX4i1 KO 54 % of wt, COX4i2 KO 61 % of wt, COX4i1/4i2 KO 49 % of wt). Cox4i1 transcript signal oscillated around the limit of detection in COX4i1 (1,2 % of wt) and COX4i1/4i2 KO (0,7 % of wt) clones as an expected consequence of COX4I1 gene KO. COX3 transcript decrease was also observed in case of COX4i2 KO clone (61 % of wt).

Levels of mtDNA-encoded CI subunit ND1 transcript were not significantly changed between wild-type and any KO cells. On the other hand, significant changes occured in case of transcripts of CI subunits ND2 (COX4i1 KO 34 % of wt, COX4i1/4i2 KO 43 % of wt) and ND6 (COX4i1 KO 45 % of wt, COX4i1/4i2 KO 43 % of wt). Downregulation of these subunits transcription may alter protein level of these subunits and contribute to decrease of CI content in Cox4i1 and COX4i1/4i2 KO clones.

Interestingly, levels of CytB (CIII) and ATP6 (CV) transcript were significantly downregulated by approximately 50 % in all KO clones. For comparison, nuclear-encoded ATP5a ($F_1\alpha$ subunit of CV) transcript levels were comparable in all analyzed samples. In contrast, SDHB subunit of CII transcripts were decreased by 25 % in COX4i2 and COX4i2/4i1 KO, but remained unchanged in COX4i1 KO.

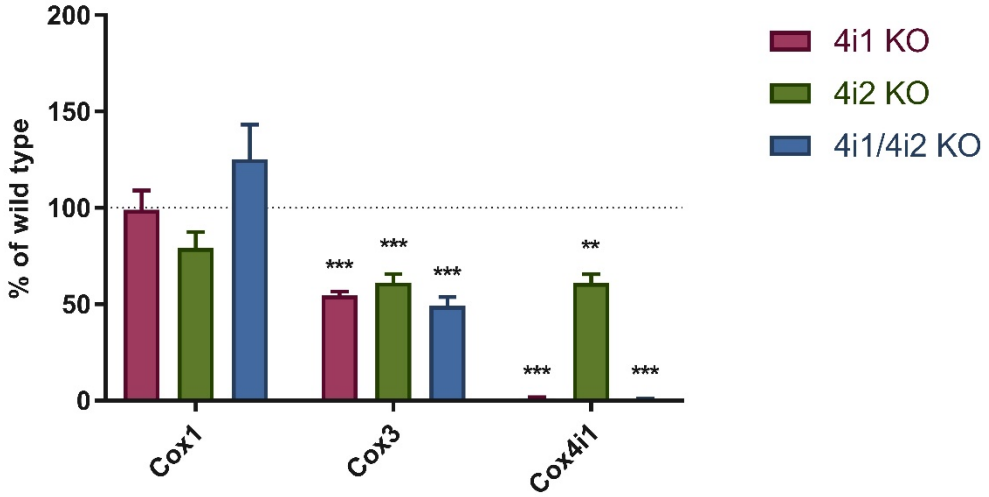

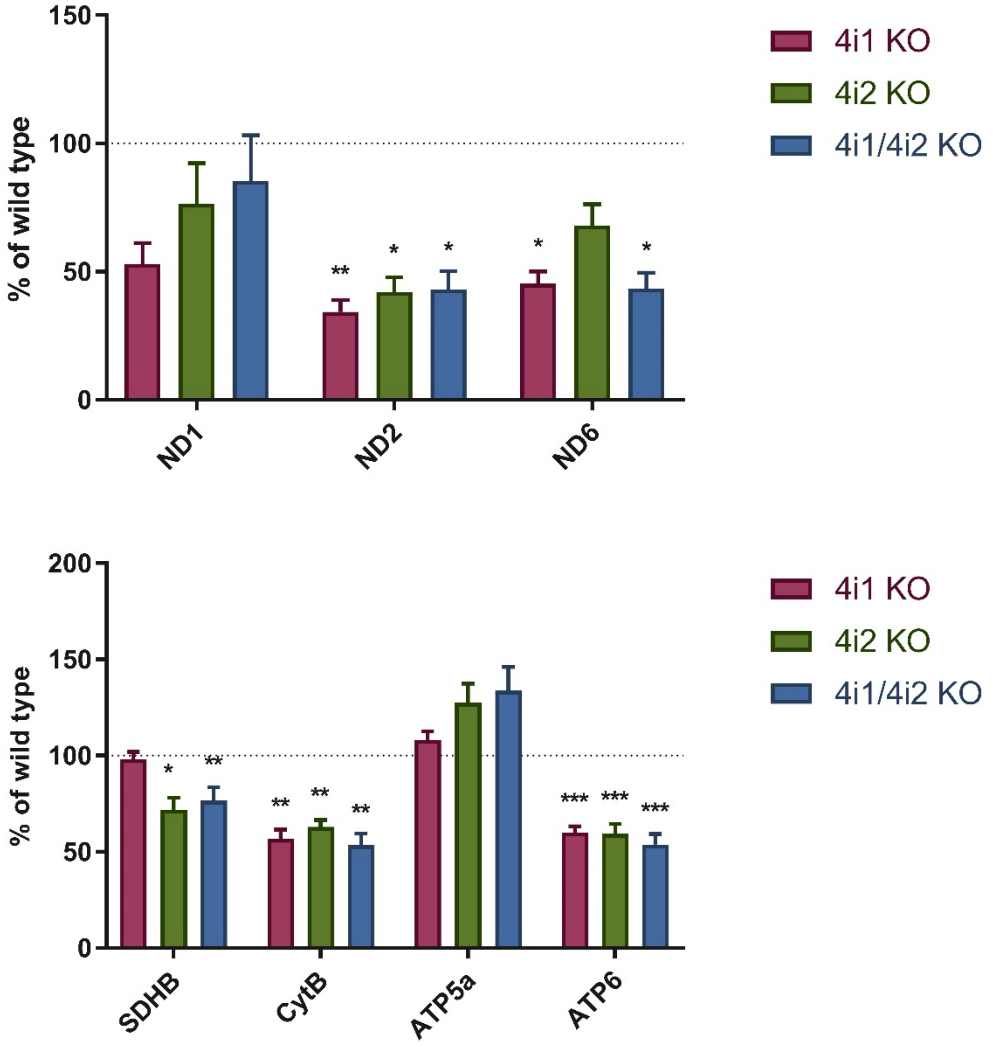

Figure 4.16: Determination of gene expression by qPCR technique. Shown data represent ratio of incriminated gene quantity per geometrical mean of two housekeeper genes quantity (B2M, HPRT-1). Asterisks (*) represent p-value: * < 0,05; ** < 0,01; *** < 0,001. Error bars represent SEM. (n = 6)

4.6. Functional characterization of Cox4 knock-out clones

4.6.1. Determination of bioenergetic phenotype

Seahorse Extracellular Flux (XF) Analyzer was used to examine rates of mitochondrial respiration and glycolysis, to characterize bioenergetic phenotype of KO clones (Figure 4.17, Figure 4.18).

During measurement, COX4i2 KO responded comparable to wild-type. After measurement of basal mitochondrial respiration (OCR, oxygen consumption rate) and glycolysis (ECAR, extracellular acidification rate), addition of oligomycin (inhibitor of CV) caused decrease of OCR, as oxygen consumption coupled to ATP synthesis was inhibited and compensated by increased glycolytic activity represented by ECAR.

Addition of chemical protonophore FCCP (which uncouples phosphorylation and oxidation processes) increased OCR, allowing to determine maximal ETC capacity. At this state, ECAR was slightly decreased. After last addition, rotenone (CI inhibitor), antimycin A (CIII inhibitor) and 2-deoxyglucose (competitive inhibitor of phosphoglucoisomerase), both OXPHOS and glycolysis were inhibited, therefore OCR and ECAR decreased to minimum and residual background rates were recorded.

As expected, COX4i1 and COX4i1/4i2 KO clones demonstrated complete absence of OXPHOS activity (OCR), neither they responded to additions of uncoupler or inhibitors. Thus, ATP production is independent on OXPHOS. Complete impairment of OXPHOS was compensated by increased glycolytic activity (ECAR) compared to control cells. Also, ECAR displayed no response to oligomycin, indicating that energy requirements of cells lacking Cox4i1 are met by steady rate of glycolysis, likely operating near its full capacity. ECAR rate seemed to be higher for COX4i1/4i2 KO clone than for COX4i1 KO clone. However, it probably reflected unique metabolic setting of individual KO clones. The recorded OCR and ECAR data from Seahorse measurement normalized to cell number are shown in Figure 4.17. In addition, basal OCR plotted versus ECAR for each cell line (phenogram) is displayed as a clear graphical data presentation enabling easy distinction between oxidative, glycolytic or quiescent cells. The same data are also displayed as OCR/ECAR ratios in Figure 4.18, indicating significant decrease in COX4i1/4i2 and COX4i1 KO, but not in COX4i2 KO cells.

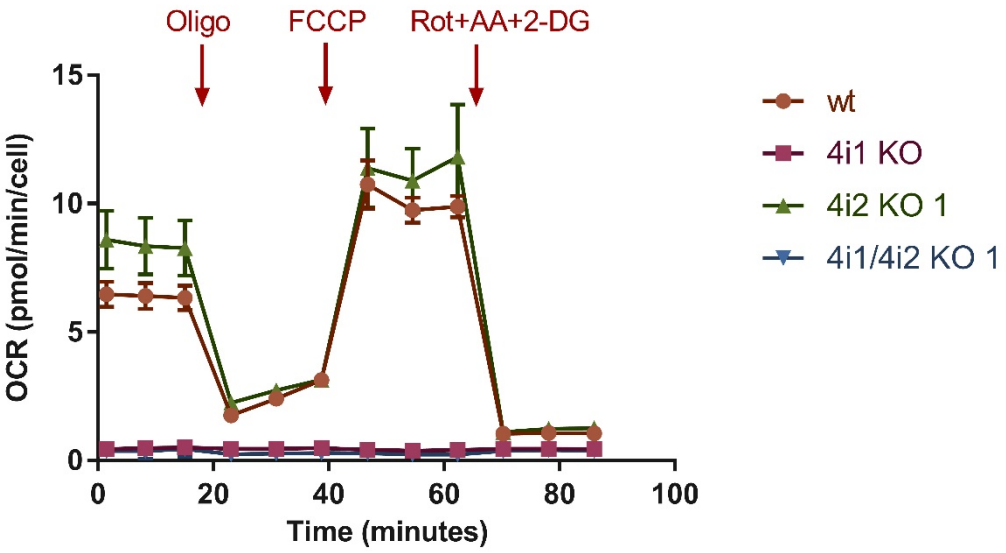

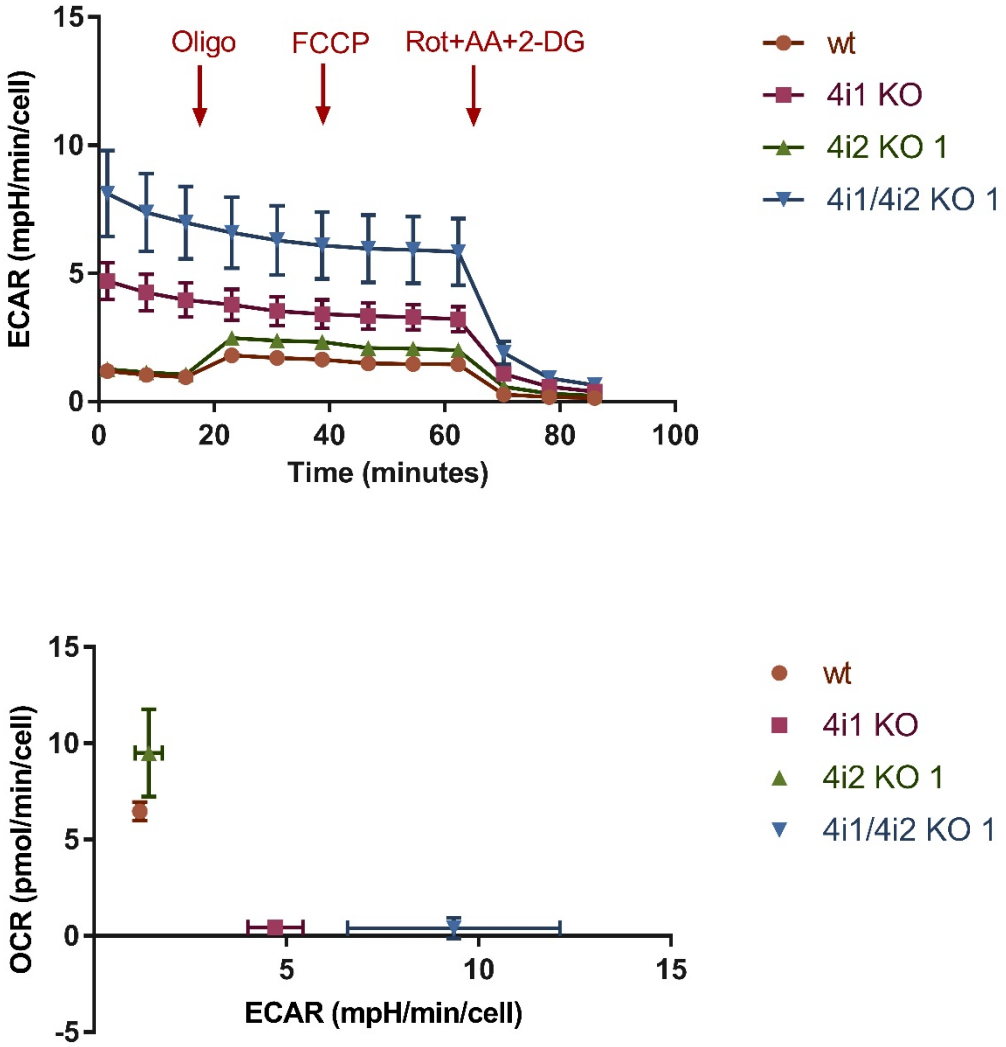

Figure 4.17: Representative parallel measurement of cellular oxygen consumption rate (OCR) and extracellular acidification rate (ECAR) demonstrate complete absence of mitochondrial OXPHOS activity in COX4i1 and COX4i1/4i2 KO clones. The shortfall of mitochondrial ATP provision is compensated by increased glycolytic activity. Scatter plot shows relation of OCR and ECAR at basal metabolic state. Metabolic phenotype of Cox4i2 KO clone is inclined to OXPHOS ATP production, while COX4i1 KO and COX4i1/4i2 KO clones are glycolytic/quiescent. (n=1)

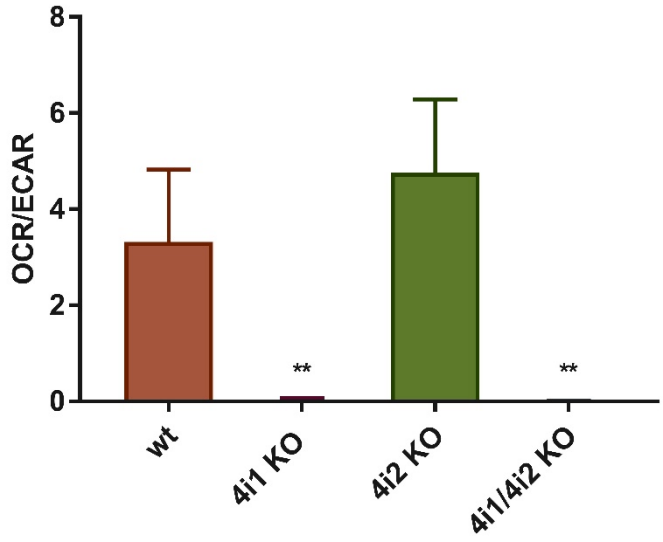

Figure 4.18: OCR/ECAR ratio at basal metabolic state represents significant decrease in COX4i1 KO and COX4i1/4i2 KO clones which corresponds to lost OXPHOS function due to COX4I1 gene KO. On the contrary, change in COX4i2 KO clones against wild-type is not significant. Asterisks (*) represent p-value: ** < 0,01. Error bars represent SD. (n =3)

4.6.2. Intact cell respiration of COX4i2 KO clones

As a complementary approach to compare intact cell respiration of COX4i2 KO clones to wild-type HEK293 cell line, high resolution respirometry using Oxygraph-2K OROBOROS was performed (Figure 4.19). Harvested cells suspended in oxygraph chamber were subjected to protocol analogous to Seahorse measurement. First, routine (basal) respiration on endogenous substrates was recorded, oligomycin was then added to inhibit OXPHOS ATP production to assess respiration compensating for proton leak. Afterwards, FCCP was used to uncouple respiration to assess maximal ETC capacity. Routine respiration and ETC capacity of COX4i2 KO 1 and COX4i2 KO 2 were not distinguishable from control. However, significant decrease of respiration in leak state was found in case of both COX4i2 KO clones.

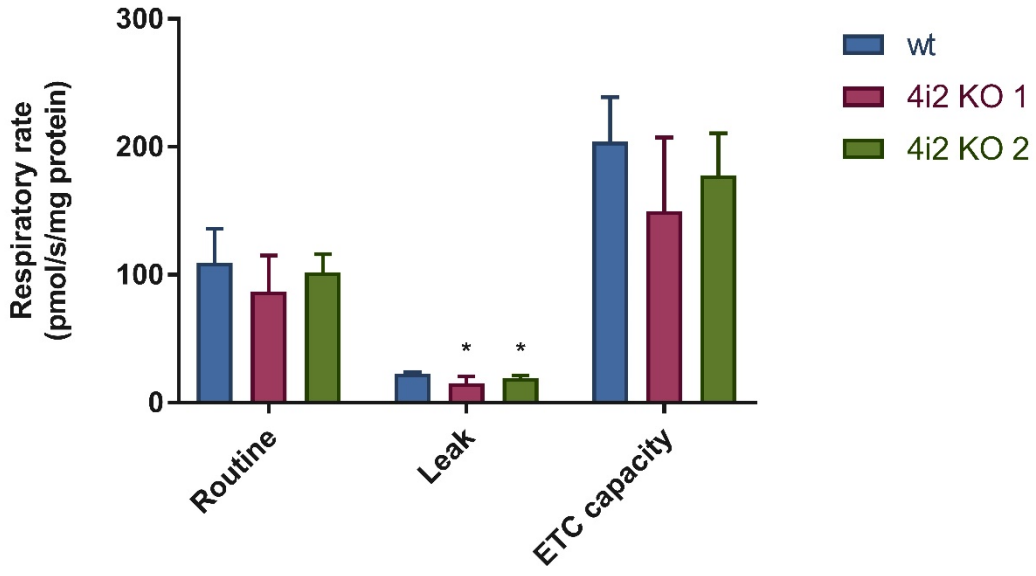

Figure 4.19: Respiratory rate of COX4i2 KO clones measured by oxygraphy OROBOROS.
Asterisk (*) represent p-value: * < 0,05. Error bars represent SD. (n=3)

5. Discussion

Cytochrome *c* oxidase, the terminal enzyme of electron transport chain, is an indispensable part of machinery needed for ATP production in mammalian cells (OXPHOS). Except three mitochondria-encoded subunits, which are necessary for COX catalytic function, ten nuclear-encoded subunits build up COX enzyme and participate on regulation of COX enzyme activity, as well as on regulation of whole OXPHOS system (Kadenbach and Merle, 1981; Tsukihara *et al.*, 1996). Even though nuclear-encoded subunits are known since 80's, the catalytic mechanism of COX enzyme involving the mitochondria-encoded subunits remained the main topic of COX research, while role of nuclear-encoded subunits was largely neglected. Since late 90's, attention of COX field has been drawn also to accessory proteins involved in COX biogenesis, triggered by identification of their mutations as a cause of severe inherited disorders. Recent discoveries of pathogenic mutations in genes encoding subunits Cox6a1, Cox6b1, Cox7b1, Cox7b2, Cox8 and Cox4i1, as well as novel genetic tools such as CRISPR technology, signal the right time to clarify the biological role of COX nuclear-encoded subunits.

5.1. HEK293 cell line as a cellular model for studying of Cox4 isoforms

Since the largest nuclear-encoded subunit's Cox4 isoforms (Cox4i1 and Cox4i2) were first described in mammals (Hüttemann, Kadenbach and Grossman, 2001), their biological relevance and differences between these two isoforms were studied on various organisms and on various tissues and cell lines with unclear Cox4i1 to Cox4i2 isoform ratio. It led to contradicting results concerning hypoxia induced isoform switch (Fukuda *et al.*, 2007; Aras *et al.*, 2015; Alexander-Shani *et al.*, 2017), activity of COX isozymes containing either Cox4i1 or Cox4i2 isoform, allosteric regulation of COX activity and role of three unique cysteine residues present in Cox4i2 isoform (Hüttemann, Kadenbach and Grossman, 2001; Oliva *et al.*, 2015; Schiffer *et al.*, 2016; Sommer *et al.*, 2017). Thus, many questions regarding COX isozymes (containing Cox4i1 or Cox4i2 isoform) biological role remain to be answered. Therefore, unique HEK293 cell line-based knock-outs of COX4i1, COX4i2 and both COX4i1/COX4i2 genes were prepared (using CRISPR knock-out technology) to establish tool for preparation of either COX4i1 or COX4i2 isoform knock-in models. These knock-in models will be used to investigate

functional differences between Cox4i1 and Cox4i2 isoforms, which represent controversial topic on the field of mitochondrial physiology.

HEK293 cell line was used for KO preparation, as other research groups study COX enzyme in this model (Fornůsková *et al.*, 2010b; Richter-Dennerlein *et al.*, 2016), and also for an excellent experience with CRISPR knock-out technology using this cell line in our laboratory. Unfortunately, COX4i1 gene locus is situated on chromosome 16, which is tetraploid within HEK293 cell line (Kim *et al.*, 2009). Therefore, COX4i1 KO sequencing screen, resulted in undecipherable overlapping nucleotide sequences. Usage of different cell line would be helpful to avoid this problem. But, for example another commonly used HeLa cell line karyotype reports 3 copies of chromosome 16 (Heneen, 1976). To prevent multiploidy, near-haploid human cell line HAP1, used in OXPHOS complexes research (He *et al.*, 2017), could be used for this study, but physiological relevance would be diminished by such an intervention on normally diploid karyotype of human cells. However, difficulties with tetraploid chromosome 16 were easily overcome by TA cloning resolving individual sequences of COX4i1 gene KO clones, while CRISPR KO introduction was still efficient despite of tetraploid chromosome 16.

Under normoxia, Cox4i2 protein is undetectable in HEK293 cell line by Western blot analysis. However, it was already published that Cox4i2 isoform is induced in HEK293 cell line after hypoxic activation (Fukuda *et al.*, 2007; Aras *et al.*, 2013). Thus, it is impossible to study Cox4 isoforms differences directly on prepared COX4i1 KO and COX4i2 KO clones under normoxia. Moreover, there is a possibility of Cox4i2 isoform expression activation under hypoxia, which may influence experiments with COX4i1 KO clones during hypoxic incubation.

With all considerations, HEK293 cell line proved suitable for preparation of CRISPR based COX4i1, COX4i2 and COX4i1/4i2 gene KO, while COX4i1/4i2 KO clone will be further used as a tool for knock-in of either COX4i1 or COX4i2 isoform to study their biological role.

5.2. COX4i2 gene KO phenotype

At first, COX4i2 gene KO clones were established. As HEK293 cells do not constitutively express Cox4i2 protein, it was easier to produce these KO clones, as we expected their viability would not be affected by COX4i2 gene knock-out as much as by

COX4i1 gene KO. Two COX4i2 KO clones (COX4i2 KO 1, COX4i2 KO 2) were selected by sequencing screen. These KO clones were used to produce COX4i1/4i2 double KO clones and subjected to various experiments to characterize their phenotype along with other cellular models established in this project.

Densitometric quantification of steady-state content of five COX subunits in COX4i2 KO clones showed changes against wild-type HEK293 cells only when data were normalized to actin levels (55 – 120 % of controls with significant decrease of Cox2 content), while upon normalization to citrate synthase levels, COX subunits content was unaffected. Citrate synthase is considered as a marker of mitochondrial amount. However, MS LFQ data mining did not reveal any significant changes in citrate synthase level against wild-type, which could have explained lower COX subunits level (upon normalization to actin level) by decreased mitochondria amount. But, interestingly, actin level was mildly decreased in both COX4i2 KO clones, which explains various significance of OXPHOS subunits changes due to different normalization. Interestingly, while actin is frequently used as a loading control, its reliability for protein normalization in semiquantitative Western blot analysis has been already questioned (Wiśniewski and Mann, 2016).

Consistently with data obtained by normalization to citrate synthase level, MS LFQ data also suggest COX subunits content of COX4i2 KO clones comparable to wild-type, with no significant changes. Combination of both approaches, SDS-PAGE followed by Western blot with immunodetection and MS LFQ, was used within this study, which proved advantageous for data interpretation. Representative subunits of OXPHOS complexes were also unaffected by COX4i2 gene KO, if we take in account changed actin level, in agreement with MS LFQ data.

However, the possibility of decreased mitochondrial amount in COX4i2 KO clones should not be completely disregarded, as significant decrease of mtDNA content was found in COX4i2 KO 1 (55 % of wild-type) and also in COX4i2 KO 2 (81 % of wild-type). However, such a decrease may also represent random fluctuation, which got fixed during the selection of single cell colonies, representing potential disadvantage of this approach. To use polyclonal cell population as an alternative is not possible, due to low efficiency of CRISPR knock-out. This could however be circumvented if CRISPR would have been used in gene-editing mode introducing selectable marker in the gRNA targeted site (Ran *et al.*, 2013). Moreover, significant decrease of some transcripts (Cox3, Cox4i1,

ND2, SDHB, CytB, ATP6) found in COX4i2 KO clones may be also altered by decrease in mtDNA quantity.

Pulse-chase experiment for examination of mtDNA-encoded OXPHOS subunits turnover revealed, that Cox1 and Cox2/Cox3 subunits display similar protein level in pulse against wild-type, as well as in chase. Difference against wild-type was observed in case of CytB, which showed lower protein level in "pulse", and faster degradation during the 24 hours of "chase". However, MS LFQ data show similar content of mitochondrial ribosomal proteins in COX4i2 KO clones compared to wild-type. Thus, mitochondrial translation is not affected by COX4i2 gene KO in HEK293 cell line.

As expected, assembly processes of COX and other OXPHOS complexes (CI, CII, CIII, CV) were not affected by COX4i2 gene KO, which correlates with finding of altered actin levels in COX4i2 KO clones, while decreased content of some subunits would affect OXPHOS complexes assembly. Also, COX-containing supercomplexes were detected in COX4i2 KO clones comparably to wild-type.

COX4i2 gene KO did not have any impact on mitochondrial respiration, as metabolic phenotype determined by Seahorse assay was comparable to wild-type. Also, respiration states of intact COX4i2 KO cells measured by OROBOROS Oxygraph-2k were not significantly changed.

Thus, no significant and functionally relevant changes in comparison with wild-type HEK293 were observed within COX4i2 KO clones, due to unexpressed Cox4i2 isoform in HEK293 cell line under normoxia. However, choosing another cell line with more reliance on isoform 2 would be complicated, as publicly available expression data reveal a single cell line enriched by Cox4i2 transcripts - SH-SY5Y7 (cell line cloned from a bone marrow biopsy derived cell line SK-N-SH) (The Human Protein Atlas, 2017). The most physiologically relevant model for Cox4i2 isoform research would be pulmonary artery smooth muscle cells (PASMCs) (Sommer *et al.*, 2017), but as a primary culture, PASMCs are not appropriate for long-term multi-passage cultivation necessary during preparation of knock-out/knock-in cellular models.

5.3. COX4i1 gene KO effect on COX enzyme

Preparation of COX4i1 gene KO clones was a risky part of this project, as it was uncertain that COX4i1 gene knock-out cells would be viable. Moreover, high-throughput

study employing CRISPR Death Screen searching for OXPHOS essential genes identified COX4i1 gene as KO-lethal (Arroyo *et al.*, 2016). Consequently, no study used COX4i1 gene mammalian KO cellular model yet.

With targeted approach, we have prepared COX4i1 KO clones and also COX4i1/4i2 KO clones using mentioned COX4i2 KOs. However, preparation was complicated due to highly glycolytic phenotype of COX4i1 gene KO cells, which was observable already during cultivation of the cells, while medium was exhausted faster against wild-type HEK293 cells. Also, only six out of 100 selected single cell clones were verified by sequencing as actual knock-outs, while they displayed the slowest proliferation rate due to severe metabolic impairment due to COX4i1 gene KO. Considering experience with COX4i1 gene KO models preparation, we suggest targeted approach in further essential OXPHOS genes KO preparation, requiring careful handling during cultivation of resulting fragile cells.

Missing Cox2 catalytic core subunit observed during Western blot selection of KO clones predicted downregulation of COX subunits content. Indeed, steady-state content of COX subunits determined by SDS-PAGE followed by Western blot in COX4i1 KO and COX4i1/4i2 KO clones showed overall significant decrease against wild-type, regardless normalization to actin or to citrate synthase level. This apparent general decrease of COX subunits was also confirmed by MS LFQ. The most affected subunit Cox2, which is below detectable level on Western blot, indicates inability to assemble COX catalytic core in COX4i1 gene KO resulting in COX loss of function.

Possible compensation of Cox4i1 isoform loss by expression of the second isoform, Cox4i2, was tested, as this mechanism was described while lost Cox7a-H was substituted by its partner, Cox7a-L isoform, in Cox7a-H KO mice heart (Hüttemann, Klewer, *et al.*, 2012). However, Cox4i2 isoform was not detected even after COX4i1 gene KO, thus substitution of missing Cox4 isoform 1 by Cox4i2 isoform was not activated in HEK293 cells. Therefore, switch of Cox4 isoforms depends on isoforms expression regulation. Isoform switch in HEK293 cells is improbable due to the fact that Cox4i2 isoform is not expressed in this cell line under normoxia.

As Cox4 is an early-assembly state subunit (Stibůrek *et al.*, 2006; Dennerlein and Rehling, 2015), impaired assembly of COX enzyme was expected in COX4i1 and COX4i1/4i2 KO clones. Native electrophoresis confirmed these expectations. Using Cox1 antibody, only unassembled Cox1 subunit was detected, most likely present as S1

intermediate. Accumulation of COX1-containing subcomplexes represents common feature of various COX assembly defects (Pecina *et al.*, 2004; Stiburek *et al.*, 2005; Stibůrek and Zeman, 2010). COX enzyme monomer and dimer were undetected. Moreover, complete absence of fully assembled COX enzyme was coupled with impairment of supercomplexes containing COX, III_2IV and $I_1III_2IV_x$ (respirasome). Therefore, Cox4 subunit is indispensable for COX assembly process (Dennerlein and Rehling, 2015).

Quantification of mtDNA revealed non-significant decrease in COX4i1 KO clone (73% of wild-type), while significant decrease was displayed by COX4i1/4i2 KO 1 (66 % of wild-type) and COX4i1/4i2 KO 2 (52% of wild-type). Decreased mtDNA content in COX4i1/4i2 KO clones might have persisted already from COX4i2 KO clones used for their preparation. However, possible decrease of mitochondria amount does not have an impact in the case of COX4i1 gene KO clones, while COX subunits content is comparably downregulated using normalization to actin or to citrate synthase level. Therefore, the advantage of establishing COX4i1 KO clones includes identifying of the genuine specific effects of COX4i1 absence in COX4i1/4i2 KO clones.

Decrease of COX subunits observed by SDS-PAGE/Western blot could be caused by overall downregulation of mitochondrial transcription, thus mtDNA-encoded subunits Cox1 and Cox3 expression was determined by qPCR technique. However, significant changes were not observed in the case of subunit Cox1 in COX4i1 KO and COX4i1/4i2 KO clones. On the other hand, Cox3 subunit transcripts displayed significantly lowered level against wild-type. Therefore, obtained data suggest that COX4i1 gene KO does not affect mitochondrial transcription in general, but levels of some transcripts may be secondarily influenced. Moreover, obtained data may be affected by decreased mtDNA content found in individual KO clones, possibly resulting in decreased transcripts quantities.

Significant decrease of steady-state level of catalytic core subunits Cox1 and Cox2 was expected to be caused by degradation of these subunits due to impaired COX enzyme assembly in COX4i1 KO and COX4i2 KO clones, i.e. faster turnover of mtDNA-encoded proteins against wild-type HEK293 cells. Interestingly, *in-vivo* metabolic labelling revealed, that turnover rate of Cox1 and Cox2/Cox3 subunits is after COX4i1 gene KO comparable to wild-type. Strikingly, difference was found already in the "pulse" samples of COX4i1 KO and COX4i1/4i2 KO clones, where Cox1 and Cox2/Cox3 protein levels

were noticeably decreased. It indicated unexpected effect of COX4i1 gene KO on mitochondrial proteosynthesis, which is impaired/downregulated. Moreover, MS LFQ data supports this hypothesis, because data analysis revealed, that compared to wild-type, mitochondrial ribosomal proteins levels are decreased. Thus, COX4i1 gene KO does not affect only COX enzyme itself, but as a secondary effect, impairs mitochondrial proteosynthesis, therefore possibly also other OXPHOS complexes.

These results correlate with published findings revealing existence of COX assembly regulation by assembly-controlled translational plasticity, while absence of early-assembly nuclear-encoded subunits (also Cox4) leads to arrest of Cox1 subunit translation, while remains present as a ribosome-nascent chain complex containing MITRAC component C12ORF62. Therefore, COX enzyme can't be assembled. Moreover, COX1 transcripts may be preferentially bound by mitochondrial ribosomes, which explains more prominent decrease of Cox2 and Cox3 subunits level in "pulse" (Richter-Dennerlein *et al.*, 2016).

Catalytic function of COX enzyme in COX4i1 KO clones was expected to be impaired, even lost, due to loss of catalytic core mtDNA-encoded subunit Cox2 indispensable for COX catalytic function (Kaila, Verkhovsky and Wikström, 2010). Results of Seahorse measurement fulfilled our expectations, while Cox4i1 KO and COX4i1/4i2 KO clones demonstrated complete absence of oxygen consumption (OCR), thus OXPHOS activity. Impaired OXPHOS function was compensated in COX4i1 KO and COX4i1/4i2 KO clones by increased glycolytic activity (ECAR). Therefore, ATP production is independent on OXPHOS and energy demands of COX4i1 KO cells are covered by ATP production on substrate level, glycolysis. ECAR rate was higher in COX4i1/4i2 KO clone than in COX4i1 KO clone. However, it likely reflects uniqueness of individual KO clones, which underwent single cell selection.

5.4. COX4i1 gene KO effect on Complex I

Studying of OXPHOS complexes already revealed, that these complexes are not linked only by its function, but also by individual complexes assembly and maintenance. The best understood is relation between CI and CIII, assembly and stability of these complexes is linked (Ugalde *et al.*, 2004; Diaz, Enríquez and Moraes, 2012). Moreover, presence of respiratory supercomplex, respirasome, is suggested as essential for assembly of CI (Moreno-Lastres *et al.*, 2013).

Phenomenon of interdependency was also found between COX and CI, while COX deficiency is coupled with decreased CI level in both monomeric and supercomplexes-associated enzyme. Moreover, interdependency occurs only in case of complete COX absence, resulting from complete block of early assembly phases (Diaz *et al.*, 2006; Li *et al.*, 2007). Results of this thesis approve the interdependency between COX and CI by various experiments.

First, steady-state levels of OXPHOS complexes displayed significant decrease of representative CI subunit NDUFA9 in COX4i1 KO and COX4i1/4i2 KO clones, which was also verified by MS LFQ data, which showed overall decrease of CI subunits compared to wild-type HEK293 cell line. Therefore, impairment of CI caused by total COX absence is noticeable even on steady-state level of its subunits content, which suggest decrease of assembled CI content.

Amount of fully assembled CI monomer was decreased in COX4i1 KO and COX4i1/4i2 KO clones (compared to wild-type) in native electrophoresis experiments. Moreover, supercomplexes loss due to COX absence was observable also by NDUFA9 immunodetection. Interestingly, one study suggested presence of respirasome as essential for CI assembly (Moreno-Lastres *et al.*, 2013). Therefore, one of possible links from COX4i1 gene KO to CI assembly impairment may be absence of respiratory supercomplexes containing COX due to total absence of fully assembled COX enzyme. This hypothesis is further developed by study, which showed that even residual portion of assembled COX enzyme, due to assembly defects, is sufficient to maintain assembled CI (Timón-Gómez *et al.*, 2017). Indeed, knock-down of Cox4i1, where residual portion of COX is maintained did not cause any decrease in CI content (Fornůsková *et al.*, 2010a). Moreover, possible link between CI and COX was found, MITRAC component MITRAC15, which besides association with ribosomes is required for COX and CI assembly (Mick *et al.*, 2012). Thus, MITRAC complex may have impact on assembled CI amount in COX4i1 gene KO clones. However, true nature of COX/CI interdependency remains to be uncovered.

Decreased amount of CI subunits, therefore assembled CI itself, could be also caused by altered mitochondrial transcription due to COX4i1 gene KO. However, qPCR experiment did not reveal clear results. MtDNA-encoded CI subunit ND1 was comparable to wild-type, while significant changes were observed in transcripts of CI subunit ND2 (COX4i1 KO 34 % of wt, COX4i1/4i2 KO 43 % of wt) and ND6 (COX4i1

KO 45 % of wt, COX4i1/4i2 KO 43 % of wt). However, overall effect of COX4i1 gene KO on mitochondrial transcription was not observed.

In contrast, interesting results yielded from in-vivo labelling of mtDNA-encoded OXPHOS subunits. Experiment revealed, that "pulse" protein levels of CI subunits (ND1, ND2, ND3, ND6) in COX4i1 KO and COX4i2 KO clones are noticeably decreased compared to wild-type. Therefore, general impairment of mitochondrial proteosynthesis affects CI, as a secondary effect of COX4i1 gene KO in HEK293 cell line. On the contrary, turnover rate of CI subunits seems to be unchanged in comparison to wild-type. Thus, expected changed turnover linked to degradation of mtDNA-encoded proteins is not observed. These results are in conflict with publication, which presents impaired stability of CI due to COX absence (caused by COX1 gene nonsense mutations). Authors explain decreased stability of CI by increased activity of mitochondrial m-AAA protease (Hornig-Do *et al.*, 2012).

5.5. COX4i1 gene KO effect on Complex II, Complex III and Complex V

COX4i1 gene KO was found to have no significant effect on other OXPHOS complexes (outside COX and CI). MS LFQ data revealed that of content of CII, CIII and CV subunits is comparable to wild-type. However, some significant changes were observable after quantification analysis of SDS-PAGE/Western blot experiment.

Interestingly, significant decrease of Core2 subunit of CIII was found in COX4i1/4i2 KO but not in COX4i1 KOs. The reason may be decreased mitochondria content displayed by decreased mtDNA content in COX4i1/4i2 KO clones (COX4i1 KO clone was unaffected). However, despite this significant change in Core2 protein level, assembly or stability of CIII was not changed. Only difference found by native electrophoresis is redistribution of CIII from supercomplexes to CIII dimer due to absent COX caused by COX4i1 gene KO.

Complex V showed significant decrease of $F_1\alpha$ in COX4i1/COX4i2 KO clones normalized to actin protein level (75% of wild-type), while normalization to citrate synthase protein level did not display decrease in both COX4i1 KO and COX4i1/4i2 KO clones. Therefore, this change is not considerable due to altered actin level found by MS LFQ in COX4i1/4i2 KO clones. On the contrary, F_Oc subunit showed significant increase in COX4i1 KO clones (normalized to both, actin and citrate synthase). This finding could

represent compensatory mechanism, similarly as was described in case of COX assembly defect caused by SURF1 mutations (Kovářová *et al.*, 2012). Interestingly, native electrophoresis revealed decreased amount of CV dimer and presence of assembly intermediates of F_1 domain. The cause of F_1 subassemblies presence in COX4i1 and COX4i1/4i2 KO clones, resembling band patterns in mild CV assembly defects (Hejzlarová *et al.*, 2014), may result from imbalance between levels of nuclear and mtDNA-encoded subunits. In fact, this may explain increased stability of F_oa detected in pulse-chase experiments, indicating that this subunit sequestered by increased pool of its interacting partners makes it less prone to proteolysis.

Difference between COX4i1 gene KO effect on CI (which is decreased) and other OXPHOS complexes (which are not significantly affected) may be explained by mechanism recently found in yeast, possibly occurring also in mammalian mitochondria. Published phenomenon of spatial partitioning of mitochondrial translation and OXPHOS complexes assembly could clarify unclarified relations between OXPHOS complexes assembly and maintenance. However, further studies are required to discover, if such a mechanism is also present in mammals (Formosa and Ryan, 2018; Stoldt *et al.*, 2018). Indeed, cell models established in this thesis may prove beneficial for such studies.

6. Conclusions

In summary, HEK293 cell line-based COX4i1, COX4i2 and COX4i1/4i2 knock-out (KO) models were prepared using CRISPR KO technology. Established COX4i1/4i2 KO clones will be used as a tool for knock-in of either Cox4i1 or Cox4i2 isoform to study their functional differences. Structural and functional aspects of cytochrome c oxidase and other OXPHOS complexes in KO cells were characterized by combination of molecular and biochemical methods.

COX4i2 gene KO did not have any relevant effect due to absence of constitutive Cox4i2 isoform expression in HEK293 cell line. On the other hand, characterization of COX4i1 gene KO clones (both, COX4i1 KO and COX4i1/4i2 KO clones) revealed overall decrease of majority of COX subunits coupled with complete loss of assembled COX enzyme. COX absence resulted in total OXPHOS dysfunction, which was compensated by increased glycolytic capacity. Moreover, COX absence also affected assembly of respiratory supercomplexes, which were lost upon COX4i1 gene KO. Interestingly, as a secondary effect, downregulation of mitochondrial proteosynthesis was observed in Cox4i1 isoform lacking cells, resulting in downregulation of Complex I, indicating interdependency of COX and CI biogenesis.

7. References

Abdulhag, U. N., Soiferman, D., Schueler-furman, O., Miller, C., Shaag, A., Elpeleg, O., Edvardson, S. and Saada, A. (2015) 'Mitochondrial complex IV deficiency , caused by mutated COX6B1 , is associated with encephalomyopathy , hydrocephalus and cardiomyopathy', *European Journal of Human Genetics*. Nature Publishing Group, 23(2), pp. 159–164. doi: 10.1038/ejhg.2014.85.

Abu-Libdeh, B., Douiev, L., Amro, S., Shahrour, M., Ta-Shma, A., Miller, C., Elpeleg, O. and Saada, A. (2017) 'Mutation in the COX4I1 gene is associated with short stature, poor weight gain and increased chromosomal breaks, simulating Fanconi anemia', *European Journal Of Human Genetics*. Macmillan Publishers Limited, part of Springer Nature., 25, p. 1142. Available at: http://dx.doi.org/10.1038/ejhg.2017.112.

Acín-Pérez, R., Fernández-Silva, P., Peleato, M. L., Pérez-Martos, A. and Enríquez, J. A. (2008) 'Respiratory Active Mitochondrial Supercomplexes', *Molecular Cell*, 32(4), pp. 529–539. doi: 10.1016/j.molcel.2008.10.021.

Acín-Pérez, R., Gatti, D. L., Bai, Y. and Manfredi, G. (2011) 'Protein phosphorylation and prevention of cytochrome oxidase inhibition by ATP: coupled mechanisms of energy metabolism regulation', *Cell Metab.*, 13(6), pp. 712–719. doi: 10.1016/j.cmet.2011.03.024.Protein.

Addgene (2018) *Enhancing Specificity with Nickases and High Fidelity Enzymes*. Available at: https://www.addgene.org/crispr/guide/ (Accessed: 25 April 2018).

Agilent (2018a) *Measuring Mitochondrial Respiration Agilent Seahorse XF Cell Mito Stress Test*. Available at: https://www.agilent.com/en/products/cell-analysis/mitochondrial-respiration-xf-cell-mito-stress-test (Accessed: 25 April 2018).

Agilent (2018b) *The Agilent Advantage - Sensitive Real-Time Assays for Glycolysis*. Available at: https://www.agilent.com/en/products/cell-analysis/glycolysis-assays-with-seahorse-xf-technology (Accessed: 25 April 2018).

Alexander-Shani, R., Mreisat, A., Smeir, E., Gerstenblith, G., Stern, M. D. and Horowitz, M. (2017) 'Long-term HIF-1α transcriptional activation is essential for heat-acclimation-mediated cross tolerance: mitochondrial target genes', *American Journal of Physiology - Regulatory, Integrative and Comparative Physiology*, 312(5), pp. R753–R762. doi: 10.1152/ajpregu.00461.2016.

Andersson, S. G. E., Zomorodipour, A., Andersson, J. O., Sicheritz-Pontén, T.,

Alsmark, U. C., Podowski, R. M., Naslund, A. K., Eriksson, A.-S. S., Winkler, H. H., Kurland, C. G., Sicheritz-Pontén, T., Alsmark, U. C., Podowski, R. M., Näslund, A. K., Eriksson, A.-S. S., Winkler, H. H. and Kurland, C. G. (1998) 'The genome sequence of Rickettsia prowazekii and the origin of mitochondria', *Nature*, 396(6707), pp. 133–140. doi: 10.1038/24094 [doi].

Aras, S., Arrabi, H., Purandare, N., Hüttemann, M., Kamholz, J., Züchner, S. and Grossman, L. I. (2017) 'Abl2 kinase phosphorylates Bi-organellar regulator MNRR1 in mitochondria, stimulating respiration', *Biochimica et Biophysica Acta - Molecular Cell Research*. Elsevier B.V., 1864(2), pp. 440–448. doi: 10.1016/j.bbamcr.2016.11.029.

Aras, S., Bai, M., Lee, I., Springett, R., Hüttemann, M. and Grossman, L. I. (2015) 'Mitochondrion MNRR1 (formerly CHCHD2) is a bi-organellar regulator of mitochondrial metabolism', *MITOCH*. © Elsevier B.V. and Mitochondria Research Society., 20, pp. 43–51. doi: 10.1016/j.mito.2014.10.003.

Aras, S., Pak, O., Sommer, N., Finley, R., Hüttemann, M., Weissmann, N. and Grossman, L. I. (2013) 'Oxygen-dependent expression of cytochrome c oxidase subunit 4-2 gene expression is mediated by transcription factors RBPJ, CXXC5 and CHCHD2', *Nucleic Acids Research*, 41(4), pp. 2255–2266. doi: 10.1093/nar/gks1454.

Arnold, S. and Kadenbach, B. (1997) 'Cell respiration is controlled by ATP, an allosteric inhibitor of cytochrome-c oxidase', *Eur. J. Biochem.*, 249, pp. 350–354.

Arroyo, J. D., Jourdain, A. A., Calvo, S. E., Ballarano, C. A., Doench, J. G., Root, D. E. and Mootha, V. K. (2016) 'A Genome-wide CRISPR Death Screen Identifies Genes Essential for Oxidative Phosphorylation HHS Public Access', *December*, 13(246), pp. 875–885. doi: 10.1016/j.cmet.2016.08.017.

Babcock, G. T. and Wikström, M. (1992) 'Oxygen activation and the conservation of energy in cell respiration', *Nature*, 356(6367), pp. 301–309. Available at: http://dx.doi.org/10.1038/356301a0.

Balsa, E., Marco, R., Perales-Clemente, E., Szklarczyk, R., Calvo, E., Landázuri, M. O. and Enríquez, J. A. (2012) 'NDUFA4 is a subunit of complex IV of the mammalian electron transport chain', *Cell Metabolism*, 16(3), pp. 378–386. doi: 10.1016/j.cmet.2012.07.015.

Bender, E. and Kadenbach, B. (2000) 'The allosteric ATP-inhibition of cytochrome c oxidase activity is reversibly switched on by cAMP-dependent phosphorylation', *FEBS*

Letters, 466, pp. 130–134.

Bentlage, H. A. C. M., Wendel, U., Schagger, H., ter Laak, H. J., Janssen, A. J. M. and Trijbels, J. M. F. (1996) 'Lethal infantile mitochondrial disease with isolated complex I deficiency in fibroblasts but with combined complex I and IV deficiencies in muscle', *Neurology*, 47(1), p. 243 LP-248. Available at: http://n.neurology.org/content/47/1/243.abstract.

Blomme, T., Vandepoele, K., De Bodt, S., Simillion, C., Maere, S. and Van de Peer, Y. (2006) 'The gain and loss of genes during 600 million years of vertebrate evolution.', *Genome Biology*, 7(5), p. R43. doi: 10.1186/gb-2006-7-5-r43.

Boczonadi, V., Giunta, M., Lane, M., Tulinius, M., Schara, U. and Horvath, R. (2015) 'Investigating the role of the physiological isoform switch of cytochrome c oxidase subunits in reversible mitochondrial disease', *International Journal of Biochemistry and Cell Biology*. Elsevier Ltd, 63, pp. 32–40. doi: 10.1016/j.biocel.2015.01.025.

Bonne, G., Seibel, P., Possekel, S., Marsac, C. and Kadenbach, B. (1993) 'Expression of human cytochrome c oxidase subunits during fetal development', *Eur. J. Biochem.*, 217, pp. 1099–1107.

Bratton, M. R., Pressler, M. A. and Hosler, J. P. (1999) 'Suicide Inactivation of Cytochrome c Oxidase: Catalytic Turnover in the Absence of Subunit III Alters the Active Site', *Biochemistry*. American Chemical Society, 38(49), pp. 16236–16245. doi: 10.1021/bi9914107.

Brzezinski, P. and Larsson, G. (2003) 'Redox-driven proton pumping by heme-copper oxidases', *Biochimica et Biophysica Acta - Bioenergetics*, 1605(1–3), pp. 1–13. doi: 10.1016/S0005-2728(03)00079-3.

Carroll, J., Fearnley, I. M., Shannon, R., Hirst, J. and Walker, J. E. (2003) 'Analysis of the Subunit Composition of Complex I from Bovine Heart Mitochondria', *Molecular & Cellular Proteomics*, 2(2), pp. 117–126. doi: 10.1074/mcp.M300014-MCP200.

Cimmino, M., Mion, F., Goglia, F., Minaire, Y. and Géloën, A. (1996) 'Demonstration of in vivo metabolic effects of 3,5-di-iodothyronine', *Journal of Endocrinology* , 149(2), pp. 319–325. doi: 10.1677/joe.0.1490319.

Cogliati, S., Calvo, E., Loureiro, M., Guaras, A. M., Nieto-Arellano, R., Garcia-Poyatos, C., Ezkurdia, I., Mercader, N., Vázquez, J. and Enríquez, J. A. (2016) 'Mechanism of super-assembly of respiratory complexes III and IV', *Nature*. Nature

Publishing Group, 539(7630), pp. 579–582. doi: 10.1038/nature20157.

Dahout-Gonzalez, C. (2006) 'Molecular, Functional, and Pathological Aspects of the Mitochondrial ADP/ATP Carrier', *Physiology*, 21(4), pp. 242–249. doi: 10.1152/physiol.00005.2006.

Das, J., Miller, S. T. and Stern, D. L. (2004) 'Comparison of Diverse Protein Sequences of the Nuclear-Encoded Subunits of Cytochrome C Oxidase Suggests Conservation of Structure Underlies Evolving Functional Sites', *Molecular Biology and Evolution*, 21(8), pp. 1572–1582. doi: 10.1093/molbev/msh161.

Dennerlein, S. and Rehling, P. (2015) 'Human mitochondrial COX1 assembly into cytochrome c oxidase at a glance', *Journal of Cell Science*, 128(5), pp. 833–837. doi: 10.1242/jcs.161729.

Dennerlein, S., Wang, C. and Rehling, P. (2017) 'Plasticity of Mitochondrial Translation', *Trends in Cell Biology*. Elsevier Ltd, 27(10), pp. 712–721. doi: 10.1016/j.tcb.2017.05.004.

Diaz, F., Enríquez, J. A. and Moraes, C. T. (2012) 'Cells Lacking Rieske Iron-Sulfur Protein Have a Reactive Oxygen Species-Associated Decrease in Respiratory Complexes I and IV', *Molecular and Cellular Biology*, 32(2), pp. 415–429. doi: 10.1128/MCB.06051-11.

Diaz, F., Fukui, H., Garcia, S. and Moraes, C. T. (2006) 'Cytochrome c Oxidase Is Required for the Assembly/Stability of Respiratory Complex I in Mouse Fibroblasts', *Molecular and Cellular Biology*, 26(13), pp. 4872–4881. doi: 10.1128/MCB.01767-05.

Durand, A., Bourbon, M., Steunou, A., Khalfaoui-hassani, B., Legrand, C., Guitton, A., Astier, C. and Ouchane, S. (2017) 'Biogenesis of the bacterial cbb 3 cytochrome c oxidase : active subcomplexes support a sequential assembly model .', 293(11), pp. 1–21. doi: 10.1074/jbc.M117.805184.

Enríquez, J. A. (2016) 'Supramolecular Organization of Respiratory Complexes', *Annual Review of Physiology*, 78(1), pp. 533–561. doi: 10.1146/annurev-physiol-021115-105031.

Ewart, G. D., Zhang, Y. Z. and Capaldi, R. A. (1991) 'Switching of bovine cytochrome c oxidase subunit Via isoforms in skeletal muscle during development', *FEBS*, 292(1,2), pp. 79–84.

Fadda, E., Yu, C. H. and Pomès, R. (2008) 'Electrostatic control of proton pumping in

cytochrome c oxidase', *Biochimica et Biophysica Acta - Bioenergetics*, 1777(3), pp. 277–284. doi: 10.1016/j.bbabio.2007.11.010.

Fontanesi, F., Soto, I. C., Horn, D. and Barrientos, A. (2006) 'Assembly of mitochondrial cytochrome c-oxidase, a complicated and highly regulated cellular process.', *American journal of physiology. Cell physiology*, 291(June 2006), pp. C1129–C1147. doi: 10.1152/ajpcell.00233.2006.

Formosa, L. E. and Ryan, M. T. (2018) 'Mitochondrial OXPHOS complex assembly lines', *Nature Cell Biology*. doi: 10.1038/s41556-018-0098-z.

Fornůsková, D., Stibůrek, L., Wenchich, L., Vinsova, K., Hansíková, H. and Zeman, J. (2010a) 'Novel insights into the assembly and function of human nuclear-encoded cytochrome c oxidase subunits 4, 5a, 6a, 7a and 7b', *Biochem J*, 428. doi: 10.1042/BJ20091714.

Fornůsková, D., Stibůrek, L., Wenchich, L., Vinsova, K., Hansíková, H. and Zeman, J. (2010b) 'Novel insights into the assembly and function of human nuclear-encoded cytochrome c oxidase subunits 4, 5a, 6a, 7a and 7b', *Biochem J*, 428, pp. 363–374. doi: 10.1042/BJ20091714.

Fukuda, R., Zhang, H., Kim, J., Shimoda, L., Dang, C. V. and Semenza, G. L. (2007) 'HIF-1 Regulates Cytochrome Oxidase Subunits to Optimize Efficiency of Respiration in Hypoxic Cells', *Cell*, 129(1), pp. 111–122. doi: 10.1016/j.cell.2007.01.047.

Galati, D., Srinivasan, S., Raza, H., Prabu, S. K., Karunakaran, C., Lopez, M., Kalyanaraman, B. and Avadhani, N. G. (2009) 'Role of nuclear encoded subunit Vb in the assembly and stability of Cytochrome C oxidase complex: Implications in Mitochondrial dysfunction and ROS Production', *Biochem J*, 420(3), pp. 439–449. doi: 10.1042/BJ20090214.Role.

Gnaiger, E. (2014) *Mitochondrial Pathways and Respiratory Control An Introduction to OXPHOS Analysis*, *Mitochondrial Physiology Network*.

Goldberg, A., Wildman, D. E., Schmidt, T. R., Hu, M., Goodman, M., Weiss, M. L. and Grossman, L. I. (2003) 'Adaptive evolution of cytochrome c oxidase subunit VIII in anthropoid primates', *Proceedings of the National Academy of Sciences of the United States of America*, 100(10), pp. 5873–5878.

Grossman, L. I., Purandare, N., Arshad, R., Gladyck, S., Somayajulu, M., Hüttemann, M. and Aras, S. (2017) 'MNRR1, a Biorganellar Regulator of Mitochondria', *Oxidative*

Medicine and Cellular Longevity, 2017. doi: 10.1155/2017/6739236.

Guo, R., Zong, S., Wu, M., Gu, J. and Yang, M. (2017) 'Architecture of Human Mitochondrial Respiratory Megacomplex I2III2IV2', *Cell*. Elsevier Inc., 170(6), p. 1247–1257.e12. doi: 10.1016/j.cell.2017.07.050.

Gupta, K. J., Zabalza, A. and Dongen, J. T. Van (2009) 'Regulation of respiration when the oxygen availability changes', *Physiologia Plantarum*, 137, pp. 383–391. doi: 10.1111/j.1399-3054.2009.01253.x.

Hällberg, B. M. and Larsson, N. G. (2014) 'Making proteins in the powerhouse', *Cell Metabolism*, 20(2), pp. 226–240. doi: 10.1016/j.cmet.2014.07.001.

Hallmann, K., Kudin, A. P., Zsurka, G., Kornblum, C., Reimann, J., Stüve, B., Waltz, S., Hattingen, E., Thiele, H., Nürnberg, P., Rüb, C., Voos, W., Kopatz, J., Neumann, H. and Kunz, W. S. (2016) 'Loss of the smallest subunit of cytochrome c oxidase, COX8A, causes Leigh-like syndrome and epilepsy', *Brain*, 139(2), pp. 338–345. Available at: http://brain.oxfordjournals.org/content/139/2/338.abstract.

Hayashi, T., Asano, Y., Shintani, Y., Aoyama, H., Kioka, H., Tsukamoto, O., Hikita, M., Shinzawa-Itoh, K., Takafuji, K., Higo, S., Kato, H., Yamazaki, S., Matsuoka, K., Nakano, A., Asanuma, H., Asakura, M., Minamino, T., Goto, Y.-I., Ogura, T., Kitakaze, M., Komuro, I., Sakata, Y., Tsukihara, T., Yoshikawa, S. and Takashima, S. (2015) 'Higd1a is a positive regulator of cytochrome c oxidase', *Proceedings of the National Academy of Sciences of the United States of America*, 112(5), pp. 1553–1558. doi: 10.1073/pnas.1419767112.

He, J., Carroll, J., Ding, S., Fearnley, I. M. and Walker, J. E. (2017) 'Permeability transition in human mitochondria persists in the absence of peripheral stalk subunits of ATP synthase', *Proceedings of the National Academy of Sciences*, 114(34), pp. 9086–9091. doi: 10.1073/pnas.1711201114.

Hejzlarová, K., Mráček, T., Vrbacký, M., Kaplanová, V., Karbanová, V., Nůsková, H., Pecina, P. and Houštěk, J. (2014) 'Nuclear genetic defects of mitochondrial ATP synthase.', *Physiological research / Academia Scientiarum Bohemoslovaca*, 63 Suppl 1(1995), pp. S57-71. Available at: http://www.ncbi.nlm.nih.gov/pubmed/24564666.

Heneen, W. K. (1976) 'HeLa cells and their possible contamination of other cell lines: Karyotype studies', *Hereditas*, 82(2), pp. 217–247. doi: 10.1111/j.1601-5223.1976.tb01560.x.

Hornig-Do, H.-T., Tatsuta, T., Buckermann, A., Bust, M., Kollberg, G., Rötig, A., Hellmich, M., Nijtmans, L. and Wiesner, R. J. (2012) 'Nonsense mutations in the COX1 subunit impair the stability of respiratory chain complexes rather than their assembly', *The EMBO Journal*, 31(5), pp. 1293–1307. doi: 10.1038/emboj.2011.477.

Horvat, S., Beyer, C. and Arnold, S. (2006) 'Effect of hypoxia on the transcription pattern of subunit isoforms and the kinetics of cytochrome c oxidase in cortical astrocytes and cerebellar neurons', *Journal of Neurochemistry*. Blackwell Publishing Ltd, 99(3), pp. 937–951. doi: 10.1111/j.1471-4159.2006.04134.x.

Hosler, J. P. (2004) 'The influence of subunit III of cytochrome c oxidase on the D pathway, the proton exit pathway and mechanism-based inactivation in subunit I', *Biochimica et Biophysica Acta - Bioenergetics*, 1655(1–3), pp. 332–339. doi: 10.1016/j.bbabio.2003.06.009.

Hosler, J. P., Ferguson-Miller, S., Calhoun, M. W., Thomas, J. W., Hill, J., Lemienx, L., Ma, J., Georgiou, C., Fetter, J., Shapleigh, J., Tecklenburg, M. M. J., Babcock, G. T. and Gennis, R. B. (1993) 'Insight into the Active-Site Structure and Function of Cytochrome Oxidase by Analysis of Site-Directed Mutants of Bacterial Cytochrome aa3 and Cytochrome bo', *Journal of Bioenergetics and Biomemranes*, 25(2), pp. 121–136.

Hüttemann, M. (2000) 'New isoforms of cytochrome c oxidase subunit IV in tuna fish', *Biochimica et Biophysica Acta*, 1492, pp. 242–246.

Hüttemann, M., Jaradat, S. and Grossman, L. I. (2003) 'Cytochrome c Oxidase of Mammals Contains a Testes-Specific Isoform of Subunit VIb — the Counterpart to Testes-Specific Cytochrome c ?', *Molecular reproduction and development*, 66(April), pp. 8–16. doi: 10.1002/mrd.10327.

Hüttemann, M., Kadenbach, B. and Grossman, L. I. (2001) 'Mammalian subunit IV isoforms of cytochrome c oxidase', *Gene*, 267(1), pp. 111–123. doi: 10.1016/S0378-1119(01)00385-7.

Hüttemann, M., Klewer, S., Lee, I., Pecinova, A., Pecina, P., Liu, J., Lee, M., Doan, J. W., Larson, D. and Slack, E. (2012) 'Mice deleted for heart-type cytochrome c oxidase subunit 7a1 develop dilated cardiomyopathy', *Mitochondrion*, 12(2), pp. 294–304. doi: 10.1016/j.mito.2011.11.002.Mice.

Hüttemann, M., Lee, I., Gao, X., Pecina, P., Pecinova, A., Liu, J., Aras, S., Sommer, N., Sanderson, T. H., Tost, M., Neff, F., Aguilar-pimentel, J. A., Becker, L., Naton, B.,

Rathkolb, B., Rozman, J., Favor, J., Hans, W., Prehn, C., Puk, O., Schrewe, A., Sun, M., Höfler, H., Adamski, J., Bekeredjian, R., Graw, J., Adler, T., Busch, D. H., Klingenspor, M., Klopstock, T., Ollert, M., Wolf, E., Fuchs, H., Gailus-durner, V., Hrabe, M., Angelis, D., Weissmann, N., Doan, J. W., Bassett, D. J. P. and Grossman, L. I. (2012) 'Cytochrome c oxidase subunit 4 isoform 2-knockout mice show reduced enzyme activity , airway hyporeactivity , and lung pathology', *The FASEB Journal*, 26, pp. 3916–3930. doi: 10.1096/fj.11-203273.

Hüttemann, M., Lee, I., Liu, J. and Grossman, L. I. (2007) 'Transcription of mammalian cytochrome c oxidase subunit IV-2 is controlled by a novel conserved oxygen responsive element.', *The FEBS journal*, 274(21), pp. 5737–48. doi: 10.1111/j.1742-4658.2007.06093.x.

Hüttemann, M., Schmidt, T. R. and Grossman, L. I. (2003) 'A third isoform of cytochrome c oxidase subunit VIII is present in mammals q', *Gene*, 312, pp. 95–102. doi: 10.1016/S0378-1119(03)00604-8.

Hwang, H. J., Lynn, S. G., Vengellur, A., Saini, Y., Grier, E. A., Ferguson-Miller, S. and LaPres, J. J. (2015) 'Hypoxia Inducible Factors Modulate Mitochondrial Oxygen Consumption and Transcriptional Regulation of Nuclear-Encoded Electron Transport Chain Genes', *Biochemistry*. American Chemical Society, 54(24), pp. 3739–3748. doi: 10.1021/bi5012892.

Chance, B., Saronio, C. and John S. Leigh, J. (1975) 'Functional Intermediates in the Reaction of Membrane-bound Cytochrome Oxidases with Oxygen', *The Journal of Biological Chemistry*, 250(24), pp. 9226–9237.

Chance, B. and Williams, G. R. (1955) 'A Method for the Localization of Sites for Oxidative Phosphorylation', *Nature*, 176, pp. 250–254.

Chazotte, B. and Hackenbrock, C. R. (1989) 'Lateral Diffusion as a Rate-limiting Step in Ubiquinone-mediated Mitochondrial Electron Transport', *The Journal of Biological Chemistry*, 264(9), pp. 4978–4985.

Chen, Y. C., Taylor, E. B., Dephoure, N., Heo, J. M., Tonhato, A., Papandreou, I., Nath, N., Denko, N. C., Gygi, S. P. and Rutter, J. (2012) 'Identification of a protein mediating respiratory supercomplex stability', *Cell Metabolism*. Elsevier Inc., 15(3), pp. 348–360. doi: 10.1016/j.cmet.2012.02.006.

Ikeda, K., Shiba, S., Horie-Inoue, K., Shimokata, K. and Inoue, S. (2013) 'A stabilizing

factor for mitochondrial respiratory supercomplex assembly regulates energy metabolism in muscle.', *Nature communications*. Nature Publishing Group, 4, p. 2147. doi: 10.1038/ncomms3147.

Indrieri, A., Rahden, V. A. Van, Tiranti, V., Morleo, M., Iaconis, D., Tammaro, R., Amato, I. D., Conte, I., Maystadt, I., Demuth, S., Zvulunov, A., Kutsche, K., Zeviani, M. and Franco, B. (2012) 'Mutations in COX7B Cause Microphthalmia with Linear Skin Lesions , an Unconventional Mitochondrial Disease', *The American Journal of Human Genetics*. The American Society of Human Genetics, 91(5), pp. 942–949. doi: 10.1016/j.ajhg.2012.09.016.

Iwata, S., Ostermeier, C., Ludwig, B. and Michel, H. (1995) 'Structure at 2.8 A resolution of cytochrome c oxidase from Paracoccus denitrificans', *Nature*, 376(6542), pp. 660–669. Available at: http://dx.doi.org/10.1038/376660a0.

Kadenbach, B. and Arnold, S. (1999) 'A second mechanism of respiratory control', *FEBS Letters*, 447, pp. 131–134.

Kadenbach, B., Arnold, S., Lee, I. and Hu, M. (2004) 'The possible role of cytochrome c oxidase in stress-induced apoptosis and degenerative diseases', *Biochimica et Biophysica Acta*, 1655, pp. 400–408. doi: 10.1016/j.bbabio.2003.06.005.

Kadenbach, B. and Hüttemann, M. (2015) 'The subunit composition and function of mammalian cytochrome c oxidase.', *Mitochondrion*. © Elsevier B.V. and Mitochondria Research Society., 24, pp. 64–76. doi: 10.1016/j.mito.2015.07.002.

Kadenbach, B., Jarausch, J., Hartmann, R. and Merle, P. (1983) 'Separation of mammalian cytochrome c oxidase into 13 polypeptides by a sodium dodecyl sulfate-gel electrophoretic procedure', *Analytical Biochemistry*, 129(2), pp. 517–521. doi: 10.1016/0003-2697(83)90586-9.

Kadenbach, B. and Merle, P. (1981) 'On the function of multiple subunits of cytochrome c oxidase from higher eukaryotes.', *FEBS Lett*, 135(1), pp. 1–11.

Kadenbach, B., Ramzan, R. and Vogt, S. (2013) 'High efficiency versus maximal performance — The cause of oxidative stress in eukaryotes : A hypothesis', *Mitochondrion*. Elsevier B.V., 13, pp. 1–6. doi: 10.1016/j.mito.2012.11.005.

Kaila, V. R. I., Verkhovsky, M. I. and Wikström, M. (2010) 'Proton-coupled electron transfer in cytochrome oxidase.', *Chemical reviews*, 110(12), pp. 7062–7081. doi: 10.1021/cr1002003.

Kamiya, K., Boero, M., Tateno, M., Shiraishi, K. and Oshiyama, A. (2007) 'Possible Mechanism of Proton Transfer through Peptide Groups in the H-Pathway of the Bovine Cytochrome c Oxidase', *Journal of the American Chemical Society*. American Chemical Society, 129(31), pp. 9663–9673. doi: 10.1021/ja070464y.

Kannt, A., Pfitzner, U., Ruitenberg, M., Hellwig, P., Ludwig, B., Ma, W., Fendler, K. and Michel, H. (1999) 'Mutation of Arg-54 Strongly Influences Heme Composition and Rate and Directionality of Electron Transfer in Paracoccus denitrificans Cytochrome c Oxidase', *The Journal of Biological Chemistry*, 274(53), pp. 37974–37981.

Khalimonchuk, O. and Rödel, G. (2005) 'Biogenesis of cytochrome c oxidase', *Mitochondrion*, 5, pp. 363–388. doi: 10.1016/j.mito.2005.08.002.

Kim, J. H., Choi, E. Y., Jung, E.-S., Kwon, Y., Lee, D. S., Hwang, D. Y. and Hwang, E. S. (2009) 'Characterization of Clones of Human Cell Line Infected with Porcine Endogenous Retrovirus (PERV) from Porcine Cell Line, PK-15', *Infection and Chemotherapy*, p. 1. doi: 10.3947/ic.2009.41.1.1.

Kocha, K. M., Reilly, K., Porplycia, D. S. M., McDonald, J., Snider, T. and Moyes, C. D. (2014) 'Evolution of the oxygen sensitivity of cytochrome c oxidase subunit 4.', *American journal of physiology. Regulatory, integrative and comparative physiology*, (23), p. ajpregu.00281.2014. doi: 10.1152/ajpregu.00281.2014.

Konstantinov, A. A., Siletsky, S., Mitchell, D., Kaulen, A. and Gennis, R. B. (1997) 'The roles of the two proton input channels in cytochrome c oxidase from Rhodobacter sphaeroides probed by the effects of site-directed mutations on time-resolved electrogenic intraprotein proton transfer', *Proceedings of the National Academy of Sciences of the United States of America*, 94(August), pp. 9085–9090.

Kovářová, N., Čížková Vrbacká, A., Pecina, P., Stránecký, V., Pronicka, E., Kmoch, S. and Houštěk, J. (2012) 'Adaptation of respiratory chain biogenesis to cytochrome c oxidase deficiency caused by SURF1 gene mutations', *Biochimica et Biophysica Acta - Molecular Basis of Disease*, 1822(7), pp. 1114–1124. doi: 10.1016/j.bbadis.2012.03.007.

Krzyzosiak, J., Mcmillan, G., Molan, P. and Vishwanath, R. (2000) 'Protein Tyrosine Phosphorylation During Prolonged In Vitro Incubation of Ejaculated Bovine Spermatozoa Is Regulated by the Oxidative State of the Medium 1', *Biology of reproduction*, 62, pp. 1615–1623.

Kwast, K. E., Burke, P. V and Poyton, R. O. (1998) 'Oxygen sensing and the

transcriptional regulation of oxygen-responsive genes in yeast', *The Journal of Experimental Biology*, 201, pp. 1177–1195.

Lang, B. F., Burger, G. and O'Kelly, C. J. (1997) 'An ancestral mitochondrial DNA resembling a eubacterial genome in miniature', *Nature*, 387, pp. 493–497.

Lanni, A., Moreno, M., Lombardi, A., Goglia, F., Generale, F., Ii, F. and Mezzocannone, V. (1996) 'Calorigenic effect of diiodothyronines in the rat', *Journal of physiology*, 494(3), pp. 831–837.

Lapuente-Brun, E., Moreno-Loshuertos, R., Acín-Pérez, R., Latorre-Pellicer, A., Colas, C., Balsa, E., Perales-Clemente, E., Quirós, P. M., Calvo, E., Rodriguez-Hernandez, M. A., Navas, P., Cruz, R., Carracedo, A., Lopez-Otin, C., Perez-Martos, A., Fernández-Silva, P., Fernández-Vizarra, E. and Enríquez, J. A. (2013) 'Supercomplex Assembly Determines Electron Flux in the Mitochondrial Electron Transport Chain', *Science*, 340(6140), pp. 1567–1570. doi: 10.1126/science.1230381.

Lazarou, M., Smith, S. M., Thorburn, D. R., Ryan, M. T. and McKenzie, M. (2009) 'Assembly of nuclear DNA-encoded subunits into mitochondrial complex IV, and their preferential integration into supercomplex forms in patient mitochondria', *FEBS Journal*, 276(22), pp. 6701–6713. doi: 10.1111/j.1742-4658.2009.07384.x.

Lee, H., Das, T. K., Rousseau, D. L., Mills, D., Ferguson-Miller, S. and Gennis, R. B. (2000) 'Mutations in the Putative H-Channel in the Cytochrome c Oxidase from Rhodobacter sphaeroides Show That This Channel Is Not Important for Proton Conduction but Reveal Modulation of the Properties of Heme a', *Biochemistry*. American Chemical Society, 39(11), pp. 2989–2996. doi: 10.1021/bi9924821.

Lee, I., Bender, E. and Kadenbach, B. (2002) 'Control of mitochondrial membrane potential and ROS formation by reversible phosphorylation of cytochrome c oxidase', *Molecular and Cellular Biochemistry*, 234(1), pp. 63–70. doi: 10.1023/A:1015921513720.

Lee, I., Salomon, A. R., Ficarro, S., Mathes, I., Lottspeich, F., Grossman, L. I. and Hu, M. (2005) 'cAMP-dependent Tyrosine Phosphorylation of Subunit I Inhibits Cytochrome c Oxidase Activity', *The Journal of Biological Chemistry*, 280(7), pp. 6094–6100. doi: 10.1074/jbc.M411335200.

Letts, J. A., Fiedorczuk, K. and Sazanov, L. A. (2016) 'The architecture of respiratory supercomplexes', *Nature*. Nature Publishing Group, 537(7622), pp. 644–648. doi:

10.1038/nature19774.

Letts, J. A. and Sazanov, L. A. (2017) ‘Clarifying the supercomplex: The higher-order organization of the mitochondrial electron transport chain’, *Nature Structural and Molecular Biology*, 24(10), pp. 800–808. doi: 10.1038/nsmb.3460.

Li, Y., D’Aurelio, M., Deng, J. H., Park, J. S., Manfredi, G., Hu, P., Lu, J. and Bai, Y. (2007) ‘An assembled complex IV maintains the stability and activity of complex I in mammalian mitochondria’, *Journal of Biological Chemistry*, 282(24), pp. 17557–17562. doi: 10.1074/jbc.M701056200.

Liang, H. (2004) ‘A rare polymorphism of the COX7B2 gene in a Cantonese family with nasopharyngeal carcinoma’, *Science in China Series C*, 47(5), p. 449. doi: 10.1360/03yc0037.

Little, A. G., Kocha, K. M., Lougheed, S. C. and Moyes, C. D. (2010) ‘Evolution of the nuclear-encoded cytochrome oxidase subunits in vertebrates.’, *Physiological genomics*, 42(1), pp. 76–84. doi: 10.1152/physiolgenomics.00015.2010.

Liu, F., Lössl, P., Rabbitts, B. M., Balaban, R. S. and Heck, A. J. R. (2018) ‘The interactome of intact mitochondria by cross-linking mass spectrometry provides evidence for coexisting respiratory supercomplexes’, *Molecular & Cellular Proteomics*, 17(2), pp. 216–232. doi: 10.1074/mcp.RA117.000470.

Ludwig, B., Bender, E., Arnold, S., Hüttemann, M., Lee, I. and Kadenbach, B. (2001) ‘Cytochrome c Oxidase and the Regulation of Oxidative Phosphorylation’, *ChemBioChem*, 2, pp. 392–403. doi: 10.1002/1439-7633(20010601)2.

Luo, F., Shinzawa-itoh, K., Hagimoto, K. and Shimada, A. (2018) ‘Structure of bovine cytochrome c oxidase in the ligand- free reduced state at neutral pH’, 2018, pp. 1–9.

Lynch, M., O’Hely, M., Walsh, B. and Force, A. (2001) ‘The probability of preservation of a newly arisen gene duplicate’, *Genetics*, 159(4), pp. 1789–1804. doi: 10.1006/scdb.1996.0068.

Massa, V., Fernández-Vizarra, E., Alshahwan, S., Bakhsh, E., Goffrini, P., Ferrero, I., Mereghetti, P., Adamo, P. D., Gasparini, P. and Zeviani, M. (2008) ‘Severe Infantile Encephalomyopathy Caused by a Mutation in COX6B1 , a Nucleus-Encoded Subunit of Cytochrome C Oxidase’, *The American Journal of Human Genetics*, 82(June), pp. 1281–1289. doi: 10.1016/j.ajhg.2008.05.002.

McDonald, A. E., Vanlerberghe, G. C. and Staples, J. F. (2009) ‘Alternative oxidase

in animals : unique characteristics and taxonomic distribution', *The Journal of Experimental Biology*, 212, pp. 2627–2634. doi: 10.1242/jeb.032151.

McEwen, J. E., Ko, C., Kloeckner-Gruissem, B. and Poyton, R. O. (1986) 'Nuclear Functions Required for Cytochrome c Oxidase Biogenesis in Saccharomyces cerevisiae', *The Journal of Biological Chemistry*, 261(25), pp. 11872–11879.

McKenzie, M., Lazarou, M. and Ryan, M. T. (2009) *Chapter 18 Analysis of Respiratory Chain Complex Assembly with Radiolabeled Nuclear- and Mitochondrial-Encoded Subunits*. 1st edn, *Methods in Enzymology*. 1st edn. Elsevier Inc. doi: 10.1016/S0076-6879(08)04418-2.

Mick, D. U., Dennerlein, S., Wiese, H., Reinhold, R., Pacheu-Grau, D., Lorenzi, I., Sasarman, F., Weraarpachai, W., Shoubridge, E. A., Warscheid, B. and Rehling, P. (2012) 'MITRAC links mitochondrial protein translocation to respiratory-chain assembly and translational regulation', *Cell*. Elsevier Inc., 151(7), pp. 1528–1541. doi: 10.1016/j.cell.2012.11.053.

Milenkovic, D., Blaza, J. N., Larsson, N. G. and Hirst, J. (2017) 'The Enigma of the Respiratory Chain Supercomplex', *Cell Metabolism*, 25(4), pp. 765–776. doi: 10.1016/j.cmet.2017.03.009.

Millett, F., De Jong, C., Paulson, L. and Capaldi, R. A. (1983) 'Identification of specific carboxylate groups on cytochrome c oxidase that are involved in binding cytochrome c', *Biochemistry*. American Chemical Society, 22(3), pp. 546–552. doi: 10.1021/bi00272a004.

Moreno-Lastres, D., Fontanesi, F., García-Consuegra, I., Martín, M. A., Arenas, J., Barrientos, A., Ugalde, C., Garcia-Consuegra, I., Martin, M. A., Arenas, J., Barrientos, A. and Ugalde, C. (2013) 'Mitochondrial Complex I plays an Essential Role in Human Respirasome Assembly', *Cell Metabolism*, 15(3), pp. 324–335. doi: 10.1016/j.cmet.2012.01.015.Mitochondrial.

Mourier, A., Matic, S., Ruzzenente, B., Larsson, N. G. and Milenkovic, D. (2014) 'The respiratory Chain supercomplex organization is independent of COX7A2L isoforms', *Cell Metabolism*, 20(6), pp. 1069–1075. doi: 10.1016/j.cmet.2014.11.005.

Napiwotzki, J. and Kadenbach, B. (1998) 'Extramitochondrial ATP / ADP-Ratios Regulate Cytochrome c Oxidase Activity via Binding to the Cytosolic Domain of Subunit IV', *Biol. Chem.*, 379, pp. 335–339. doi: 10.1515/bchm.1998.379.3.335.

Nicholls, D. G. and Ferguson, S. J. (2013) ‘5 - Respiratory Chains BT - Bioenergetics (Fourth Edition)’, in. Boston: Academic Press, pp. 91–157. doi: http://dx.doi.org/10.1016/B978-0-12-388425-1.00005-1.

Nijtmans, L. G. J., Taanman, J., Muijsers, A. O., Speijer, D. and Bogert, C. V. A. N. D. E. N. (1998) ‘Assembly of cytochrome- c oxidase in cultured human cells’, *Eur. J. Biochem*, 254, pp. 389–394.

Oliva, C. R., Markert, T., Gillespie, G. Y. and Griguer, C. E. (2015) ‘Nuclear-encoded cytochrome c oxidase subunit 4 regulates BMI1 expression and determines proliferative capacity of high-grade gliomas’, *Oncotarget*, 6(6), pp. 4330–4344.

Pecina, P., Houšťková, H., Hansíková, H., Zeman, J. and Houštěk, J. (2004) ‘Genetic defects of cytochrome C oxidase assembly’, *Physiological Research*, 53, pp. S213–S223.

Pfitzner, U., Odenwald, A., Ostermann, T., Weingard, L., Ludwig, B. and Richter, O. M. (1998) ‘Cytochrome c oxidase (heme aa3) from Paracoccus denitrificans: analysis of mutations in putative proton channels of subunit I.’, *Journal of bioenergetics and biomembranes*. UNITED STATES, 30(1), pp. 89–97.

Pierron, D., Wildman, D. E., Hüttemann, M. and Markondapatnaikuni, G. C. (2012) ‘Cytochrome c oxidase: Evolution of control via nuclear subunit addition’, *Biochimica et Biophysica Acta*, 1817(4), pp. 590–597. doi: 10.1016/j.biotechadv.2011.08.021.Secreted.

Piherov, L., Kidd, K., Acott, P. D., Crocker, J. F. S., Oussedik, Y., Str, V., Anna, P., Mallet, M., Zivn, M., Sovov, J., Jedli, I., Bare, V., Robins, V., Vrback, M., Pecina, P., Thibeault, Y., Hou, J., Bleyer, A. J. and Kmoch, S. (2018) ‘Acadian variant of Fanconi syndrome is caused by mitochondrial respiratory chain complex I deficiency due to a non-coding mutation in complex I assembly factor NDUFAF6 Hana Hartmannov a neck y rina Hoda n kov a a c st e s Mr a Vilma Kaplanov a’, 25(18), pp. 4062–4079. doi: 10.1093/hmg/ddw245.

Pitceathly, R. D. S., Rahman, S., Wedatilake, Y., Polke, J. M., Cirak, S., Foley, A. R., Sailer, A., Hurles, M. E., Stalker, J., Hargreaves, I., Woodward, C. E., Sweeney, M. G., Muntoni, F., Houlden, H., Taanman, J.-W. and Hanna, M. (2013) ‘NDUFA4 Mutations Underlie Dysfunction of a Cytochrome c Oxidase Subunit Linked to Human Neurological Disease’, *Cell Reports*. The Authors, 3(6), pp. 1795–1805. doi: 10.1016/j.celrep.2013.05.005.

Pitceathly, R. D. S. and Taanman, J.-W. (2018) ‘NDUFA4 (Renamed COXFA4) Is a

Cytochrome -c Oxidase Subunit', *Trends in Endocrinology & Metabolism*. Elsevier Ltd, xx, pp. 2–3. doi: 10.1016/j.tem.2018.03.009.

Porplycia, D. S. M., Lau, G. Y., McDonald, J., Chen, Z., Richards, J. G. and Moyes, C. D. (2017) 'Subfunctionalization of COX4 paralogs in fish', *American Journal of Physiology - Regulatory, Integrative and Comparative Physiology*, 312(5), pp. R671–R680. doi: 10.1152/ajpregu.00479.2016.

Poyton, R. O., Goehring, B., Droste, M., Sevarino, K., Allen, L. and Zhao, X.-J. (1996) 'Saccharomyces cerevisiae By has emerged as a useful model for studying both the crosstalk between', *Methods in enzymology*, 260, pp. 97–116.

Radford, N. B., Wan, B., Richman, A., Szczepaniak, L. S., Li, J., Li, K., Pfeiffer, K., Scha, H., Garry, D. J., Moreadith, R. W., Nina, B., Wan, B., Richman, A., Szczepaniak, S., Li, J., Li, K., Pfeiffer, K., Garry, D. J. and Randall, W. (2002) 'Cardiac dysfunction in mice lacking cytochrome- c oxidase subunit VIaH', *American Journal of Physiology Heart and Circulatory Physiology*, 282, pp. 726–733.

Ramzan, R., Staniek, K., Kadenbach, B. and Vogt, S. (2010) 'Mitochondrial respiration and membrane potential are regulated by the allosteric ATP-inhibition of cytochrome c oxidase', *BBA - Bioenergetics*. Elsevier B.V., 1797(9), pp. 1672–1680. doi: 10.1016/j.bbabio.2010.06.005.

Ran, F. A., Hsu, P. D., Lin, C., Gootenberg, J. S., Trevino, A., Scott, D. A., Inoue, A. and Matoba, S. (2014) 'HHS Public Access', *Cell*, 154(6), pp. 1380–1389. doi: 10.1016/j.cell.2013.08.021.Double.

Ran, F. A., Hsu, P. D. P., Wright, J., Agarwala, V., Scott, D. a and Zhang, F. (2013) 'Genome engineering using the CRISPR-Cas9 system', *Nature protocols*, 8(11), pp. 2281–2308. doi: 10.1038/nprot.2013.143.Genome.

Rich, P. R. (2017) 'Mitochondrial cytochrome c oxidase: catalysis, coupling and controversies', *Biochemical Society Transactions*, 45(3), p. 813 LP-829. Available at: http://www.biochemsoctrans.org/content/45/3/813.abstract.

Richter-Dennerlein, R., Oeljeklaus, S., Lorenzi, I., Ronsör, C., Bareth, B., Schendzielorz, A. B., Wang, C., Warscheid, B., Rehling, P. and Dennerlein, S. (2016) 'Mitochondrial Protein Synthesis Adapts to Influx of Nuclear-Encoded Protein', *Cell*, 167(2), p. 471–483.e10. doi: 10.1016/j.cell.2016.09.003.

Ruitenberg, M., Kannt, A., Bamberg, E., Ludwig, B., Michel, H. and Fendler, K.

(2000) ‘Single-electron reduction of the oxidized state is coupled to proton uptake via the K pathway in Paracoccus denitrificans cytochrome c oxidase’, *Proceedings of the National Academy of Sciences of the United States of America*, 97(9), pp. 4632–4636.

Salje, J., Ludwig, B. and Richter, O. H. (2005) ‘Is a third proton-conducting pathway operative in bacterial cytochrome c oxidase ?’, *Biochemical Society Transactions*, 33(4), pp. 829–831.

Sampson, V. and Alleyne, T. (2001) ‘Cytochrome c / cytochrome c oxidase interaction - Direct structural evidence for conformational changes during enzyme turnover’, *Eur. J. Biochem.*, 268, pp. 6534–6544.

Seagroves, T. N., Ryan, H. E., Lu, H. A. N., Wouters, B. G., Knapp, M., Thibault, P., Laderoute, K. and Johnson, R. S. (2001) ‘Transcription Factor HIF-1 Is a Necessary Mediator of the Pasteur Effect in Mammalian Cells’, *Molecular and Cellular Biology*, 21(10), pp. 3436–3444. doi: 10.1128/MCB.21.10.3436.

Segade, F., Hurlé, B., Claudio, E., Ramos, S. and Lazo, P. S. (1996) ‘Identification of an additional member of the cytochrome c oxidase subunit VIIa family of proteins’, *Journal of Biological Chemistry*, 271(21), pp. 12343–12349. doi: 10.1074/jbc.271.21.12343.

Sharma, V., Ala-Vannesluoma, P., Vattulainen, I., Wikström, M. and Róg, T. (2015) ‘Role of subunit III and its lipids in the molecular mechanism of cytochrome c oxidase’, *Biochimica et Biophysica Acta - Bioenergetics*. Elsevier B.V., 1847(8), pp. 690–697. doi: 10.1016/j.bbabio.2015.04.007.

Shimokata, K., Katayama, Y., Murayama, H., Suematsu, M., Tsukihara, T., Muramoto, K., Aoyama, H., Yoshikawa, S. and Shimada, H. (2007) ‘The proton pumping pathway of bovine heart cytochrome c oxidase.’, *Proceedings of the National Academy of Sciences of the United States of America*, 104(10), pp. 4200–4205. doi: 10.1073/pnas.0611627104.

Schäfer, E., Seelert, H., Reifschneider, N. H., Krause, F., Dencher, N. A. and Vonck, J. (2006) ‘Architecture of Active Mammalian Respiratory Chain’, *The Journal of Biological Chemistry*, 281(22), pp. 15370–15375. doi: 10.1074/jbc.M513525200.

Schägger, H. (2006) ‘Tricine–SDS-PAGE’, *Nature Protocols*, 1(1), pp. 16–22. doi: 10.1038/nprot.2006.4.

Schägger, H. and von Jagow, G. (1987) ‘Tricine-sodium dodecyl sulfate-

polyacrylamide gel electrophoresis for the separation of proteins in the range from 1 to 100 kDa', *Analytical Biochemistry*. Academic Press, 166(2), pp. 368–379. doi: 10.1016/0003-2697(87)90587-2.

Schägger, H. and Pfeiffer, K. (2000) 'Supercomplexes in the respiratory chains of yeast and mammalian mitochondria', *The EMBO Journal*, 19(8), pp. 1777–1783.

Schiffer, T. A., Peleli, M., Sundqvist, M. L., Ekblom, B., Lundberg, J. O., Weitzberg, E. and Larsen, F. J. (2016) 'Control of Human Energy Expenditure by Cytochrome C Oxidase Subunit IV-2.', *American journal of physiology. Cell physiology*, (9), p. ajpcell.00099.2016. doi: 10.1152/ajpcell.00099.2016.

Schmidt, T. R., Goodman, M. and Grossman, L. I. (1999) 'Molecular evolution of the COX7A gene family in primates.', *Molecular biology and evolution*, 16(5), pp. 619–626.

Singh, S., Misiak, M., Beyer, C. and Arnold, S. (2009) 'Cytochrome c Oxidase Isoform IV-2 is Involved in 3-Nitropropionic Acid-Induced Toxicity in Striatal Astrocytes', *Glia*, 57, pp. 1480–1491. doi: 10.1002/glia.20864.

Sommer, N., Hüttemann, M., Pak, O., Scheibe, S., Knoepp, F., Sinkler, C., Malczyk, M., Gierhardt, M., Esfandiary, A., Kraut, S., Jonas, F., Veith, C., Aras, S., Sydykov, A., Alebrahimdehkordi, N., Giehl, K., Hecker, M., Brandes, R. P., Seeger, W., Grimminger, F., Ghofrani, H. A., Schermuly, R. T., Grossman, L. I. and Weissmann, N. (2017) 'Mitochondrial Complex IV Subunit 4 Isoform 2 Is Essential for Acute Pulmonary Oxygen Sensing', *Circulation Research*, 121(4), pp. 424–438. doi: 10.1161/CIRCRESAHA.116.310482.

Stibůrek, L., Hansíková, H., Tesařová, M., Cerna, L. and Zeman, J. (2006) 'Biogenesis of Eukaryotic Cytochrome c Oxidase', *Physiol. Res.*, 55(2), pp. 27–41.

Stiburek, L., Vesela, K., Hansikova, H., Pecina, P., Tesarova, M. and Cerna, L. (2005) 'Tissue-specific cytochrome c oxidase assembly defects due to mutations in SCO2 and SURF1', 632, pp. 625–632. doi: 10.1042/BJ20050807.

Stibůrek, L. and Zeman, J. (2010) 'Assembly factors and ATP-dependent proteases in cytochrome c oxidase biogenesis', *BBA - Bioenergetics*. Elsevier B.V., 1797(6–7), pp. 1149–1158. doi: 10.1016/j.bbabio.2010.04.006.

Stoldt, S., Wenzel, D., Kehrein, K., Riedel, D., Ott, M. and Jakobs, S. (2018) 'Spatial orchestration of mitochondrial translation and OXPHOS complex assembly', *Nature Cell Biology*. doi: 10.1038/s41556-018-0090-7.

Strogolova, V., Furness, A., Robb-McGrath, M., Garlich, J. and Stuart, R. A. (2012) 'Rcf1 and Rcf2, members of the hypoxia-induced gene 1 protein family, are critical components of the mitochondrial cytochrome bc1-cytochrome c oxidase supercomplex', *Molecular and cellular biology*, 32(8), pp. 1363–1373. doi: 10.1128/MCB.06369-11.

Szklarczyk, R. and Huynen, M. A. (2010) 'Mosaic origin of the mitochondrial proteome', *Proteomics*, 10, pp. 4012–4024. doi: 10.1002/pmic.201000329.

Tamiya, G., Makino, S., Hayashi, M., Abe, A., Numakura, C., Ueki, M., Tanaka, A., Ito, C., Toshimori, K., Ogawa, N., Terashima, T., Maegawa, H., Yanagisawa, D., Tooyama, I., Tada, M., Onodera, O. and Hayasaka, K. (2014) 'A Mutation of COX6A1 Causes a Recessive Axonal or Mixed Form of Charcot-Marie-Tooth Disease', *The American Journal of Human Genetics*. The American Society of Human Genetics, 95(3), pp. 294–300. doi: 10.1016/j.ajhg.2014.07.013.

The Human Protein Atlas (2017) *COX4I2 RNA expression*. Available at: https://www.proteinatlas.org/ENSG00000131055-COX4I2/cell (Accessed: 25 April 2018).

Timón-Gómez, A., Nývltová, E., Abriata, L. A., Vila, A. J., Hosler, J. and Barrientos, A. (2017) 'Mitochondrial cytochrome c oxidase biogenesis: Recent developments', *Seminars in Cell & Developmental Biology*, pp. 1–16. doi: 10.1016/j.semcdb.2017.08.055.

Tsukihara, T., Aoyama, H., Tomizaki, T., Yamaguchi, H., Nakashima, R., Yaono, R. and Yoshikawa, S. (1996) 'The Whole Structure of the 13-Subunit Oxidized Cytochrome c Oxidase at 2.8 A', *SCIENCE*, 272(31), pp. 1136–1144.

Tzagoloff, A. and Dieckmann, C. L. (1990) 'PET Genes of Saccharomyces cerevisiae', *Microbiological Reviews*, 54(9), pp. 211–225.

Ugalde, C., Janssen, R. J. R. J., van den Heuvel, L. P., Smeitink, J. A. M. and Nijtmans, L. G. J. (2004) 'Differences in assembly or stability of complex I and other mitochondrial OXPHOS complexes in inherited complex I deficiency', *Human Molecular Genetics*, 13(6), pp. 659–667. doi: 10.1093/hmg/ddh071.

Vidoni, S., Harbour, M. E., Guerrero-Castillo, S., Signes, A., Ding, S., Fearnley, I. M., Taylor, R. W., Tiranti, V., Arnold, S., Fernández-Vizarra, E. and Zeviani, M. (2017) 'MR-1S Interacts with PET100 and PET117 in Module-Based Assembly of Human Cytochrome c Oxidase', *Cell Reports*. ElsevierCompany., 18(7), pp. 1727–1738. doi:

10.1016/j.celrep.2017.01.044.

Vygodina, T. V, Capitanio, N., Papa, S. and Konstantinov, A. A. (1997) 'Proton pumping by cytochrome c oxidase is coupled to peroxidase half of its catalytic cycle', *FEBS Letters*. Federation of European Biochemical Societies, 412(3), pp. 405–409. doi: 10.1016/S0014-5793(97)00649-2.

Weishaupt, A. and Kadenbach, B. (1992) 'Selective removal of subunit VIb increases the activity of cytochrome c oxidase', *Biochemistry*. American Chemical Society, 31(46), pp. 11477–11481. doi: 10.1021/bi00161a028.

Wikström, M., Sharma, V., Kaila, V. R. I., Hosler, J. P. and Hummer, G. (2015) 'New Perspectives on Proton Pumping in Cellular Respiration', *Chemical Reviews*. American Chemical Society, 115(5), pp. 2196–2221. doi: 10.1021/cr500448t.

Wikström, M., Verkhovsky, M. I. and Hummer, G. (2003) 'Water-gated mechanism of proton translocation by cytochrome c oxidase', *Biochimica et Biophysica Acta - Bioenergetics*, 1604(2), pp. 61–65. doi: 10.1016/S0005-2728(03)00041-0.

Williams, L., Valnot, I., Rustin, P. and Taanman, J. (2004) 'Cytochrome c Oxidase Subassemblies in Fibroblast Cultures from Patients Carrying Mutations in COX10 , SCO1 , or SURF1', *The Journal of Biological Chemistry*, 279(9), pp. 7462–7469. doi: 10.1074/jbc.M309232200.

Wiśniewski, J. R. and Mann, M. (2016) 'A proteomics approach to the protein normalization problem: Selection of unvarying proteins for MS-based proteomics and western blotting', *Journal of Proteome Research*, 15(7), pp. 2321–2326. doi: 10.1021/acs.jproteome.6b00403.

Wittig, I., Braun, H.-P. and Schägger, H. (2006) 'Blue native PAGE.', *Nature protocols*, 1(1), pp. 418–428. doi: 10.1038/nprot.2006.62.

Wittig, I. and Schägger, H. (2005) 'Advantages and limitations of clear-native PAGE', *Proteomics*, 5, pp. 4338–4346. doi: 10.1002/pmic.200500081.

Wu, M., Gu, J., Guo, R., Huang, Y. and Yang, M. (2016) 'Structure of Mammalian Respiratory Supercomplex I1III2IV1', *Cell*. Elsevier, 167(6), p. 1598–1609.e10. doi: 10.1016/j.cell.2016.11.012.

Yang, W.-L., Iacono, L., Tang, W.-M. and Chin, K.-V. (1998) 'Novel Function of the Regulatory Subunit of Protein Kinase A: Regulation of Cytochrome c Oxidase Activity and Cytochrome c Release', *Biochemistry*. American Chemical Society, 37(40), pp.

14175–14180. doi: 10.1021/bi981402a.

Yano, N., Muramoto, K., Shimada, A., Takemura, S., Baba, J., Fujisawa, H., Mochizuki, M., Shinzawa-Itoh, K., Yamashita, E., Tsukihara, T. and Yoshikawa, S. (2016) 'The Mg2+-containing water cluster of mammalian cytochrome c oxidase collects four pumping proton equivalents in each catalytic cycle', *Journal of Biological Chemistry*, 291(46), pp. 23882–23894. doi: 10.1074/jbc.M115.711770.

Yoshikawa, S. and Shimada, A. (2015) 'Reaction Mechanism of Cytochrome c Oxidase', *Chemical Reviews*. American Chemical Society, 115(4), pp. 1936–1989. doi: 10.1021/cr500266a.

Yoshikawa, S., Shinzawa-itoh, K., Nakashima, R., Yaono, R., Yamashita, E., Inoue, N., Yao, M., Fei, M. J., Libeu, C. P., Mizushima, T., Yamaguchi, H., Tomizaki, T. and Tsukihara, T. (1998) 'Redox-Coupled Crystal Structural Changes in Bovine Heart Cytochrome c Oxidase', *SCIENCE*, 280(June), pp. 1723–1729.